Cape Peninsula
University of Technology

Faculty of Engineering

Department of Electrical Engineering

DEVELOPMENT OF A NONCONTACT CURRENT SENSOR BASED ON MEMS TECHNOLOGY

A thesis submitted in fulfilment
of the requirements for the Master's degree in Technology (M.Tech)
in the Faculty of Engineering

of the Cape Peninsula University of Technology

by

Mr. Haithem Ali Babiker Mustafa

Supervisor: Prof MTE Kahn

Bellville Campus
December 2007

Declaration

I, *HAB Mustafa*, hereby declare that development of a non-contact current sensor based on MEMS technology is my own original work and that all sources have been accurately reported and acknowledged, and that this document has not previously, in its entirety or in part, been submitted at any university in order to obtain an academic qualification.

HAB Mustafa September 2007

Title

DEVELOPMENT OF A NON-CONTACT CURRENT SENSOR BASED ON MEMS TECHNOLOGY

Author

Haithem Ali Babiker Mustafa

Keywords

MEMS, Capacitance Transducer, Differential capacitance, Magnetic moment

Abstract

Development of a non-contact current sensor based on MEMS Technology
HAB Mustafa
Master degree of Technology Thesis
Department of Electrical Engineering
Cape Peninsula University of Technology

Most of MEMS sensors are based on the micro-cantilever technology, which use wide range of different design materials and structures. The benefit of MEMS technology is in developing devices having lower cost, lower power consumption, higher performance, and integration. A free-end cantilever-beam made of magnetic material (Permalloy) and a movable mass attached to the free-end has been designed using MEMS software tools. The magnetic material was used to improve the sensitivity of the cantilever-beam to an external applied magnetic field. The deflection of the cantilever was detected using capacitive sensing method. The aim of this research was to develop a non-contact current sensor based on MEMS technology by analysing the simulation of the system design of the micro cantilever when subjected to a magnetic field produced by a current-carrying conductor. When the signal, a sinusoidal current with a constant frequency is applied, the cantilever-beam exhibits a vibration motion along the vertical axis when it is placed closer to the line current. This creates corresponding capacitance changes and generates a voltage output proportional to the capacitive change in the signal processing circuitry attached to the micro cantilever.

Modelling of the magnetic moment of a magnetic cantilever-beam placed in a field, the deflection of the beam, the natural frequency of the cantilever-beam, the maximum deflection, the change in differential capacitive sensing technique, linearity of the differential capacitive, and capacitive sensitivity the circuit designed for readout was derived. The resonance frequency of the sensor structure was investigated and the simulation results were analyzed.

The analysis of the simulation result showed change in capacitance sensing in a certain range (50m A/meter to 1K A/meter) of external AC applied field. The change in the capacitance showed both a linear and nonlinear relationship beyond that range. The sensitivity of the differential capacitive in the range of the linearity of the system was calculated ($0.0212 \times 10^{-15} \frac{Farad}{A/meter}$). The output voltage due the capacitance change showed a linear relationship in a certain range and nonlinear beyond.

The use of the sensor in how to measure a current flowing in single or double wires was discussed in terms of the sensor position to the line current and the equation of the measurement was modelled for

the linear output of the sensor in both cases single and double wire. The main application of this micro cantilever is in current measurements with the aim to develop a non-contact current sensor mote.

September 2007

ACKNOWLEDGMENTS

First of all, I would like to thank my God, and then my Supervisor, Professor Khan for his support, patience and trust in me. Many thanks, to my family for their support and who stood by my side to reach this stage. Other thanks are to be extended to my brothers and friends in Cape Town city who fully supported and encouraged me during this period of study.

The financial assistance of the Cape Peninsula University of Technology is acknowledged as well.

LIST OF TABLES

Table **Page**

LIST OF FIGURES

Figure **Page**

CONTENTS

CHAPTER 1

NATURE AND SCOPE OF THE STUDY

1.1 BACKGROUND

Remote measurement in the energy technology rector is a topic of current value and concern. Presently, measurements are done with voltage divider network, current shunt and current transformers. Special purpose IC's are currently under development to facilitate such measurement without highly expensive isolation amplifiers for the low voltage electronics. A case of this development is the PIC 16F9xx interfaced with MCP3905 currently being researched by a student under the B-Tech department.

Electrical power sensors could be developed using new technology in applications such as determining the power consumption of big cities during the peak usage period. MEMS technology can offer a good solution by designing a non-contact current sensor which can be used to measure the power consumption. The idea behind wireless is to provide an accurate reading, since we are measuring power consumption by means of a non-contact current detection, as well as safety.

Electrical power sensors are used to measure characteristics of electric power such as voltage, current, power, and potential degradation of insulation due to age. For AC circuits, an electric power sensor can also be used to measure power quality. Some electrical power sensors are incorporated into transformers or other components of the power distribution grid. Typically, these electrical power sensors measure one or more physical characteristics and convert them into electrical signals. Basic electric power sensor categories include electrical capacitance, electrical frequency, electrical resistance, and electrical conductance sensors.

Electrical power sensors use different technologies to measure electrical characteristics. For example, Hall Effect sensors measure voltage, current, and power levels by using a current perpendicular to a magnetic field to cause an electric potential [S. V. Marshall, G. G. Skitek, 1990]. To measure the condition of aging insulation, sensing methods include degree of polymerization, insulation resistance, power frequency dissipation factor, and polarization index measurement. Additional methods use voltage response measurements, in which the electrical characteristics of a circuit are determined from the amplitude and phase of a test current flowing through a circuit

In this research we will achieve current measurement by means of a non-destructive, non invasive technique based on MEMS technology. We will overcome the problem of isolation circuitry and develop a unique non-invasive electric utility measurement device that can be deployed virtually anywhere including distributed generation and end user facilities.

1.2 RESEARCH TOPIC

The title of this study is:

Development of a non-contact current sensor based on MEMS technology.

1.3 RESEARCH OBJECTIVES

The primary objective of this study is to develop a non-contact current sensor based on MEMS technology. In particular, the study investigates the design, modelling, and simulation of micro-structure cantilever-beam and the capacitive transducer for current measurement.

In the process of realizing the primary objective, several secondary objectives are also identified as follows:

1.3.1 ANALYSIS OF MEMS CANTILEVER BEAM

In this part we look at the material structure, design specification, modelling and analysis of specific cantilever design. For certain applications, materials have to be selected based on their electrical and magnetic properties. The dynamic analysis of the cantilever will be investigated which includes the beam deflection due to external applied magnetic field, effective dimensions of the cantilever, and resonance frequencies of the cantilever. ConventorWare software will be used to design and analyze the micro-cantilever.

1.3.2 CAPACITIVE TRANSDUCER

In this part we will design a capacitive transducer based on the actuator designed. This includes modelling, linearization and sensitivity analysis of the capacitive transducer. We also need to look

at the circuit design for sensor readout in order to predict the behaviour of the sensor. The simulation analysis of capacitive transducer integrated with the circuit readout is possible by using CoventorWare and utilizes comparison between the sensor modelling and the simulation results.

Since this is an emerging academic field, the study should conclude by indicating areas for further research.

1.4 OUTLINE OF THE LITERATURE STUDY

The literature study follows a logical approach in which the starting point is a general discussion about MEMS magnetic and current sensors, including their basic principles operations.

The strategy review begins with chapter two which is an involved introduction to MEMS technology by presenting some of the historical background, applications, and progress through the use of this technology in developing current sensors.

The study continues by discussing current measurement and sensing techniques in chapter three. It explores characteristics of current measurements and it identifies the field of the research interest. The literature study concludes with a review of MEMS current sensor and the progress through the use of the technology in the field of current measurements.

1.5 THE SCOPE AND LIMITATIONS OF THE STUDY

This study will be geographically confined to the design, modelling, and simulation analysis. However there are some limitations as described below.

1.5.1 Limitations

The study will incorporate the latest findings and material in the literature and in practice. The following topics will not be part of this study:

(I) RF for interfacing.
(II) The specific silicon fabrication of MEMS sensor.

1.6 RESEARCH METHOD APPROACH

Having formulated the objectives, research question and motivated the scope of the study, the specific research method approach to be followed is discussed.

The literature study will provide background and insights into the research statement and permit an in-depth analysis.

The literature study will involve:

- a study of the relevant journals, books, newspapers, electronic publications, websites, and all other forms of published material
- the examination of papers presented at conferences
- personal communications with local and international experts in the field
- the use of keyword searches in the full text academic research databases such as Emerald, EBSCO Host and ScienceDirect
- the application of web search engines such as Google

The core fields of study will include:

- Structure and Designs of MEMS cantilever
- Model approach of the sensor dynamics
- Capacitive Transducer design
- Linearization analysis
- Simulation analysis of the sensor

Further fields of study may be revealed by cross-references or citations. These will be followed up and studied for their relevance.

1.7 LAYOUT OF THE DISSERTATION

In order to achieve the objectives of the study discussed above the following chapters and content of this dissertation are structured as follows:

Chapter 2: This chapter introduces MEMS Technology by presenting some of history background and applications.

Chapter 3: This chapter reviews the techniques of current measurement including: shunt resistor, current transformer, Hall Effect sensor, Rogowiski coil, Fluxgate current sensor, SQUID sensor, nuclear precession, fibre optics, and other techniques. It concludes with a review of Micro-electromechanical sensors.

Chapter 4: This chapter discusses the modelling of the equation that describes the sensor dynamic. This include modelling of the magnetic moment of a magnetic cantilever-beam placed in a magnetic field, the deflection of the beam, the natural frequency of the cantilever-beam, the maximum deflection, the change in differential capacitive sensing technique, linearity of the differential capacitive, and capacitive sensitivity. The chapter also presents the circuit designed that will be used for sensor readout, as well as the electrostatic modelling.

Chapter 5: This chapter presents a full description of the sensor, including cantilever-beam designed with capacitive sensing techniques and some description of the main steps of simulating the sensor design using CoventorWare software.

Chapter 6: This chapter presents the simulation and analysis result of the sensor design. Analyzing discussion of each simulation used to verify the sensor model will be included in this chapter.

Chapter 7: This chapter concludes the thesis. It reviews the study in terms of the research problem, sensor development modelling, design, simulation, analysis and ends with recommendations for further study.

1.8 SUMMARY

This chapter introduced the background and context of the study. It covered the research topic title and the objective of the research. The primary research objective was discussed, which is to develop a non-contact current sensor based on MEMS technology. Secondary objectives are to investigate the design, modelling, and simulation analysis of micro-structure cantilever-beam and the capacitive transducer of a current sensor.

The chapter concluded with the layout of the dissertation in order to achieve the objectives of the study. The next chapter introduces MEMS Technology in a brief discussion of the historical background and application.

CHAPTER 2

2 INTRODUCTION TO MEMS TECHNOLOGY

2.1 INTRODUCTION

In this chapter, a brief introduction to MEMS technology will be presented to provide a background of the field and its interest in developing devices and sensors. This includes the MEMS historical background and some applications.

2.2 MEMS BACKGROUND

Micro-electromechanical system (MEMS) is the integration of the element, sensors, actuator, and electronics in a common silicon substrate through micro-fabrication technology. MEMS technology has grown from early implementations in products such as pressure sensors to a pervasive technology used to produce high-volume solutions such as automotive airbag sensors and aerospace equipment. MEMS manufacturing uses high volume, integrated-circuit (IC)-style batch processing. There are multiple ways to manufacture MEMS, because the technology encompasses several different approaches [Lyshevski, S. E, 2002].

MEMS has a unique ability to collect information, process it, determine a course of action, and then act as a trigger by communicating through an electronic interface. These capabilities allow MEMS to provide advanced applications for smart devices technology, such as collision avoidance systems and wireless handsets. Integrating electro-mechanical, optical, and electronic circuits all on the same chip simplifies design and fabrication, and improves reliability because of fewer interconnects and components. As a result, MEMS is seen as a cost-effective candidate for the next-generation solution across multiple markets.

2.3 MEMS HISTORY

An amazing accurate description of MEMS technology was predicted in 1960 by Nobel Laureate Richard Feynman of Caltech. In this speech, Feynman pointed out the new obvious possibilities of mass information storage in atom units and scaling issues in an attempt to micromechanics [Feynman R, 1960]. After more than twenty years, he clearly predicted the sacrificial layer technology and many

production techniques in making micromotors and microtools. The first silicon-based micromechanics structure was developed way back in 1965 by Nathanson and Wickstrom [Nathanson H C, and Wickstrom R A, 1965] when they published their work on resonant gate transistor (RGT).

The Electrical Engineering department of Stanford and Case Western Reserve University pioneered the fabrication of pressure sensors using piezoresistive and capacitive sensing methods in 1970 [Ko W H, Hynecek J, and Boettcher S F, 1976, Wise K D, and Clark S K, 1978]. The lamb wave ultrasonic device using thin film deposition of aluminium and zinc oxide as well as silicon etching was developed by a group at UC Berkeley [White R M, 1970].

The historic paper in the 1980s, written by Kurt Petersen in 1982, was "Silicon as a mechanical material" which outlined the important mechanical properties of silicon and many processing techniques that were taking place intermittently at the time [Petersen K E, 1982]. The paper provided the following three major reasons as of how silicon-based micromachine can be successful: 1) they provide functions which cannot easily be duplicated by any conventional analogue or digital circuit, 2) they satisfactorily solve the inherent problems of mechanical reliability and reproducibility, 3) the fabrication techniques are totally compatible with standard IC processes since low-cost high-yield device technologies are most liked only if well established mass fabrication processes can be employed. Ink jet nozzle arrays, torsion optical mirror scanners accelerometers, electromechanical switches, cantilever light modulators were applications of MEMS described, therefore recognizing silicon-based technology micromachining as a technology field of its own.

Microvalves and pressure sensors in Japan were pioneered by Esashi [Esashi M, 1993]. Neural probes for neural prosthesis were advanced by Wise's group at university of Michigan and silicon devices for biomedical engineering applications were led by Ko at case Western Reserve university. Polysilicon surface micromaching started with Howe's chemical vapour sensor in 1984 (Howe R T, & Muller R S, 1988). In Germany, a fabrication technique for high aspect ratio tall structure was developed from post-war nuclear technology with the high energy [Ehrfeld et *al,* 1987]. Hybrid fabrication processes bridging different baseline processes has been developing since 1990. Some of the processes involved the interaction between the surface and bulk micromachining [Konishi S & Fujita H, 1993]. As we begin the 21st century, MEMS Technology seems to have the potential to penetrate almost any technology known to mankind. The trend of MEMS, being mostly microsensors, will evolve into a microactuators-led technology [Gabriel K J, 1995]. Technically the development of Microelectronics and Integrated Circuit (IC) led to the MEMS field, as demonstrated in Figure 2.1 [Noh H M, 2007].

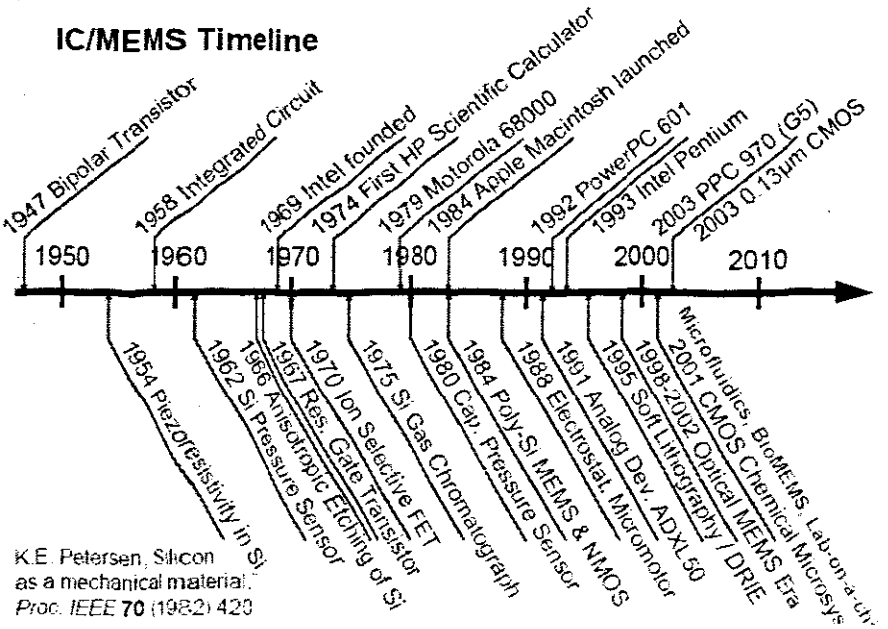

Figure2.1: From IC to MEMS

2.4 MEMS APPLICATION AND MARKETS

There are several applications for MEMS technology [Lyshevski, S. E, 2002]. The diagram in figure 2.2 shows the MEMS application field since 2004 and the prediction of future application in 2009 [Salomon P R, 2007].

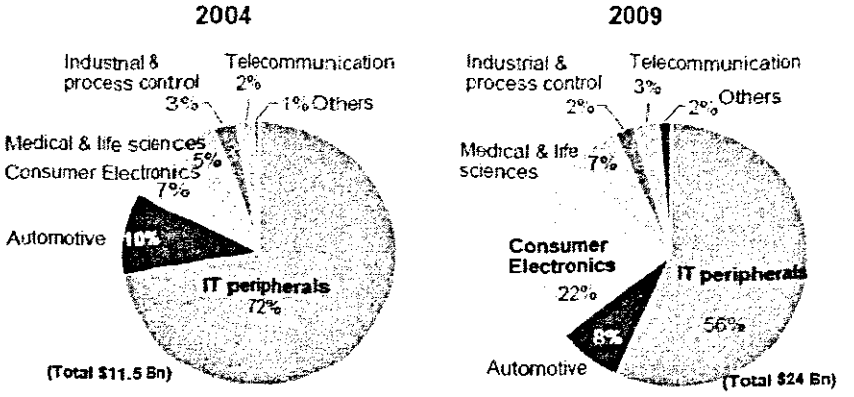

Figure2.2: MEMS Application field in 2004 and 2009

Medical and life Sciences

MEMS technology is enabling new discoveries in science and engineering such as the Polymerase Chain Reaction (PCR) micro-systems for DNA amplification and identification, micro-machined Scanning Tunnelling Microscopes (STMs), biochips for detection of hazardous chemical and biological agents, and micro-systems for high-throughput drug screening and selection [Lyshevski, S. E, 2002]. This field of application is predicted to increase in the next few years as shown in the figure 2.2.

Telecommunications

High frequency circuits will benefit considerably from the advent of the RF-MEMS technology. Electrical components such as inductors and tunable capacitors can be improved significantly compared to their integrated counterparts if they are made using MEMS technology [Lyshevski, S. E, 2002]. With the integration of such components, the performance of communication circuits will improve, while the total circuit area, power consumption and cost will be reduced. The telecommunication application has not taken a large capacity compared to the medical application, though it is predicted to increase slightly in the coming years as clearly demonstrated in the diagram.

Automotive

Automotive application has taken a large capacity in the field of MEMS application. The well-known sensors in this field are accelerometers and gyroscopes. MEMS accelerometers are used in industrial and automotive applications where detection of motion is required [Veijola T, Kuisma H & J Lahdenperä, 1998]. Recently, small-sized and high-performance acceleration sensors have been fabricated using MEMS cantilever technology and equivalent electrical circuit techniques. This technology has made it a possibility to integrate the accelerometer and electronics onto a single silicon chip at a lower cost, therefore being more functional, lighter, and more reliable. Unfortunately, the future of this application is not growing. In fact it is decreasing slightly. Figure 2.3 shows the market breakout of MEMS products from 2004 to 2009 [Salomon P R, 2007].

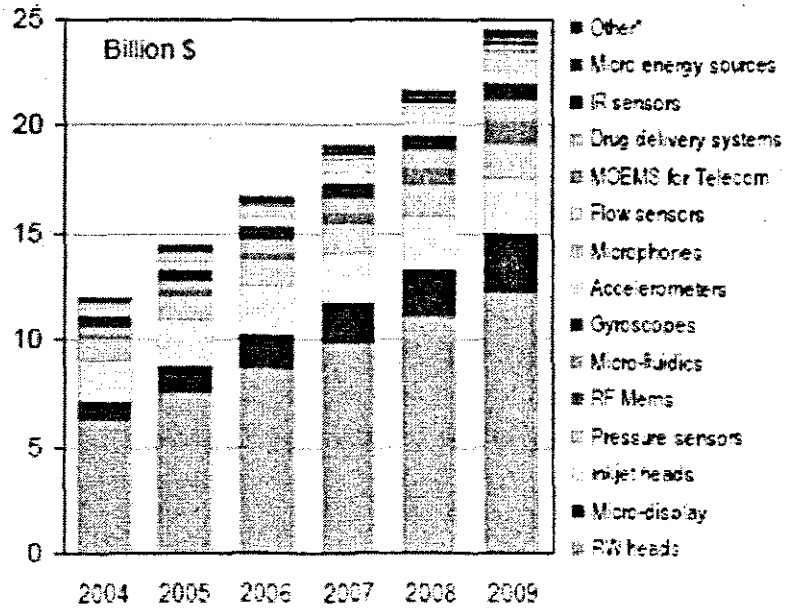

Figure2.3: Market breakout by product

2.5 SUMMRY

In conclusion, the chapter introduced MEMS Technology by presenting some of history background and applications.

CHAPTER 3

3 CURRENT MEASUREMENT AND SENSING TECHNOLOGIES

3.1 INTRODUCTION

Shunt resistor, transformers, and Hall sensors are traditional technologies that have been used to measure a current flowing in a wire. Shunt resistor techniques are used to directly measure the amount of current, while transformer techniques are used to indirectly measure the current through the secondary winding. Hall sensor techniques are based on the Hall Effect principle, which is a means of sensing the magnetic field produced by a current. While research is growing in magnetic field sensing technology, development of other technologies has also emerged. Many types of magnetic sensors with different techniques and various applications have been developed. One of the main applications is in current measurement and sensing techniques. The main advantage of the current sensing technique is sensing the magnetic field produced by the current under test in a contact-less measurement, due to the safety needed in case of high current measurement. In this chapter, an overview of the traditional current sensing technologies will be presented as well as the new technologies that were used in the magnetic field sensing techniques. This will also include MEMS techniques.

3.2 MAGNETIC FIELD SENSING TECHNOLOGIES

Several methods have been developed and used for sensing magnetic fields. The most common methods and their practical limits of sensing magnetic field are illustrated in Figure 3.1[Lenz J E, 1990, Bahreyni, 2006]. The average value of the magnetic field that any one of these technologies can be used to detect high or low field is around the order of $10^{-3}T$. The output of the magnetic sensors is either analogue or digital, therefore allowing it to be divided into two groups. Analogue sensors output provide a continuous signal with change of the present magnetic field. Most magnetic field sensors belong to this group. However, in many cases, a sensory system has to communicate with a digital processor and the use of an analogue-to-digital converter is inevitable if an analogue sensor is used as it adds to the overall cost of the system [Bahreyni, 2006]. A digital output on the sensor can be used more easily for such an application.

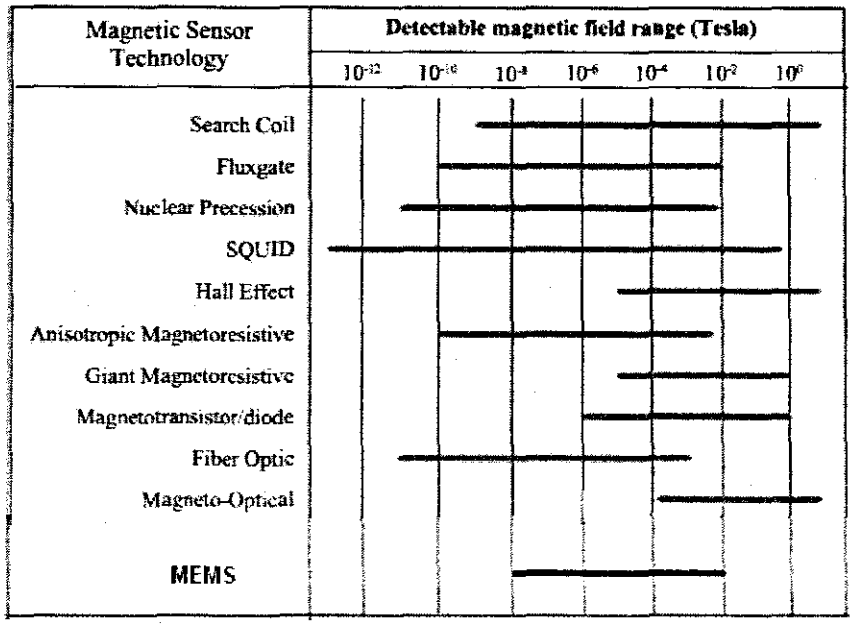

Figure 3.1: Technologies of sensing magnetic field

Figure 3.1 shows a comparison of various magnetic sensor technologies and the detectable magnetic field range. As is evident, devices using SQUID are very broad in range and sensitivity while others like Magneto optical are applicable over only a short range of magnetic field strength.

A brief discussion of the principles of the magnetic field sensing technologies will take place in the sections that follow as part of current sensing technologies.

3.3 CURRENT SENSING TECHNOLOGIES

3.3.1 CURRENT SHUNT RESISTORS

Shunt resistors are simply a resistive element placed in series with the load. The principle is based on Ohms law where the voltage drop across the device is proportional to the current [Ripka, 2004, Koon W, 2007]. This technology can provide an accurate measurement for low current but in the case of large current, they are impractical if not impossible because the shunts become bulky and heavy and the voltage drop causes heat dissipation. They are also not insulated and the conductor should be disconnected for mounting purposes [Dickinson R & Milano S, 2002]. Shunt resistors with high perform-

ance thermal packaging have been developed for large currents, although they still result in insertion loss. In addition, they do not provide a measurement isolated from transient voltage potential on the load. Shunt resistors also require other circuitry such as instrumentation amplifiers to generate distinguishable signals for measurement [Koon W, 2007].

3.3.2 CURRENT TRANSFORMERS

Current transformers are relatively simple to implement and are passive devices that do not require driving circuitry to operate. These transformers have a primary coil with a few turns and a secondary coil which should ideally be short circuits [Ripka P, 2004, Koon W, 2007]. The primary AC current will generate a magnetic which is coupled into secondary coil by Faraday's law. The magnitude of the secondary current is proportional to the number of turns in the coil. which is typically as high as >1000. The secondary current is then sensed through a sense resistor to convert the output to voltage.

The current transformers amplitude and phase errors depend on the core material and size, coil geometry, amplitude and frequency of the measured current, and also on the value of the burden. Relative current ratio error of a transformer with Nano-crystalline Vitroperm 500 F is very small and phase error is almost constant, even for law value of the primary current [Dickinson R & Milano S, 2002]. The advantages of current transformers are: contact-less current measurement, detecting high current, low power consumption, and low temperature shift.

3.3.3 CURRENT SENSORS USING HALL EFFECT

Hall sensors are among the most commonly-used types of magnetic field sensors [Lenz J E, 1990, Van Dau *et al*, 1995, Carvou *et al*, 2002, Dickinson R & Milano S, 2002]. The magnetic force on a moving electron in a conductor will produce a slight displacement between the electrons and the positive ions of the stationary lattice structures. As a result of this a voltage will be generated perpendicular to both the current and the field. This principle is known as the Hall Effect. This principle has found applications in many sensor devices.

When a magnetic field is perpendicular to a current and thin metal sheet, as shown in Figure 3.2, a Lorentz force is exerted on the current [Marshall & Skitek, 1990]. This force disturbs the current distribution, resulting in a potential difference (voltage) across the output. This voltage is called Hall voltage V_H, and is directly proportional to the current and the magnetic field, albeit of being of very small in order (micro-Tesla).

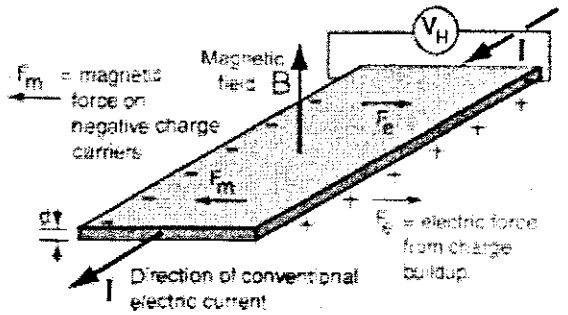

Figure 3.2: Hall Effect principle

The relationship is given by:

$$V_H = \frac{IB}{n_e q_e d} \tag{3.1}$$

where n_e and q_e is the free electron density and electron charge respectively, and d is the width of the conductor metal sheet.

The most sensitive Hall sensors are made of InSb and III-V semiconductors. However, sensors made of InSb require dedicated fabrication processes.

3.3.4 ROGOWSKI COIL CURRENT SENSORS (SEARCH COIL)

Rogowski coil also known as di/dt coil, is used to measure AC current, transient current, and change in DC current. It is based on search coil technique for sensing magnetic field. Schematic on figure 3.3 shows simple search coil. It is made of coil with or without core. The operation principle of these sensors is based on Faraday's Law of Induction. If the magnetic flux inside the coil changes a voltage proportional to the rate of change of the flux is generated between the coil leads [Lenz J E, 1990, Ripka P, 2001]. The sensitivity of the search coil depends on the permeability of the core material (ferromagnetic core increases the sensitivity), the area of the coil, the number of turns and the rate of change of the magnetic flux through the coil.

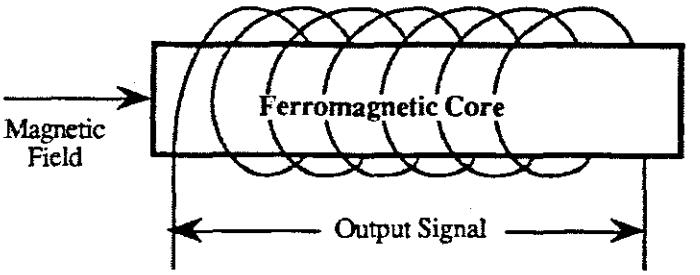

Figure 3.3: Search coil schematic

The Rogowski coil is designed to cancel the far field while the near field will remain. This is to avoid the possibility of interference occurring which is usually far field related. Rogowski devices are extremely linear and have air cores which make construction simple. However, in terms of signal processing, the output of the coil should be integrated because it is sensitive to the rate of the current (di/dt) [Ripka P, 2004]. The advantage that the Rogowski coil have in addition to that of current transformers is that no DC or high current saturation is possible. This is because the saturation of the air-core in a Rogowski coil is extremely high compared with ferrite cores of normal current transformers. The air core also has a linear phase response and low cost [Koon W, 2007].

3.3.5 FLUXGATE CURRENT SENSORS

Fluxgate sensors measure the magnitude and direction of the DC or low AC magnetic field in the range shown in Figure 3.1 [Lenz J E, 1990, Ripka P, 2001]. These sensors are one of the most sensitive magnetic field sensors. The basic sensor principle is illustrated in Figure 3.4. As all ferromagnetic materials exhibit hysteresis, a sinusoidal current applied to drive coil causes the core to reach its saturation magnetization once every half cycle. The sense coil then detects a nonlinearly distorted signal. The output signal includes even harmonics of drive signal, and most importantly, the second harmonic. The voltage associated with harmonics is proportional to the external magnetic field [Ripka P, 2001].

A novel DC/AC current sensor based on the fluxgate principle has been presented [Ripka *et al*, 2005]. The sensor is embedded in a print circuit board (PCB) that required the current to be sensed by passing a current carrying wire through an opening in the centre of the PCB. A linear characteristic with error of 10% has shown. Other fluxgate current sensor integrated in printed circuit board with different characteristics has been introduced [O'Donnell *et al*, 2006].

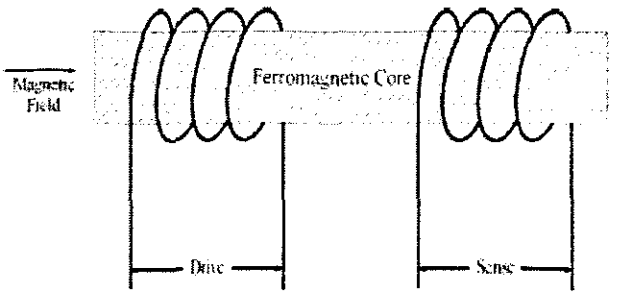

Figure 3.4: Fluxgate sensors schematic

3.3.6 SQUID CURRENT SENSORS

Superconducting Quantum Interference Devices (SQUID) are one of the most sensitive magnetic sensors available. [Lenz J E, 1990, Janawadkar *et al*, 1999, Krause H J *et al*, 2002, Fujita H, 2006]. The sensitivity of these sensors is on the order of femto-teslas. Besides their use in the laboratory, they have a rich application potential in areas such as geophysics, bio-magnetism and non-destructive testing of materials. The basic phenomena governing the operation of SQUID devices are flux quantization in superconducting loops and the Josephson Effect. For more details descriptions refer to Ripka [Ripka, 2001]. SQUIDs are operated as either RF or DC SQUIDs biased on Josephson junctions. Figure 3.5 shows superconducting flux transformer inductively coupled to SQUID. SQUID devices have been used to detect magnetic field in several applications [Penna S D, 2006]. One of the main applications besides current measurement is in medical imaging purposes, whereby measuring the neuro-magnetic field of the humans. Some other applications include: modulated excitation arrays, rotating field schemes, sensor multiplexing, magnetic moment detection, and microscopy setups [Krause H J & Kreutzbruck M.v, 2002].

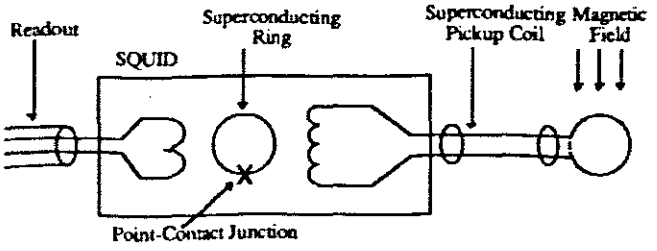

Figure 3.5: Superconducting flux transformer inductively coupled to SQUID

Odawara (2003) has developed a non-contact current measurement system using SQUID [Odawara *et al*, 2003]. The sensor converts the measured magnetic flux distribution into a current distribution with high sensitivity. The sensor has been applied in solar cell system to visualize the area of the solar cell that does not generate electrical power.

3.3.7 NUCLEAR PRECESSION

Nuclear precession is also known as nuclear magnetic resonators taking the advantage of the response to the magnetic field nuclei of atoms in hydrocarbon fluid [Lenz J E, 1990, Bahreyni, 2006, Ripka, 2001]. The principle of operation is based on the fact that the protons have small magnetic moment. When inside a liquid, these protons can be aligned by generating a uniform field around them using a coil. Switching off the generated magnetic field makes the protons precess about the ambient magnetic field. This transitional state of protons induces a signal in the coil which is a function of the strength of the magnetic field. Figure 3.6 shows a schematic of the sensor principle.

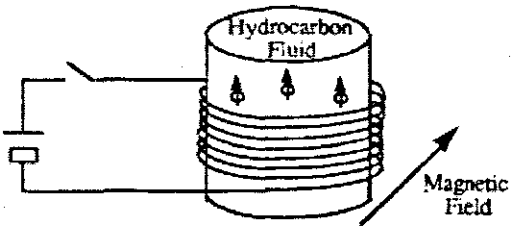

Figure 3.6: Nuclear precession magnetic sensor principle

3.3.8 FIBER OPTICS SENSORS

A fiber optic sensor uses the advantage of some material properties such as the magnetostrictive effect. Magnetostriction is a property of ferromagnetic materials. When this material is placed in a magnetic field, changes in size will occur [Lenz J E, 1990, Bahreyni, 2006, Ripka, 2001]. A piece of optical fibre is coated with a magnetostrictive material and is used as a leg of Mach-Zender interferometer as shown in Figure 3.7. When the sensor is placed in a magnetic field, a phase shift will be caused between the two legs due to the change in the coated leg dimension. Other optical fibre technology uses the Kerr effect and External Fabry-Perrot interferometry.

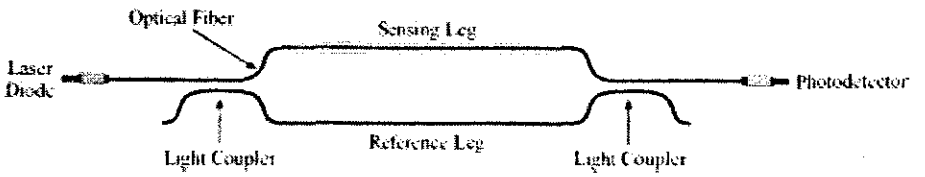

Figure 3.7: Fibre-optic magnetic field

3.3.9 OTHER TECHNOLOGIES

An external magnetic field can induce changes in the resistivity of the physical magnetoresistor due to material specifications [Lenz J E, 1990, Bahreyni, 2006, Ripka, 2001]. Material such as permalloy can be given a preferred initial magnetic orientation. Inside the magnetic field, the direction of magnetization rotates, which result in the reduction of the material resistance as a function of the magnetic field. The operation principle is similar to the Hall Effect as shown in Figure 3.8. The difference is that one of the electrodes is divided into two equal segments.

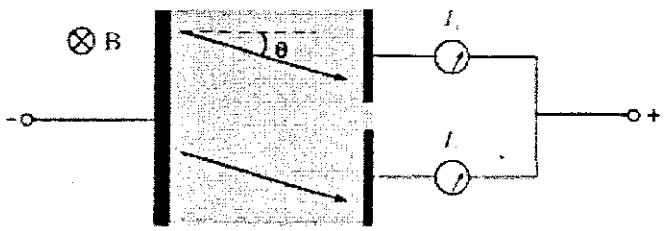

Figure 3.8: Magnetoresistive sensor schematic

The Giant Magnetoresistive (GMR) effect is based on the behaviour of electrons travelling through a magnetic field [Hardner H T, 2000, Simpson J, 2000]. The GMR of several thin layers of magnetic and non-magnetic material stacked together and over each other changes in magnetic field and electrons scattered in each layer differently based on their spin. GMR effect is similar to the giant magnetoimpedance effect (GMI); the impedance of the material changing rather than the resistor inside the magnetic field. GMR sensors have several applications in different fields such as automotive industry and magnetic hard drives.

A magnetodiode is basically a semiconductor diode or PN junction as illustrated in Figure 3.9. The two regions p and n are separated by undoped silicon [Lenz J E, 1990, Bahreyni, 2006, Ripka, 2001].

When the diode is forward biased and placed a magnetic field, electrons and holes are deflected in the same direction. The resistance of this region is a function of electron-hole recombination, which itself is a function of the external applied magnetic field. The sensitivity of these sensors is better than silicon Hall devices but their fabrication is more expensive [Ripka, 2001].

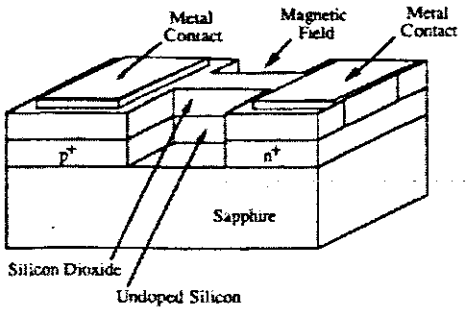

Figure 3.9: Magnetodiode sensor

Magnetotransistor sensors are similar to the magnetodiode sensors. They are a version of npn transistor [Ripka, 2001, Schneider *et al*, 1995]. The difference is that there are two collectors instead of one as illustrated in Figure 3.10. Both collectors have the same number of charge carriers in the absence of a magnetic field. In the presence of the magnetic field, the charge carriers are deflected toward one of the collectors depending on the field direction. The difference of amplifier voltage of the two collectors is proportional to the applied field. Hall effect is used in magnetotransistor to detect the magnetic field [Ripka, 2001].

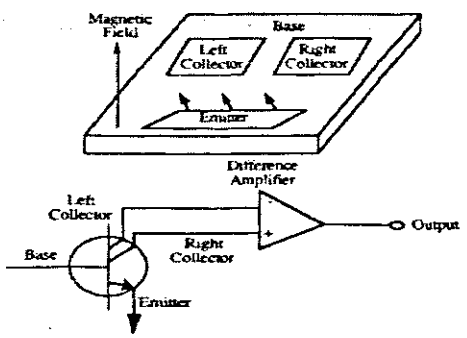

Figure 3.10: Magnetotransistor sensor

3.3.10 MICROMECHANICAL SENSORS

Recently MEMS have been used for sensing magnetic field for various applications [Leichle *et al*, 2003, Pister K S J, 1998, Bourquin F & Joly M, 2005]. The principle of these sensors is the interaction of the magnetic field with MEMS. A review of some of these sensors will be presented in this section.

Cowburn (1997) has designed a micro-cantilever for sensing magnetic field [Cowburn *et al*, 1997]. The cantilever was coated with a magnetic material in order to make it sensitive to an external applied magnetic field. The deflection is measured using a sensitive optical detection system. The sensor has shown a sensitivity in the order of 10^{-4} G (10 nT), and a good linearity over five orders of magnitude of applied field strength. Other techniques for measuring the deflection may also be used piezoresistive or piezoelectrics which were used by Beroulle and Pister, [Beroulle *et al*, 2001, Pister K S J, 1998], but the most common method is via capacitive sensing.

In 1998, Kaienburg and his associates developed a new surface micromachined silicon sensor for detecting magnetic field with highly accurate angle detection [Kaienburg *et al*, 1998]. A differential capacitance sensing technique was used to measure the deflection. The transducer may also serve as a reliable position and magnetic field sensor. In contrast to other angle detection sensors, this sensor is completely based on surface micromachining technology. The fabrication of the transducer is therefore fully compatible to the fabrication of other surface micromachined sensors like accelerometers. The same technique of measuring a moving structure has been used to develop a magnetic field sensor. The magnitude of the deflection is increased by resonant operation in vacuum to increase sensitivity of the sensor to the magnetic field [Emmerich H & Schofthaler M, 2000].

Kadar has introduced, in 1994 a resonant magnetic sensor based on the principle on Lorentz force [Kadar *et al*, 1994]. The resonator is a flexible thin silicon plate supported by two torsion bars and a rectangular coil attached on top of the plate. When a sinusoidal current is passed through the coil and an external magnetic field is present, the plate will vibrate. The displacement was detected via capacitive sensing. A capacitive feedback loop was used to enable the sensor to have a large dynamic range because of the high quality factor of the resonator. The sensor has a nonlinear response which is easy to solve using the feedback.

The resonating microstructures have the advantage of providing a large output signal and many micromechanical sensors has utilized this advantage to improve their sensitivity or dynamic range [Kadar *et al*, 1994, Leichle *et al*, 2001, Temnykh A B & Lovelace R V E 2001, Sunier *et al*, 2006, De Angelis

et al, 2007]. These sensors use different mechanisms to bring and hold mechanical structure under resonance.

In current sensing application, most of MEMS-based current sensors are designed to operate by sensing and determining the current in a first conductor by making use of either the force acting between a conductor carrying an unknown current and a reference current positioned in the magnetic field produced by the unknown current carrying conductor or the mutual inductance induced between terminals of a reference conductor [Berkan *et al*, 2006]. For example, a MEMS-based current sensor has been developed for industrial automation application [DeNatale *et al*, 2003]. The sensor consists of a current carrying beams mechanically coupled using a rigid backbone support. A perpendicular external magnetic field to the sensor substrate will deflect the beam laterally. This deflection is sensed capacitively using integrated comb structures. The sensor provides 16-bit resolution over a 4-20 mA range.

Another kind of design based on the magnetic field torque has taken a place in MEMS current sensors. Goedeke (2004) introduced a current sensor using a cobalt-coated micro-cantilever as a detector element to detect the magnetic field generated by a current carrying wire at point up to 5mm from the sensor [Goedeke *et al*, 2004]. Different structures have been investigated to a chief high sensitivity and performance. An optical readout based on dual fibre probe technique has been used to sense the cantilever deflection. This technique is not sensitive to motion as some others optical techniques, but it has the advantage that it can be used with LED. Other techniques for sensing the deflection due to the magnetic moment used is piezoelectric material [Leland E S, 2007]. The idea is that the mechanical element consists of piezoelectric material. A deformation of this material will produce a voltage that is proportional to the deformation which is a function of the external magnetic field.

3.4 SUMMARY

In conclusion, this chapter discussed the techniques of current measurement. This included, shunt resistor, current transformer, Hall Effect sensor, Rogowiski coil, Fluxgate current sensor, SQUID sensor, nuclear precession, fibre optics, other techniques, and Micro-electromechanical sensors.

CHAPTER 4

4 SENSOR MODELLING

4.1 INTRODUCTION

In this chapter the modelling and the operating principles of the sensor will be discussed. In the modelling section concerning modelling, an analysis of the sensor behaviour under normal conditions will be presented. The electromechanical modelling of a magnetic cantilever-beam is first described. This includes modelling of the natural frequency of the structure, large scale deflection of the beam, capacitive transducer operation, and the derivation of the sensitivity.

4.2 MAGNETIC CANTILEVER-BEAM

In this section the equation of the deflection of the magnetic cantilever-beam subjected to a sinusoidally alternating magnetic field is described based on the work completed by Ruan, Shen and Weeler [Ruan M, Shen J, & Wheeler C B, 2001]. The proposed application of the cantilever is to measure the beam deflection when it is placed closer to a current-carrying conductor. This will make the cantilever vibrate in relation to the applied magnetic field, and generate a voltage output proportional to the capacitive change in the micro cantilever. It is known that a current-carrying conductor generates a magnetic field around the conductor. This magnetic field is represented by

$$H = \frac{i}{2\pi r} \tag{4.1}$$

where H is the magnetic field, i is the current, and r is the distance from the centre of the conductor.

When a magnetic cantilever-beam is subjected to an external applied magnetic field, the free-end of the magnetic beam will rotate along the y-axis if the magnetic field lies along the z-axis and the beam is along the x-axis. The rotation is proportional to the applied field and the magnetic sensitivity of the beam material. If a permanent magnetic field is applied along the beam-length, it will induce sufficient magnetization depending on the magnitude of the field and the magnetic properties of the beam-material. Higher magnetization ensures high sensitivity to an external field. In this case the magnetiza-

tion direction is along the beam-length by neglecting the effect of the others component along the thickness and the width. Figure 4.1 shows the proposed of the cantilever-beam.

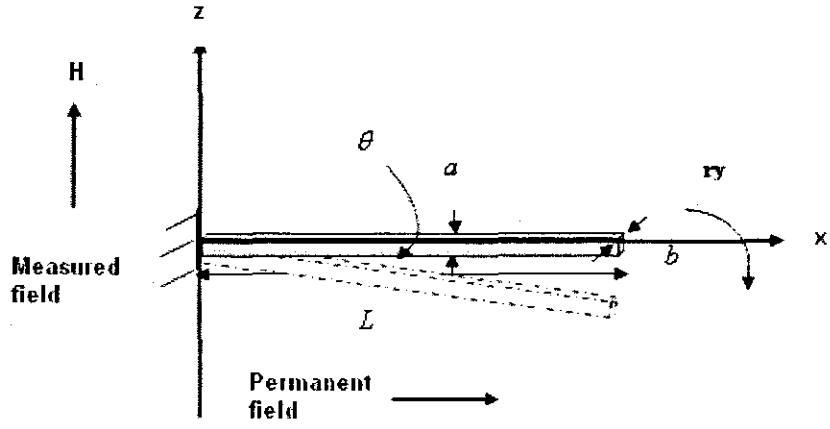

Figure 4.1: Schematic of the proposed micro-magnetic cantilever beam

The assumption is that the beam material is isotropic and homogeneous and has a uniform magnetization along the beam-length. The magnetic moment of the beam can be expressed as

$$\bar{m} = \bar{M}V \qquad (4.2)$$

Where M is the magnetization in the beam and is determined by the external magnetic field (H). V is the volume of the beam. The beam is initially straight having a rectangular uniform shape before it deforms by the external magnetic field [Youhe Z & Xiaojing Z, 1997]. The magnetic bending moment (τ_m) that causes this deformation is obtained using the formula below:

$$\tau_m = \bar{m} \times \bar{B} = \mu_o \bar{m} \times \bar{H} \qquad (4.3)$$

where

$\mu_o = 4\pi \times 10^{-7} H/m$ is the permeability of free space. Here we considered an AC field and magnetization ($\bar{B} = B_0 \sin w_f t.\bar{z}$, $\bar{m} = m_0 \sin w_f t.\bar{x}$) produced by an AC current-currying conductor, therefore, the magnetic force that acts on the beam-ends to rotatesthe beam can be derived as follows

$$\tau_m = \mu_o m_o H_o \sin^2(w_f t) = \frac{\tau_o}{2}[1 - \cos(2w_f t)] \quad (4.4)$$

$$\tau_o = \mu_o m_o H_o \quad (4.5)$$

where $w_f = 2\pi f$ is the circular frequency of the current signal, and f is the frequency of the current signal. The magnetic force that act sat the beam-ends can be obtained by

$$F_m = \frac{\tau_m}{L} \quad (4.6)$$

$$F_m = \frac{\tau_o}{2L}[1 - \cos(2w_f t)] \quad (4.7)$$

Equation 4.7 represents the magnetic force that acts at the end of the beam and makes it vibrate around its equilibrium position.

4.3 STATIC ANALYSIS OF THE BEAM

The dynamic characteristics of this system depend on the geometrical dimension and the material properties of structure [Hu Y C, Chang C M, & Huang S C, 2004]. There are some considerations that need to be taken into account to simplify the dynamic system analysis. The material of the beam follows Hook's Law in that the flexure is a linear spring and the maximum flexure stress in the beam is less than the elastic limit of the beam.

The relation between the bending moment and the curvature of the beam where the curvature is equal to the second derivative of the deflection is given by

$$\tau(x) = EI \frac{\partial^2 z(x)}{\partial^2 x} \quad (4.8)$$

where E is the Young's Modulus, $I = \frac{ab^3}{12}$ is the moment of inertia, and (EI) is called flexural rigidity. The bending moment at a distance x along the beam obtained by

$$\tau(x) = -F(L - x) \tag{4.9}$$

If we substitute equation (4.9) into equation (4.8) we can derive the deflection equation as fellows:

$$EI \frac{\partial z(x)}{\partial x} = -\int_{x=0}^{x} F(L - x)dx$$

$$EI \frac{\partial z(x)}{\partial x} = -F\left(Lx - \frac{x^2}{2}\right)$$

$$z(x) = -\int_{x=0}^{x} \frac{F}{EI}\left(Lx - \frac{x^2}{2}\right)dx$$

$$z(x) = -\frac{F}{EI}\left(L\frac{x^2}{2} - \frac{x^3}{6}\right) \tag{4.10}$$

Equation 4.10 represents the deflection of the beam varying along the beam length but we are interested in the maximum displacement which occurs by the free-end of the beam (x = L) and obtained by

$$z(L)_{max} = -\frac{FL^3}{3EI} \tag{4.11}$$

The angular deflection can also be represented by the slope of the beam deflection as in equation (4.12) and also it's varying along the beam length.

$$\theta(x) = \frac{\partial z(x)}{\partial x} = -\frac{F}{EI}\left(Lx - \frac{x^2}{2}\right) \tag{4.12}$$

The maximum angular deflection is given by taking (x = L) and substituting it into equation (4.12) obtaining

$$\theta(L)_{max} = -\frac{FL^2}{2EI} \tag{4.13}$$

By substitute equations 4.3 and 4.6 into equation 4.13, we obtained

$$\theta(L)_{\max} = -\frac{L}{2EI}\tau_m \tag{4.14}$$

$$\theta(L)_{\max} = -\frac{L}{2EI}\mu_o \vec{m} \times \vec{H} \tag{4.15}$$

Equation 4.15 represents the deflection at x=L (refer to Figure 4.1) and is proportional to the field and the magnetization.

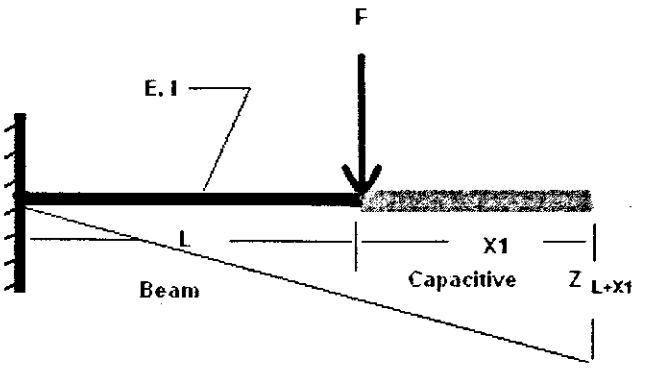

Figure 4.2: Schematic of the sensor dynamic

Figure 4.2 shows the beam and the capacitive attached together. In order to derive the deflection at the end of the attached mass by means at point (L+X1), assuming that the maximum angular deflection is very small and $\theta(L)_{\max} = \theta(L + X1)_{\max}$, then we can write

$$Z_{L+X_1} = (L + X_1)\theta(L)_{\max} \tag{4.16}$$

Substitute 4.10 into 4.11, we then obtained

$$Z_{L+X_1} = -\frac{FL^2}{2EI}(L + X_1) \tag{4.17}$$

$$Z_{L+X_1} = -\frac{\mu_o L}{2EI}(L + X_1)\bar{m} \times \bar{H} \tag{4.18}$$

Equation 4.18 represents the displacement at a distance $Z(L + X_1)$ from the fixed beam-end. This equation shows that displacement is a function of the magnetization and the external applied magnetic field. In order to ensure a sensing displacement due to a very small external applied field, the initial value of the magnetization should be high enough. This can be achieved by increasing the permanent magnetic field along the beam-length to increase the magnetization.

4.4 LARGE DEFLECTION OF THE BEAM

Large deflection of a free-end cantilever beam has been studied in both linear and non-linear situations by many researchers. Recently, a solution of a large deflection cantilever beam of non-linear elastic material under combined loading was done by Lee Kyangoo. [Kyungwoo L, 2002]. Here we are going to consider a linear elastic material. The maximum applied force that does not bend the beam determines the large deflection of the beam. In other words, the total force that causes the maximum stress. When the beam stress is bigger than the fracture strength the beam will break. Assume that a force is applied at the free-end of the beam, then the maximum stress (σ_{max}) is at the anchor of the cantilever-beam given by

$$\sigma_{max} = \frac{6LF_{total}}{ab^2} \tag{4.19}$$

The maximum magnetic force that can be applied to the cantilever-beam is estimated by taking ($\sigma_{max} = \sigma$), where σ is the fracture strength constant of the material of the beam. Then we write the maximum force which is called the maximum detectable signal in equation (3.9).

$$F_{total} = \frac{ab^2\sigma}{6L} \tag{4.20}$$

Once the fracture strength of the beam material is known, we can estimate the maximum force that does not break the beam. This force includes the maximum magnetic force and any other factors like electrostatic force and damping force. Zero damping will take place in this model because the dielec-

tric material between the beam and the base is considered to be a free space as the damping forces present a challenge in observing the oscillation behaviour of the system [Harmany Z, 2003].

In some applications, the height of the cantilever-beam from the sensor substrate needs to be modelled in order to avoid contact during the vibration motion. In this case, the ratio of the cantilever-beam deflection and the height (initial gap) should be very small-that is, the deflection is very small compared to the beam-height but it can still make sense in the capacitive transducer.

4.5 NATURAL FREQUENCY ANALYSIS

In order to avoid the effect of the resonance frequency on the beam structure, we should predict the natural frequency of the structure [Rossit C A & Laura P A A, 2001]. The natural frequency of the cantilever-beam depends on the equivalent spring constant and the effective-mass defined by equation 4.21. Higher natural frequency requires higher ratio of stiffness to effective mass. In other words, the stiffness must be greater than the effective mass.

$$f_n = \frac{1}{2\pi}\sqrt{\frac{K_{eq}}{M_{eq}}} \tag{4.21}$$

where

K_{eq} , M_{eq} is the equivalent mass and spring constant of the structure.

$$K_{eq} = -\frac{F}{Z(L+X_1)} \tag{4.22}$$

$$K_{eq} = \frac{2EI}{L^2(L+X_1)} = \frac{ab^3E}{6L^2(L+X_1)} \tag{4.23}$$

$$M_{eq} = 0.23\,(m + M) \tag{4.24}$$

where $m = abL\,\rho_p$ is the beam-mass and $M = 2X_1Y_1Z_1\rho_a$ is the mass of the plates attached to the beam free-end.

$$f_n = \frac{1}{2\pi}\sqrt{\frac{ab^3E}{6L^2(L + X_1)0.23(m + M)}} \tag{4.25}$$

Using the dimensions of the cantilever and the material properties, presented in the next chapter, the natural frequency can be calculated (0.766 kHz), and compared to the resonance frequency later in chapter 6.

4.6 DIFFERENTIAL CAPACITIVE TRANSDUCER

4.6.1 LINEARIZATION ANALYSIS

In this scenario, it is assumed that the movable plate is rigid and moving toward the fixed plate with a small angular displacement while a magnetic field is applied on the beam. In this case, a small angle tilted-plate capacitor is assumed for the capacitance sensor between the movable plate and the fixed plate. This kind of capacitor has two unparallel electrode plates with a small angle between them, as seen in Figure 4.3. The total capacitance (C) of this capacitor is derived from the theory of parallel plate capacitance and is given by equation 4.26.

Figure 4.3: Small angle tilted-plate capacitor

$$C = \varepsilon\frac{A_{eff}}{d_{average}} \tag{4.26}$$

Here ε is the dielectric constant, A_{eff} is the effective area, and $d_{average}$ is the average distance between the two plates. The area of the movable plate is the effective area, which is designed to be smaller than the area of the fixed plates. Referring to the Figure 4.3, which is constructing a differential capacitive, we can write the equations of the capacitors as

$$C_L(t) = \varepsilon \frac{A_{eff}}{d_o - \frac{z(t)}{2}} = \varepsilon \frac{A_{eff}}{d_o(1 - z(t)/2d_o)} \tag{4.27}$$

$$C_U(t) = \varepsilon \frac{A_{eff}}{d_o + \frac{z(t)}{2}} = \varepsilon \frac{A_{eff}}{d_o(1 + z(t)/2d_o)} \tag{4.28}$$

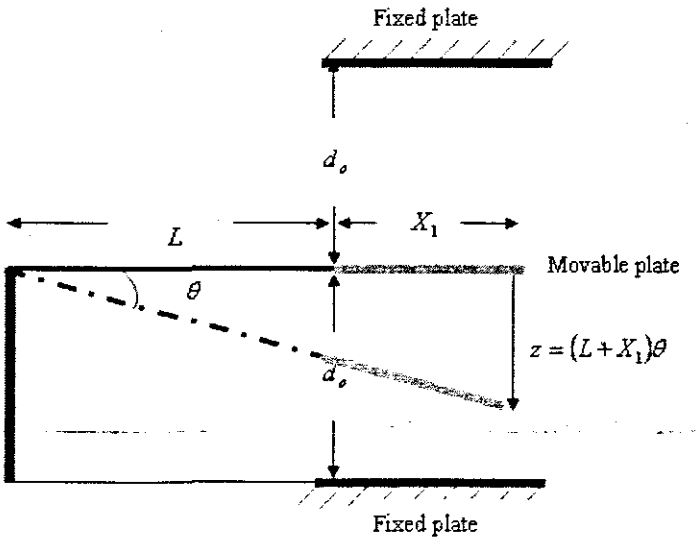

Figure 4.4: Differential capacitive sensing dimensions

where $C_L(t)$, $C_U(t)$ represents the capacitance of the Lower and Upper capacitors respectively. The difference in the differential capacitive sensor is given by equation 4.29. Now, let

$$C_L(t) = C_o + \Delta C(t) \tag{4-29}$$

$$C_U(t) = C_0 - \Delta C(t) \tag{4-30}$$

where C_o is the initial capacitance value of both lower and upper capacitors and $\Delta C(t)$ is the change in capacitance.

$$C_o = \varepsilon \frac{A_{eff}}{d_o} \tag{4.31}$$

$$\Delta C(t) = \frac{1}{2}\left[C_L(t) - C_U(t)\right] \tag{4.32}$$

By substituting equations (4.27) and (4.28) into equation (4.32), we obtained

$$\Delta C(t) = \frac{1}{2}\varepsilon \frac{A_{eff}}{d_o}\left[\frac{\frac{z(t)}{d_o}}{1-\left(\frac{z(t)}{2d_o}\right)^2}\right] \tag{4.33}$$

Then the approximation assumption

$1-\left[\frac{z(t)}{2d_o}\right]^2 \approx 1$ when $\left[\frac{z(t)}{2d_o}\right]^2 \prec\prec 1$ is used. This assumption ensures that the ratio of the displacement double the initial gap is small enough, therefore, equation (4.33) can be written as

$$\Delta C(t) = \frac{C_0}{2}\left[\frac{z(t)}{d_o}\right] \tag{4.34}$$

$$\Delta C(t) = \frac{C_0}{2}\left[\frac{L + X_1}{d_o}\right]\theta(t) \tag{4.35}$$

Equation 4.34 shows the capacitance difference proportional to the angle deflection linearly with a constant determined by the initial gap, initial capacitance, beam-length, and the movable plate width.

4.7 CAPACITIVE SENSITIVITY ANALYSIS

The sensitivity of the cantilever beam is defined by the change in capacitance per applied magnetic force. Therefore, the sensitivity formula can be derived as follows

Substitute equation (4.15) into equation (4.35).

$$\Delta C = C_o \left[\frac{L + X_1}{d_o} \right] \frac{L \mu_o}{2 EI} \bar{m} \times \bar{H} \tag{4.36}$$

Then

$$Sen = \frac{\Delta C}{H} = C_o \left[\frac{L + X_1}{d_o} \right] \frac{6 L \mu_o}{ab^3 E} |\bar{m}| \sin(m, H) \tag{4.37}$$

The effect of the beam parameters on the sensitivity can be extracted from equation 4.37. The equation shows that the sensitivity is proportional to the beam-length and inversely proportional to the beam-width, thickness and the beam-elasticity as well.

4.8 ELECTROSTATIC MODELLING

Electrostatic actuation is a common method that is used in MEMS sensors and actuators for the reasons given below [Veijola T, 2001, Murnane *et al*, 1996, Boser B E, 1996]:

- The steady state power requirements
- Ease of fabrication
- Constructed from poly-silicon or metals which are usually available in micro-machined process
- The same structure that is used for actuation can be used for capacitive sensing

In addition, they are easy to use and can be adapted to many different applications. Micro-machined electrostatic actuators are controlled by applying different voltages to the electrodes rather than directly putting a certain amount of charge on a plate [Boser B E, 1996, Veijola T *et al*, 1998]. As a result, the force between two electrodes is always attractive and this means it can be used to pull, not push. This force is called an electrostatic force and exists between any structures which are either

changed independently from each other or proportionally. The magnitudes of these forces depend on the voltage difference between the objects, their geometry, and the distance between them. The electrostatic force is represented by the following equation:

$$F_{eletro} = -C_0 \frac{V^2}{d_{ave}^2} \tag{4.38}$$

4.9 MEMS CAPACITIVE READ OUT

This section describes the circuit design as part of this research which was used to measure the capacitive change and to convert the mechanical energy into electrical energy. Bridge circuits are traditional techniques which are basically used to measure changes in resistors or capacitors in the arms of the circuit [Kester W, 2007]. For the majority of the sensor applications employing bridges, however, the deviation of one or more capacitors in a bridge from an initial value is measured as an indication of the magnitude or change in the measured variable [Kester W, 2007]. In this case, the change in the output voltage is an indication of capacitance change. The change it might be as small as tens of nano or micro-volts due to a very small capacitance changes.

Since capacitive sensors are used in variety of sensing applications such as acceleration, force, pressure, displacement and so forth, different circuits designed for measuring capacitance change have been developed [Ignjatovic Z & Bocko M F, 2005, Niemainen *et al*, 2004]. This provides either analogue or digital readouts for both single and double differential capacitors. The presence of parasitic capacitances associated with the signal traces connecting the MEMS capacitive sensor is the major problem in the measurement of MEMS capacitive.

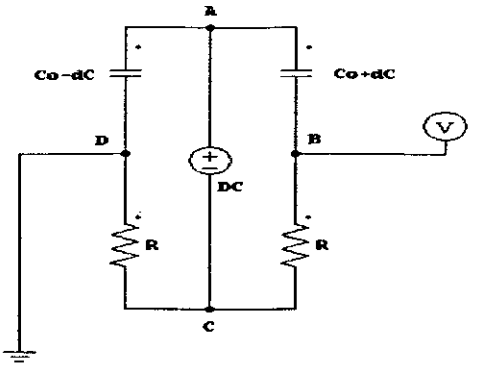

Figure 4.5: Circuit design for readout

The voltage output of the circuit in Figure 4.5 is depends on the capacitance value and can be given by

$$V_B = V_{C+\Delta C} - V_{C-\Delta C} \tag{4.39}$$

4.10 SUMMARY

In conclusion, the chapter discussed the modelling of the equation that described the sensor dynamics. This includes the modelling of the magnetic moment of a magnetic cantilever-beam placed in a field, the deflection of the beam, the natural frequency of the cantilever-beam, the maximum deflection, the change in differential capacitive sensing technique, linearity of the differential capacitive, and capacitive sensitivity. The chapter also presented the circuit design that will be used for sensor readout and the electrostatic modelling as well.

CHAPTER 5

5 SENSOR DESIGN

5.1 INTRODUCTION

In this chapter, a complete geometrical description and material properties of the electromechanical part of the sensor will be described, in addition to a brief introduction to Coventor software will be presented in this chapter as well. The main steps of designing the sensor by using the software will also be presented.

5.2 INTRODUCTION TO COVENTOR

Many laboratory techniques have been developed in recent years to manufacture micro-devices. Software has also been developed to simulate these devices to assist studies of physical structures, layouts and analysis of these miniature systems. Coventorware is a software package designed to accurately reproduce MEMS design models and support both system level and physical design approaches. The system level approach uses libraries of tools with a high speed system simulator to create 2-D layer outputs and the physical approach convert the 2-D to a 3-D model. The major components of this software are the Material Properties Database (MPD), Processor Editor, Architect, Designer, Meshing, and Analyzer.

Material Properties Database (MPD) is a file provided with the software that contains common materials used in MEMS processing. The software allows the user to add or delete new material with access of modifying their relevant mechanical, electrical, thermal, fluidic, and other properties.

Process Editor allows the user to create a simulating process flow for micro-fabrication of MEMS and Micro-fluidics design. Process Editor has three components: process library, process description, and step parameters. Process library contains folders that include modelling actions (deposit or etching) such as conformal shell, delete, planar fill, stack material, and straight cut. Process steps such as action, material, layer name, layer thickness, step number, step name, and more are provided by the process description. Editing of selected step parameters are provided by the step parameters.

Architect parametric library has been developed to allow the designer user to simulate and evaluate multiple design configurations. The parametric components are building blocks. Each block has a connection point that can be used to connect several blocks together in order to simulate MEMS device. These blocks also have variable characteristics determined by the user. Parametric library contain several libraries, which are electromechanical, dampers, magneto-mechanics, optics, sensors and actuators, and fluidics. With Architect, the user can employ high-level design techniques to create a system model of a device that can be simulated using Saber. Saber allows the user to connect and simulate a system model that can contain a mixed signal either analogue or digital with mixed technology: electrical, mechanical, optical, or fluidic using the parametric library component.

Designer is a creation tools especially for MEMS layout. These tools can be used to extract a MEMS design from an Architect schematic or it can be used to build a device from a process file. Designer allows the user to access the 2-D layout and convert it to a 3-D solid model for mechanical and electrical analysis provided by the analyzer.

Meshing is one of the techniques that were used to determine the stress and strain on a certain physical structure, which is called finite element methods (FEM) [Mendels *et al*, 2006]. The idea of FEM is to discrete the actual shape of the structures into finite geometrical elements, where each element represents a portion of the physical structure and all are joined by shared nodes. The collection of these elements and nodes is called a mesh [CoventorWare, 2006]. The Coventor provides a meshing tool which is easy to use to mesh a solid model. Then the result can be used by Analyzer solvers for various FEM simulations.

Analyzer solvers allow many different types of simulations to be used to compute electrostatic, mechanical, thermal, and fluidics solutions, such as capacitance and charge, deformation, harmonic analysis, natural vibration frequencies, pull in analysis, boundary conditions, and more.

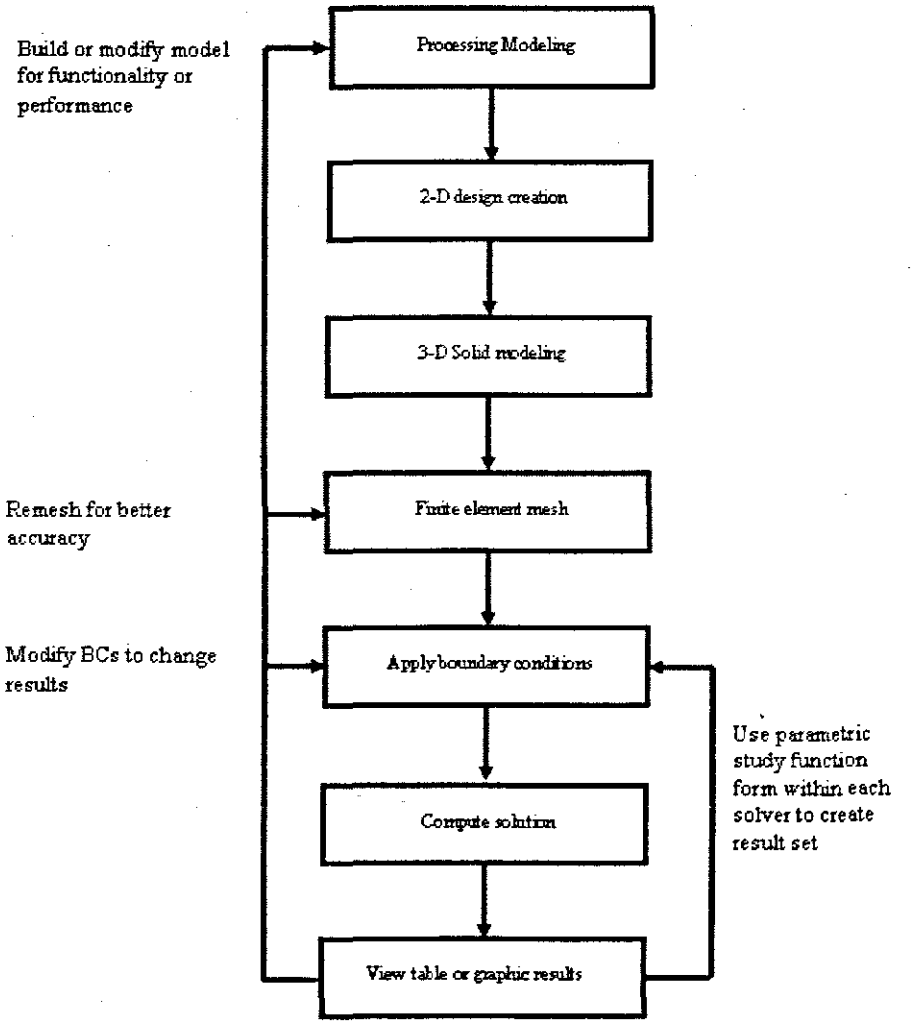

Figure 5.1: Typical Design Flow. The flow shows simulation and analysis steps of a micro-device model using Coventor

5.3 STRUCTURE AND DESIGN

A micro-cantilever beam has been designed using MEMS tools in CoventorWare 2006 to sense the magnetic field. A differential capacitive was attached to the beam to measure the deflection of the beam. Silicon was the basic material that was used as substrate to build over the micro miniature cantilever. The beam material is made of Permalloy (80% Ni and 20% Fe) as one of MEMS material which has been developed with highly magnetic properties (high magnetic permeability and electrical resistivity) for the use of this kind of application [Liu C & Yi Y W, 1999]. Some of the physical properties of the materials are shown in Table 5.1.

The beam was designed to be fixed at one end while the other end is free. This cantilever design is called a free-end cantilever-beam. A movable mass has attached to the free-end of the beam. Two electrodes layers of aluminium has attached to the bottom and top of the movable mass to compose a differential capacitance with a fixed aluminium layers under and above it. In this case, the motion of the movable mass will change the capacitance of both upper and lower capacitors, therefore increasing the sensitivity of the sensor. Figure 5.2 shows the 3D model of the cantilever designed. The longitudinal motion and the extension of the beam material due to an external magnetic field reflected in the overlapping area between the two, fixed and movable plates. The area of the movable plates is designed to be smaller than the area of the fixed plates in order to achieve an overlapping area depending on the area of the movable plate (effective area). Table 5.2 shows the dimensions of the cantilever and the capacitive sensing techniques.

The lateral deflection of the beam in response to an externally applied magnetic field perpendicular to the beam-length generated by a current-carrying conductor is used to change the capacitance and thereby to measure the current as a function of the magnetic force. To increase the dynamic range and the sensitivity of the cantilever beam, an applied field along the beam-length can be used as a permanent field to induce the magnetization in the material. The source of this permanent field can be an external embedded source, such as coil.

Table 5.1: Cantilever-beam Materials properties

Properties	Permalloy	Aluminum	mass
Young's modulus N/m^2	6.5×10^{10}	7.7×10^{10}	7.91×10^{10}
Poisson's ratio	0.3	0.3	0.25
Density kg/m^3	8.69×10^3	2.3×10^3	5.32×10^3
Fracture strength N/m^2	$\approx 600 \times 10^{10}$	—	—

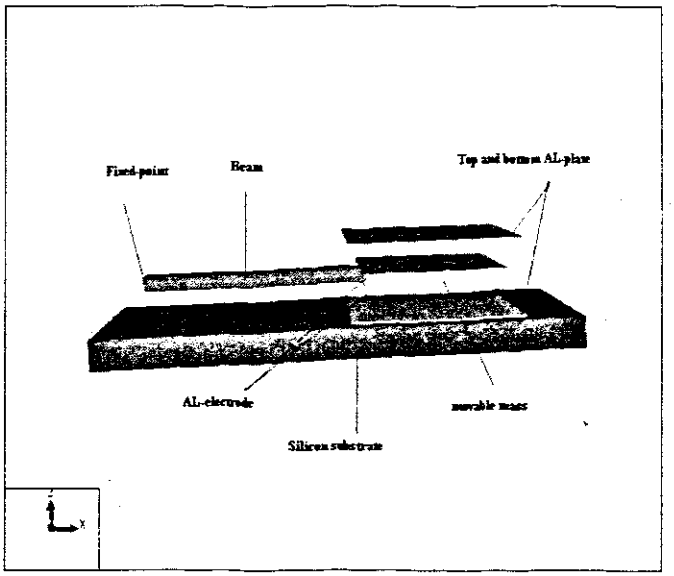

Figure 5.2: Sensor Design Model

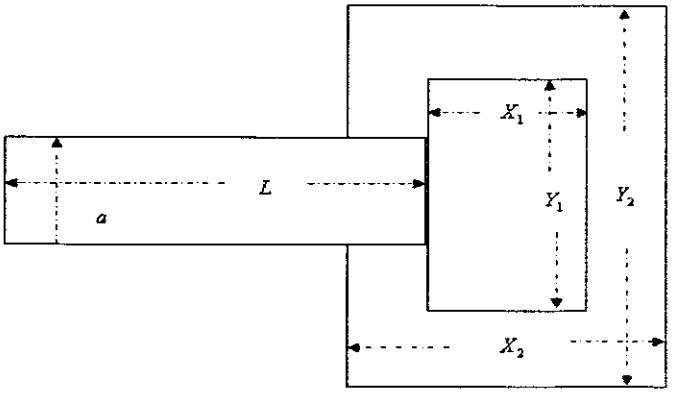

Figure 5.3: Geometrics of the sensor plane

Table 5.2: Dimensions of the sensor

Dimension	**Length (μm)**
Beam Length L	700
Beam width a	100
Beam thickness b	5
Movable mass length Y_1	600
Movable mass width X_1	400
Movable plates thickness Z_1	5
Fixed plates length Y_2	700
Fixed plates width X_2	500
Fixed plates thickness Z_2	0.5
Thickness of the Aluminium electrode film	0.1
Initial gap d_o	10

5.4 SENSOR DESIGN STEPS IN COVENTOR

In this section, sensor designed steps in Coventor are described. Figures 5.4 to 5.11 show all the main steps of sensor design from processing flow through to the 3D solid model, and integrating it with electronic sensing circuit readout.

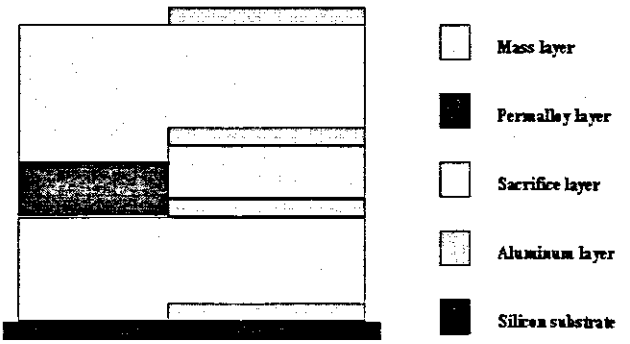

Figure 5.4: Process flow

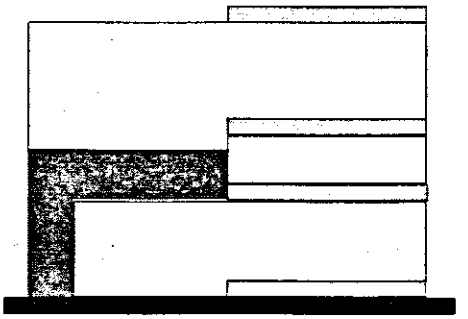

Figure 5.5: Process flow

Figures 5.4 and 5.5 show the sensor process flow that can be used to fabricate the sensor. This is a sequences of layers created in the process editor. A full description of this flow to show the thickness and type of the material and the process description, such as deposit or etch, is shown in Figure 5.6 in (Appendix A). The beam-layer is stack deposit material in Figure 5.4 and conformal shell deposit in Figure 5.5.

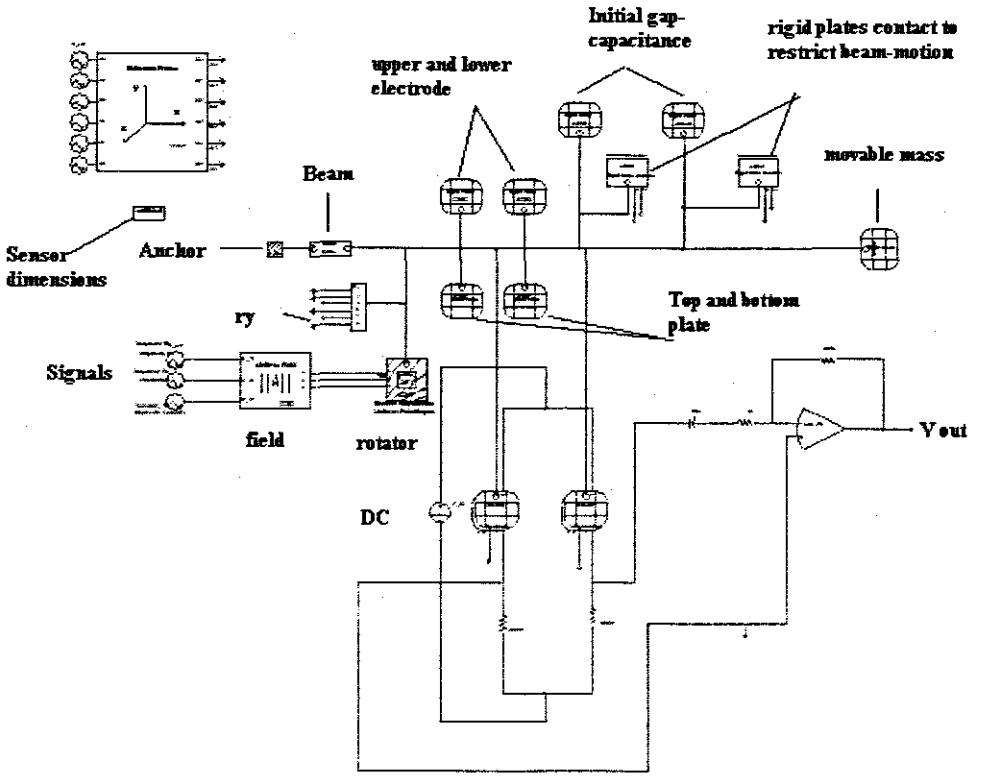

Figure 5.5: Sensor schematic in architect

Figure 5.6 shows integration of the mechanical part with the electronics part of the sensor design which has been created using the tools in Architect library. In this step, the dimensions of the sensor length, width, and some others mechanical connection point, such as kont, anchor (beam support) and physical material properties have been setup. This setup has been shown in Figures attached in appendix A. Right setups will allow access to 2D of the sensor model.

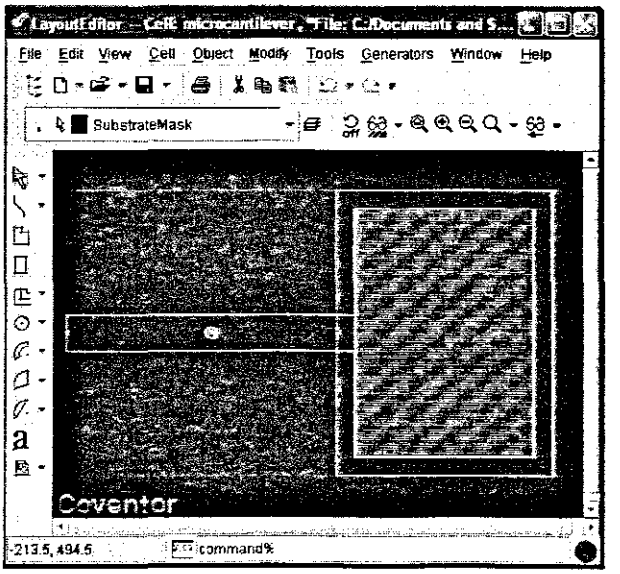

Figure 5.6: Sensor in layout editor

Figure 5.7 shows the 2D view of the sensor design in Layout Editor. The Layout verifications report has been attached in Appendix A and displays no error. Success of the 2D layout led to the building of a 3D solid model, as shown in Figures 5.8 to 5.11.

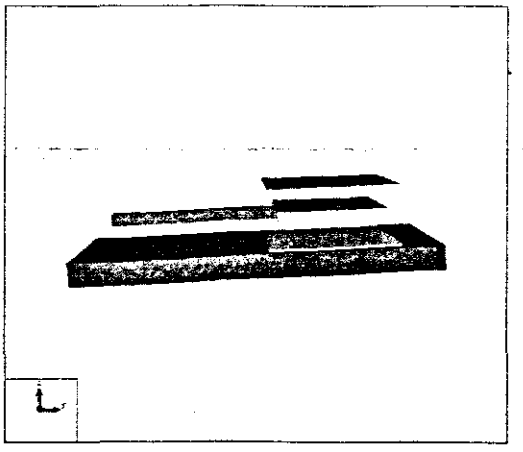

Figure 5.7: Side view of the 3D solid model of the sensor

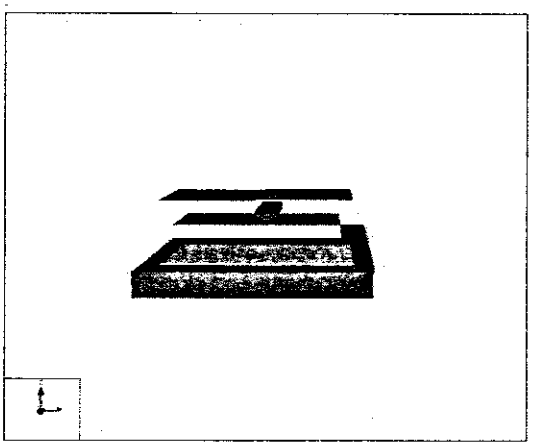

Figure 5.8: Front view of the 3D solid model of the sensor

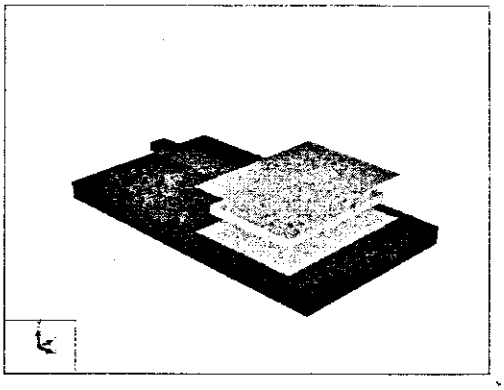

Figure 5.9: F Front view of the 3D solid model of the sensor

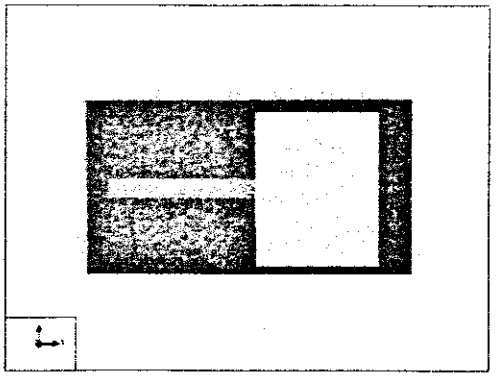

Figure 5.10: Top view of the 3D solid model of the sensor

Size approximation of the actuator packaging

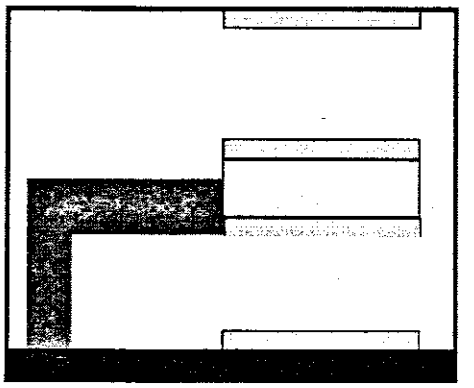

Figure 5.11: Sensor in box size 1130 µm x 605 µm x 30 µm

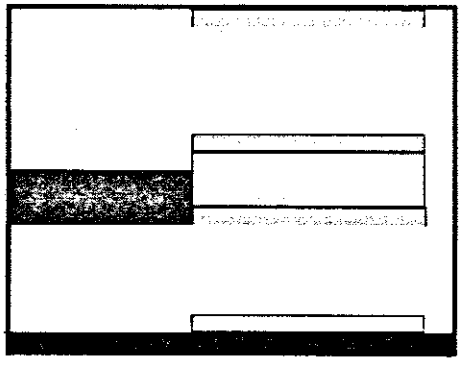

Figure 5.12: Sensor in box size 1105 µm x 605 µm x 30 µm

5.5 SUMMARY

In conclusion, a full description of the sensor design, dimensions, materials type and their properties has been presented. An introduction to the CoventorWare software and some description of the main steps of simulating the sensor design has been presented as well.

CHAPTER 6

6 SENSOR SIMULATION AND ANALYSIS

6.1 INTRODUCTION

Different types of simulations were performed to predict the sensor performance, to verify the modelling results, and to validate the assumptions made during the modelling of the sensor. Moreover, simulations provided insight into aspects of the sensor performance whose modelling was not possible or did not yield an easy-to-use result (e.g. the magnetization of such magnetic materials).

CoventorWare's Architect suite has several different parametric libraries such as electromechanical, dampers, magneto-mechanics and so on. Architect provides a system simulator module, Saber. This simulator allows the user to integrate and simulate a system model using the tools in MAST and parametric libraries. Saber Solver provides DC operating point analysis, DC transfer analysis, small signal AC analysis, Vary analysis, Transient analysis, Sensitivity and Monte Carlo analysis.

Small signal AC and Vary Analysis were performed to determine and analyze the resonant frequency of the actuator structures. Any structure has a resonance frequencies in six directions named by x, y, z, rx, ry, and rz, where r means the rotation along these axes(x, y, and z). Thèse frequencies are sensitive to any change whether in materials properties or in parameters of the structures.
Transient Analysis was performed to simulate and analyze the behaviour of the sensor. All the simulations results are attached in Appendix B and some examples will be presented through the dissection of magnetic deflection of the beam, capacitive transducer, linearity and non-linearity, and sensor calibration.

Sensitivity analysis using these simulation results to predict the sensitivity and the performance of the sensor will be discussed in this chapter.

6.2 RESONANCE FREQUENCY ANALYSIS

When a plate of magnetic material is placed in an external magnetic field, the plate will be subjected to bending due to the magnetic force acting on the plate [Zheng X & Wang X, 2003, Zheng *et al*,

1999]. The cantilever-beam is designed to deflect vertically if an external magnetic field is applied along the beam vertically. To simplify the dynamic motion, the cantilever-beam must move in a single-degree of freedom in the direction along the vertical axis of the beam. If the beam is caused to vibrate due to the magnetic force, capacitance changes occur between the movable plate and the fixed plate. In this case, it is important to ensure that the basic vibration mode of the structure causes the capacitance change, and not higher modes that could affect the reading due to smaller variations in the capacitance value [Wang L, 2005]. Therefore, small signal analysis simulation was performed to analyze the vibration modes of the cantilever-beam in six directions (x, y, z, rx, ry, and rz) as shown in Figure 6.1.

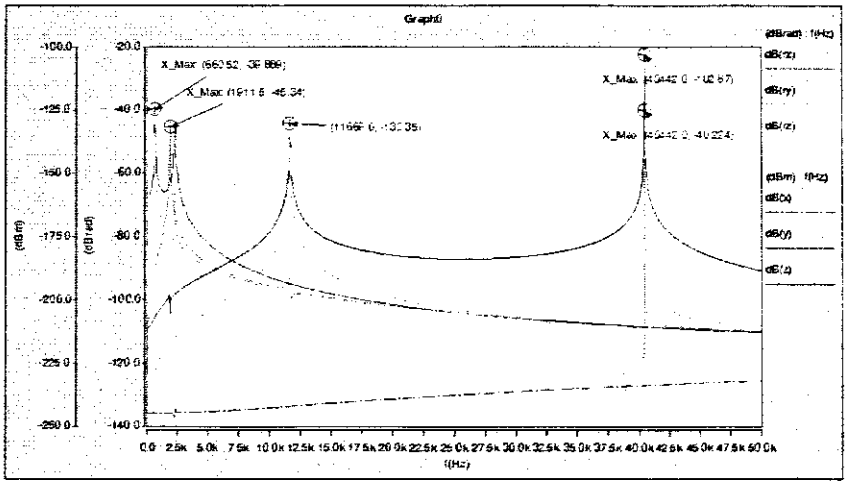

Figure 6.1: Resonance frequencies analysis in six directions x, y, z, rx, ry, and rz. The values of these frequencies are varying from 660-40442 Hz

Considering the beam bending moment is along the width (y-axis), leading to a displacement along the vertical (z-axis) of the beam length, the vibration modes in the directions of ry and z are interesting because they can make change in the capacitance by changing the average distance between the plates [Wang L, 2005]. The resonance frequencies of those two directions are shown in Figure 6.2. Both of them show two different modes of lower and higher values (660 and 2275Hz) in the range of the simulation performed, as shown in Figures 6.3 and 6.4.

Lateral vibration can normally show more than one modes. The resonance frequencies of rx which is the rotation of the beam structure along the beam-length does not change the average distance between the plates, and the effective area remains constant due to the area of the movable plate (effective area)

being smaller than the fixed plate. The vibration mode of the beam structure along x, the longitudinal vibration, does not change the average distance and the effective area of the capacitance.

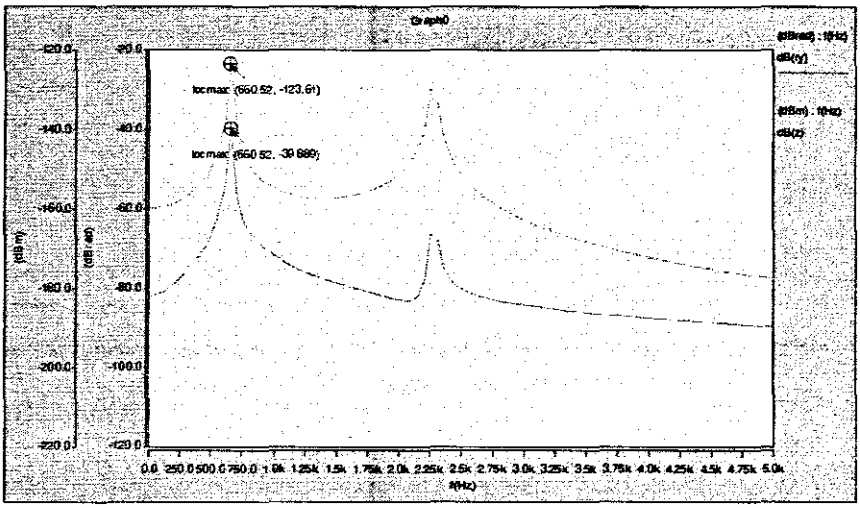

Figure 6.2: Resonance frequencies in z and ry directions. Two modes have shown in this simulation for lateral vibration of the structure

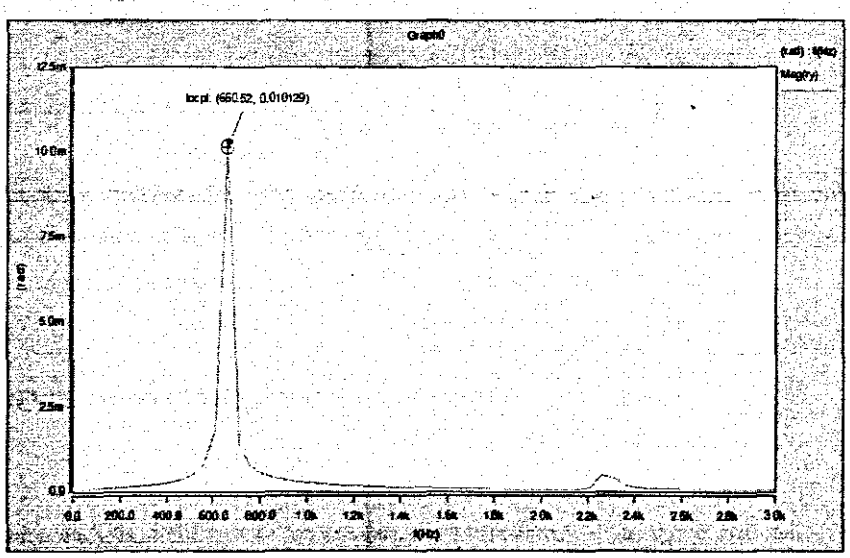

Figure 6.3: The fundamental frequency mode is the lower resonance frequency of the sensor structures in ry direction

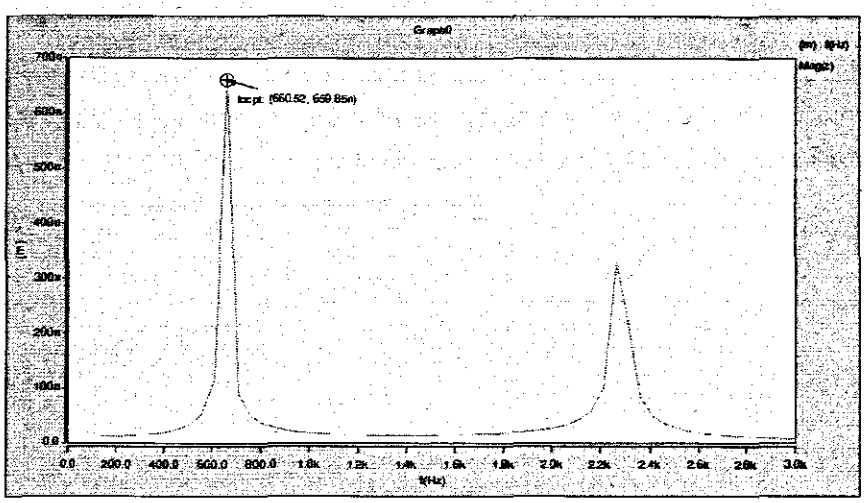

Figure 6.4: The fundamental frequency mode is the lowest resonance frequency of the sensor structures in z direction

The beam vibration mode along the y and rz does not change the average distance and the effective area. If we refer to equation 4.26 of small angle tilted-capacitor, the capacitance will remain constant and hence the mode x, y, rx, and rz has no affect on the capacitance. In this case one has to consider a small angle tilted-capacitor design or eliminate the high frequency from measurements. Therefore, effects of modes x, y, rx, and rz can be ignored because the frequencies that are generated are much higher when compared to the first mode of ry and z.

As a result of this analysis, the lower resonance frequency (660Hz) is suitable for the sensor requirement because there is a vibration mode along z and ry direction, normally called the fundamental frequency or the natural frequency.

6.3 DEFLECTION OF THE CANTILEVER-BEAM

The transient analysis simulation of the sensor aids in estimation of the spring constant and the amount of deflection and displacement of the cantilever-beam. The magnetic cantilever-beam is designed to case lateral deflection when a magnetic field is applied along the normal of the beam, considering that the magnetization of the material-beam takes a direction along the beam length.

The magnetization of the beam material depends on the external applied magnetic field along the length (horizontal) of the beam [Ruan *et al*, 2001]. Higher magnetic field along the beam-length will induce high magnetization on the magnetic material of cantilever-beam. A permanent sinusoid magnetic field signal (Hx = 1kA/m) along the beam-length, therefore, has been applied in this simulation analysis to achieve higher magnetization, see Figure 6.5.

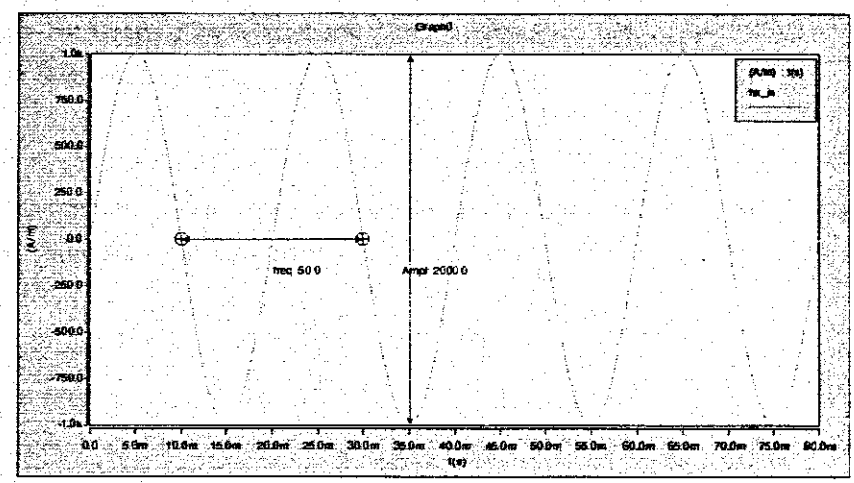

Figure 6.5: Signal of permanent input field in x-axis direction (along the beam-length) with a fixed amplitude of 1k A/m and frequency of 50Hz

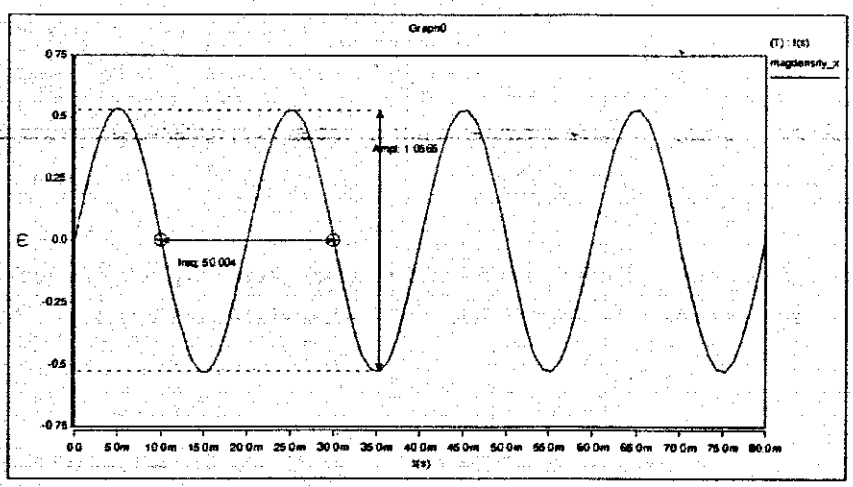

Figure 6.6: Magnetization density of the beam material of zero applied fields. This is the initial value of the magnetization before reaching the saturation value while the input field is increasing

Figure 6.6 shows the magnetization density induced by the permanent field when no field is applied along the vertical of the beam. Very small fluctuations of the beam motion due to very small magnetic force are discovered in the simulation in the diagram of Figure 6.7.

The small fluctuation is because of the lateral free vibration which will make very small drift in the beam length axis from the permanent applied field and then yield to divide permanent field into two components- one along the beam length and the other normal to it. But the one along the beam length is very high compared to the other.

Therefore, the deflection, in this case, is considered to be zero, neglecting the small fluctuation of the beam motion due to the effective mass and other factors that do not make sense on the capacitive sensing system. This will be evident in the upcoming in the section regarding the capacitive transducer.

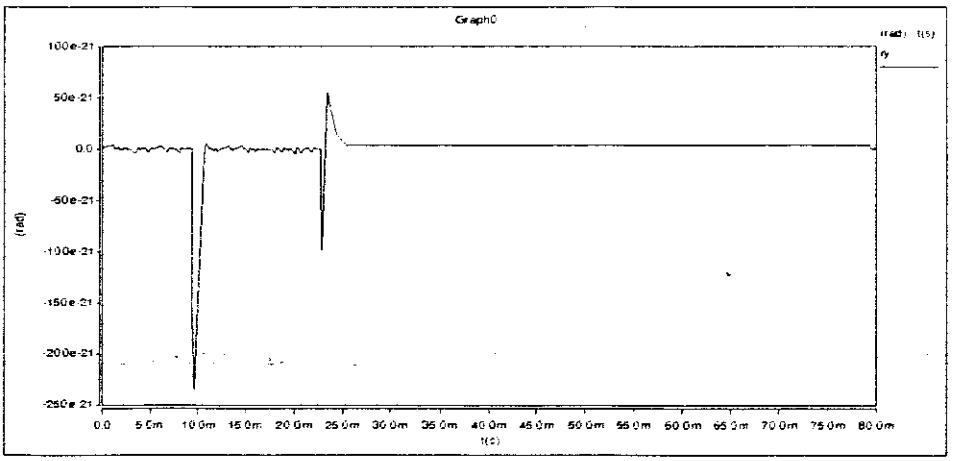

Figure 6.7: Beam deflection of zero applied field. The deflection is zero by neglecting the small fluctuations of the beam due to the DC voltage and the weight of the effective mass

When an external magnetic field is applied along the normal of the beam length (z-axis), a deflection of order of micro-rad to mil-rad range has been measured. Simulation analysis of various amplitude values of applied fields with frequency of 50 Hz vertically along the beam to predict the sensor behaviour including deflection. The simulation has been done by applying various fields in a range of 50m A/meter to 5k A/meter.

When a magnetic field of 50m A/meter and 5k A/meter has been applied vertically along the beam length, as in Figures 6.8 and 6.9, a deflection of 0.085 μ rad and 9427.4 μ rad respectively has been measured, as shown in Figure 6.12 and 6.13. The magnetization (M) in this case, as shown in Figures 6.10 and 6.11 is increased from the initial value that measured when no field was applied. This is because of the deflection which changes the net of the horizontal field component. The increases in magnetization reach a point at which it is no longer able to continue. This point is called the saturation point and it is easy to determine, as shown in Figure 6.14.

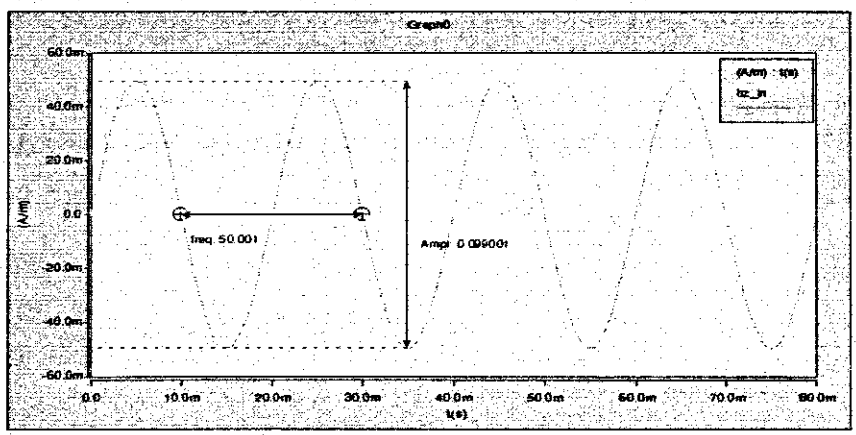

Figure 6.8: Applied magnetic field along the normal of the beam-length of amplitude of 50m A/meter and frequency of 50Hz

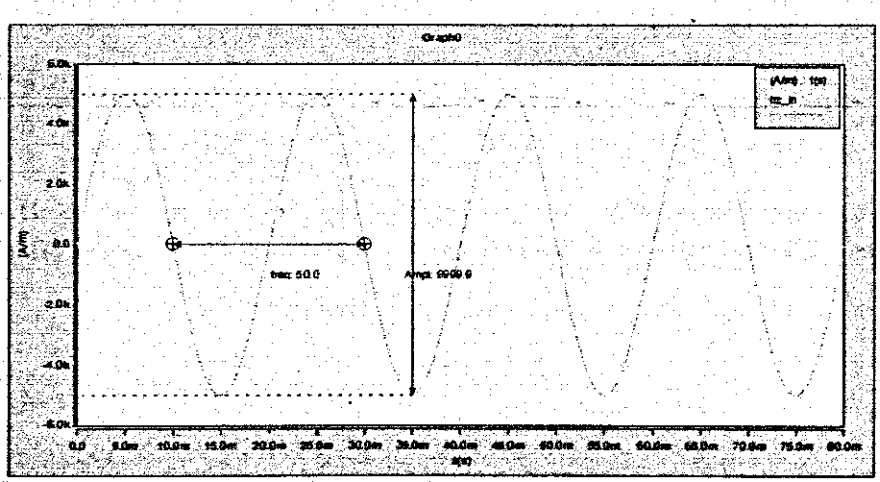

Figure 6.9: Applied magnetic field along the normal of the beam-length of amplitude of 5k A/meter and frequency of 50Hz

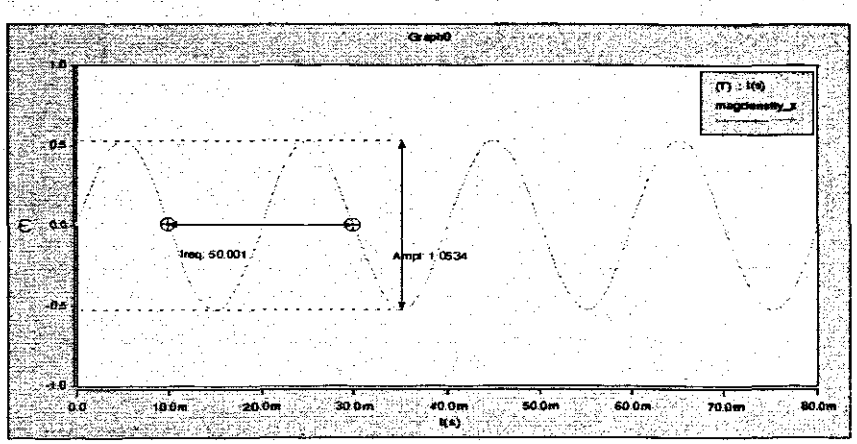

Figure 6.10: Magnetization density of the beam material of input field 50m A/meter along the beam-length (x-axis). The amplitude of the signal is increased with small value of the initial amplitude of zero input fields

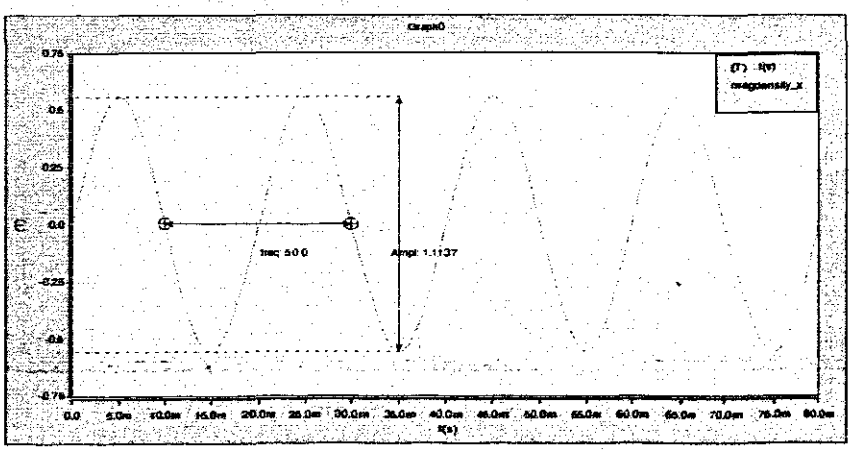

Figure 6.11: Magnetization density of the beam material of input field 5k A/meter along the beam-length (x-axis). The amplitude of the signal is increased with small value of the initial amplitude of zero input fields

(L+X1) from the beam fixed point (Anchor) can be calculated using the formula in equation 4.18. Figure 6.15 shows a plot diagram of the maximum displacement against the applied magnetic field.

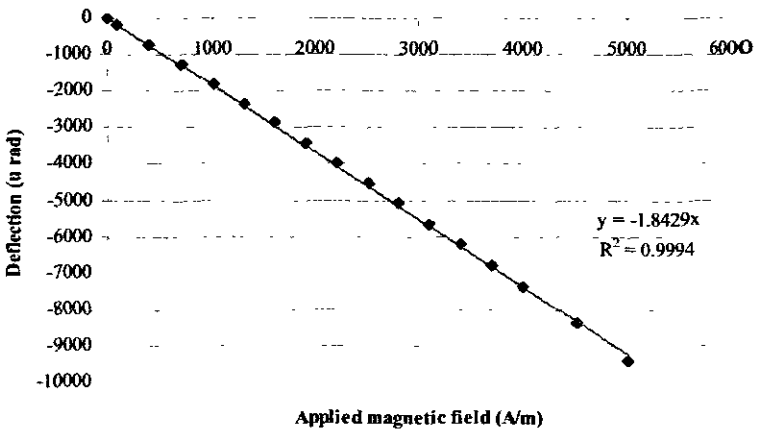

Figure 6.14: Linearization analysis of the beam deflection due to the applied magnetic field. The beam shows linear relationship with highly regression coefficient

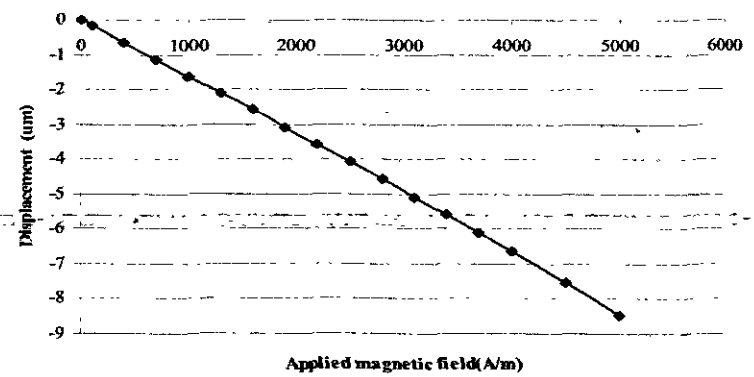

Figure 6.15: Maximum displacement at distance of (L+X1) from the fixed point of the beam against the applied magnetic field

Table 6.1: Measurements of deflection, magnetization, capacitance change, and voltage output when different values of magnetic field have been applied along the vertical of the beam-length

Hz A/m	Bz μTesla	Magdenx Tesla	Def μ rad	Delta C fF	VB nV	Vout
0	0	1.0665	-0	0	0	0
0.05	0.06283	1.0534	-0.08505	0.000996	0.000202	0.178745
1	1.2566	1.0557	-1.7689	0.020542	0.004072	3.92445
100	125.66	1.0641	-179.02	2.1002	0.40421	380.375
400	502.64	1.0644	-716.04	8.40825	1.62845	1526.1
700	879.62	1.065	-1252.6	14.754	2.84175	2677.05
1000	1256.6	1.0566	-1792.5	21.2225	4.1003	3839.15
1300	1633.58	1.0673	-2335.1	27.8335	5.365	5043
1600	2010.56	1.0689	-2871.9	34.6415	6.6645	6262
1900	2387.54	1.0709	-3422.6	41.7595	8.0025	7503
2200	2764.52	1.0733	-3972.3	49.1385	9.3965	8840.5
2500	3141.5	1.076	-4520.8	56.929	10.894	10227
2800	3518.48	1.0791	-5085.1	65.3425	12.4405	11671.5
3100	3895.46	1.0825	-5651.7	74.351	14.143	13280.5
3400	4272.44	1.0863	-6217.5	83.929	16.051	14973.5
3700	4649.42	1.0905	-6798.5	94.5785	18.085	16955.5
4000	5026.4	1.0952	-7377.5	106.5315	20.6315	19199.5
4500	5654.7	1.1038	-8378.4	130.244	25.555	24077.5
5000	6283	1.1137	-9427.4	161.118	32.931	31304.5

6.4 EFFECTIVE BEAM-DIMENSIONS

In this section, the effect of the beam cantilever dimension has been studied to achieve an optimal geometrical which led to a sensitive beam. This has been done by studying the deflection against different size of the beam dimensions- length, width, and thickness. The results have been shown in Figures 6.16, 6.17 and 6.18.

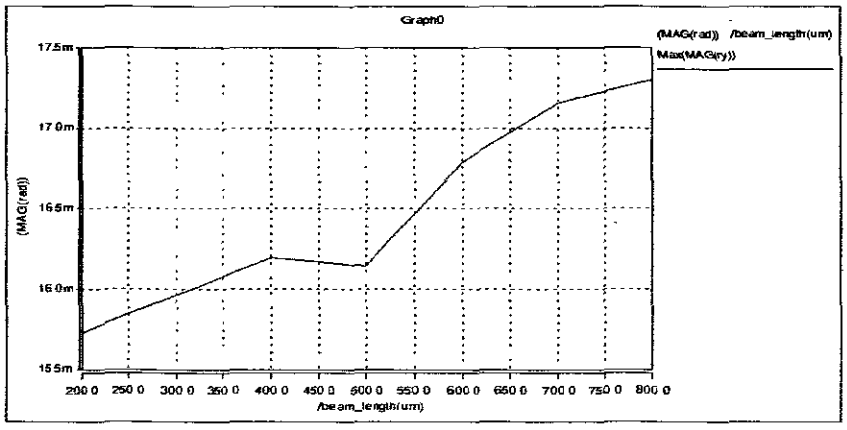

Figure 6.16: Deflection of the cantilever-beam for discreet values of the beam-length

Figure 6.16 shows linear increment with different slope in deflection, while the beam length increases in different ranges, 200-400, 500-600,600-700, and 700-800 μm. The slope of range 700-800 μm is very small compared to the others. In range of 400-500 μm, the deflection has decreased in a very small range- in other words, the difference in the deflection at length 400 μm and at length 500 μm is very small compared to the others. As result, the 700 μm beam length that used in the sensor simulation can still achieve a good sensitivity.

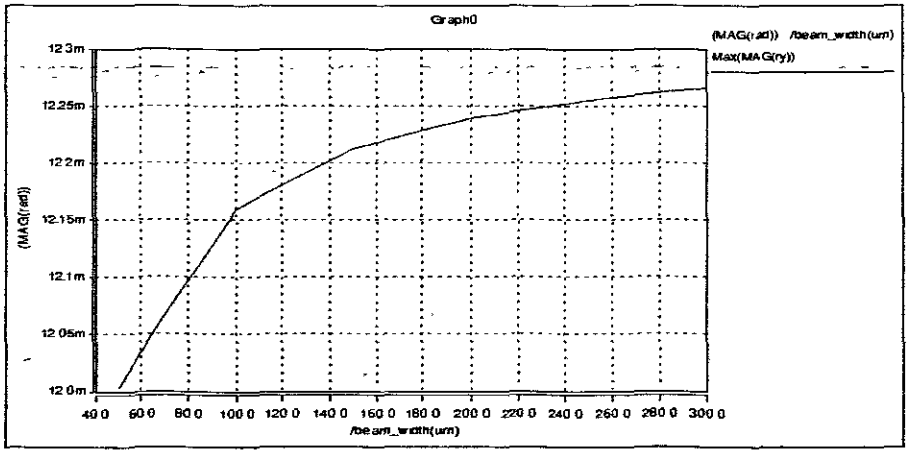

Figure 6-17: Deflection of the cantilever-beam for discreet values of the beam-width

Figure 6.17 is showed the deflection against different values of the width in range of 50-300 μm. A linear relation for a range of 50-100 μm and 100-150 μm of the width with different slopes has been

observed as in the diagram. From 150 μm up to 300 μm , the deflection is increasing but not linear. Also the change is very small compared to linear part. As a result, the beam-width that was used in the sensor simulation, which was 100 μm, can still achieve a good sensitivity.

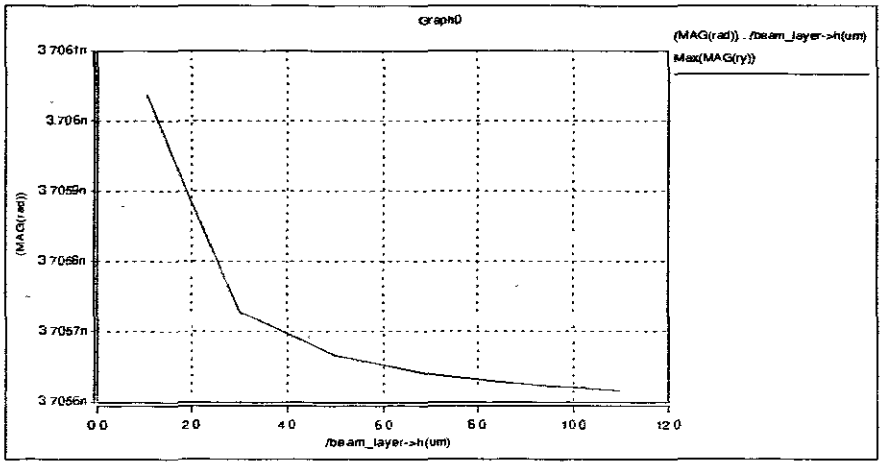

Figure 6.18: Deflection of the cantilever-beam for discreet values of the beam-thickness

Figure 6.18 shows the deflection against different values of the thickness in range of 1-11 μm. The result of increasing the beam-thickness is decreasing the beam deflection. From 1 μm up to 5 μm of the beam-thickness, the deflection is decreasing more rapidly than the decreasing in the range from 5-11 μm. As a result, the beam-width that was used in the sensor simulation, which was 5 μm, can still achieve a good sensitivity.

6.5 CAPACITIVE TRANSDUCER

One way to readout the position of a moving part of a MEMS device is by optical methods, including: Doppler vibrometers, which usually are employed at relativity high speed; and Interferometeric techniques, which are usually used for low frequency [Cowburn *et al*, 1997, Lenz J E, 1990, Bahreyni B, 2006]. The sensitivity of these methods can be in the sub-nm range, although they are limited. Capacitive readout is one of the most widely used in MEMS applications due to its simplicity and ease of implementation [Li X & Meijer G C M, 2002, Toth *et al*, 1996]. It is particularly well-suited for Micro machined MEMS, where capacitances between moving structures are measured. Capacitive sensing is used in commercially available accelerometers, gyroscope, and other various applications of Microsystems. The advantages of these devices are the simplicity and the low cost of fabrication process [Li X & Meijer G C M, 2002, van der Goes F M L & Meijer G C M, 1996, Toth *et al*, 1996].

Therefore, a differential capacitive is designed to measure the beam deflection due to an external applied magnetic field. As outlined in the previous sections the beam does not move from its initial position when no field (Hz=0) applied along the vertical of the beam-length but a very small deflection is measured due to the mass of the structure and others factors. The small deflection does not make sense in the initial capacitance, as we can see in Figure 6.15. The initial values of both capacitors are equals and the measured values is (212.5f Farad), which is extremely close to the model calculation value (212.4f Farad).

When the AC external applied magnetic field is increased to different values with constant frequency for example, two different amplitudes of applied fields(50m A/meter and 5k A/meter) has shown change in the differential capacitance due to the deflection of the cantilever-beam. The change occur in each capacitor has the same frequency response of the beam vibration which is double of the frequency of the applied field.

The lower capacitor shows an increase while the upper is decreasing in the measured capacitance value. The change is proportional to the magnitude of the applied magnetic field. This can led to the fact that the difference in capacitance also should be increased with increasing the applied magnetic field.

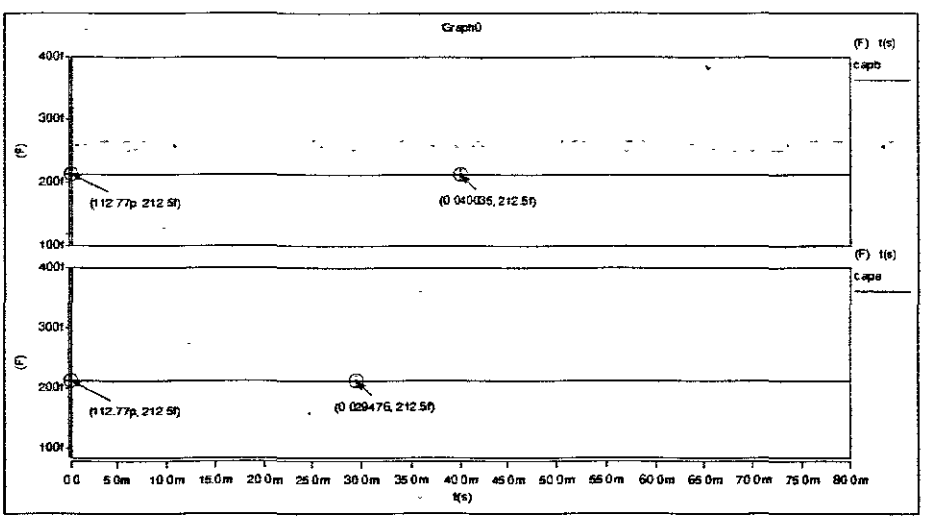

Figure 6.19: Capacitance measurement when no external field has been applied. The capacitance has shown the initials values

Figure 6.19 is showed the measurements of the capacitance when no external field was applied along the normal of the beam-length. The top graph in figure 6.19 is the capacitance measured value of the upper capacitor and the bottom graph is the measured value of the lower capacitor. Both capacitors they showed equally measured values at response time of 112.77 p sec.

Figures 6.20, 6.21, 6.22, and 6.23 are showed the measurements of the differential capacitance of the applied field of 50m A/meter and 5k A/meter with 50 Hz. The measured signal has shown a frequency value of double the applied field in all cases.

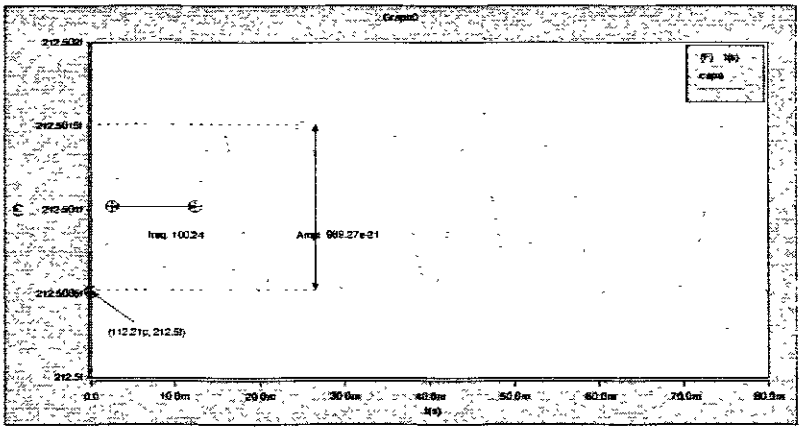

Figure 6.20: Lower capacitor signal of input field of 50m A/meter. The amplitude of the signal is increasing, beginning with the initial value until it reaches a maximum value as a function of the input field

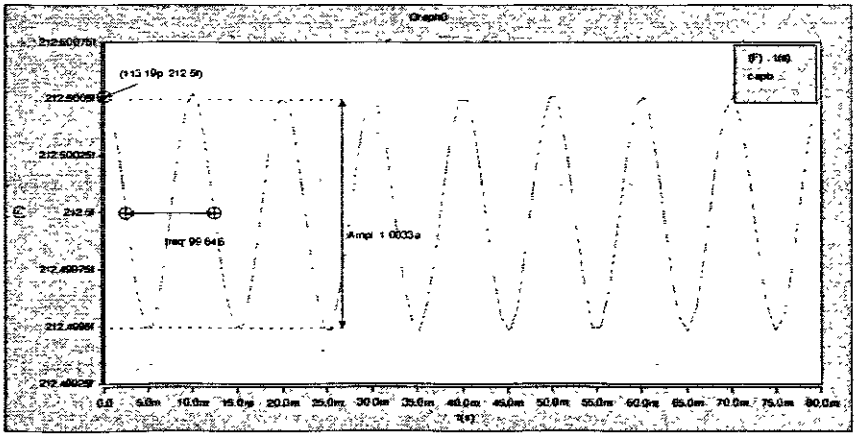

Figure 6.21: Upper capacitor signal of input field of 50m A/meter. The amplitude of the signal is decreasing, beginning with the initial value until it reaches a minimum value as a function of the input field

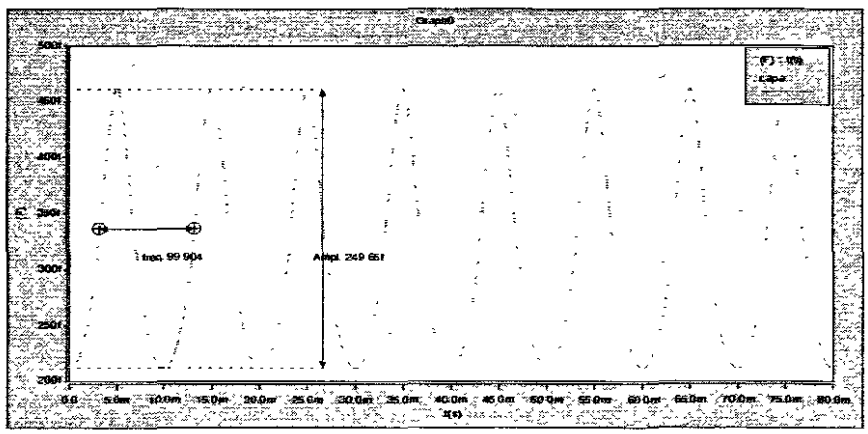

Figure 6.22: Lower capacitor signal of input field of 5k A/meter. The amplitude of the signal is increasing , beginning with the initial value until it reaches a maximum value as a function of the input field

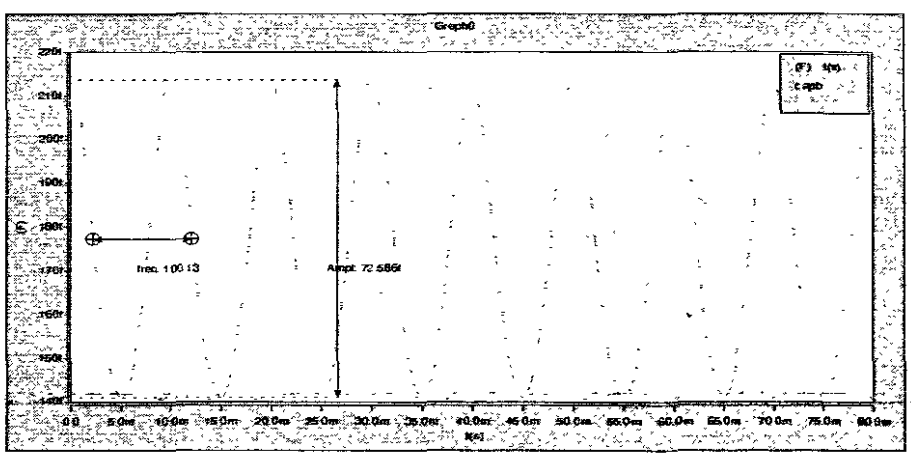

Figure 6.23: Upper capacitor signal of input field of 5k A/meter. The amplitude of the signal is decreasing, beginning with the initial value until it reaches a minimum value as a function of the input field

6.6 LINEARITY AND NON-LINEARITY OF CAPACITANCE CHANGE

The change in capacitance measurements that were obtained for different values of the applied magnetic field as shown in Table 5.1, has been used to study linearity and non-linearity of the capacitance change. The plotting diagram of these measurements against the applied magnetic field and the beam

deflection has shown non-linear relation as in Figures 6.24 and 6.25 respectively. A highly linear relation can be achieved if we considered a smaller deflection compared to the initial capacitance gap-in other words, to satisfy the approximation condition that lead to modelled equation 4.34. This is clearly evident in the diagram in Figure 6.26. An equation of a good linear relation can be extracted if we considered a deflection of up to where the curve drifts from the linear line. As a result of this analysis, the dynamic instability of the capacitive system will be influenced by the nonlinear effect when large deflection is considered.

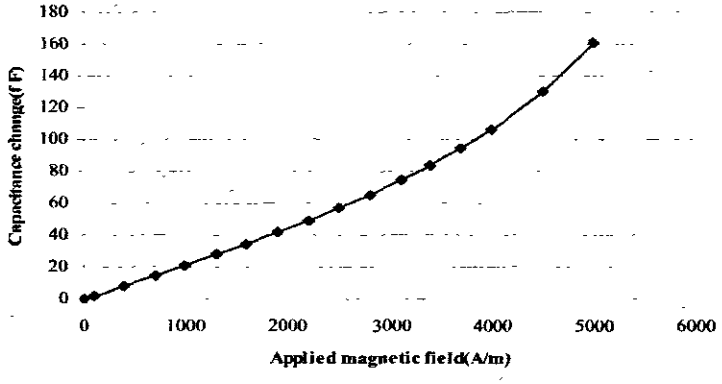

Figure 6.24: Non-linearity of the capacitance change when large deflection compared to the initial capacitance gap has been considered

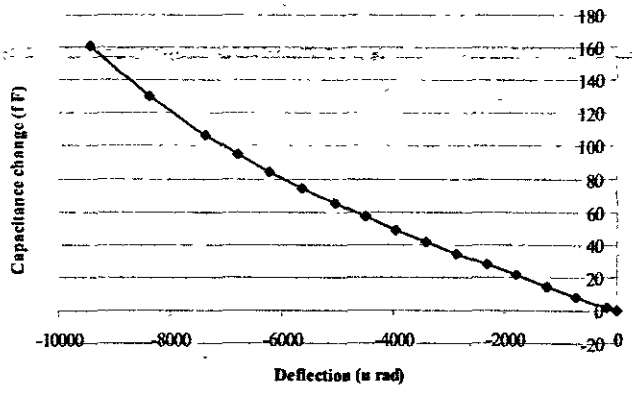

Figure 6.25: Capacitance change against deflection. The linearity is obvious for lower deflection and nonlinearity for higher deflection

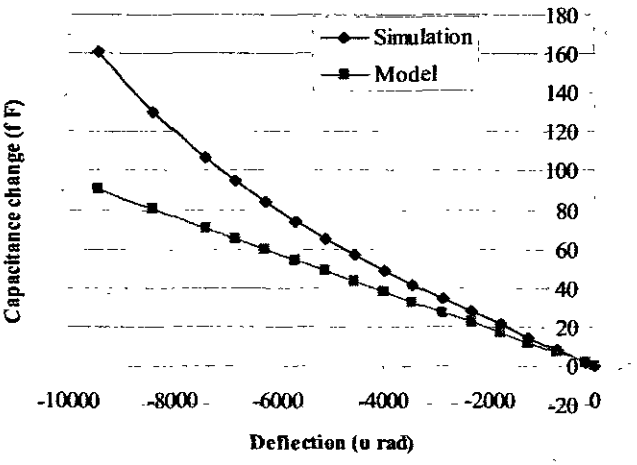

Figure 6.26: The diagram shows capacitance change against deflection. The curve plotted using the simulation results and the linear line is a plot of the modelled equation 4.22

6.7 DIFFERENTIAL CAPACITIVE SENSITIVITY

Since the different capacitive has shown a linear relationship for low field, as seen in the diagram in Figure 6.27 below, the sensitivity of the capacitive can be easily calculated by the determining the linear equation.

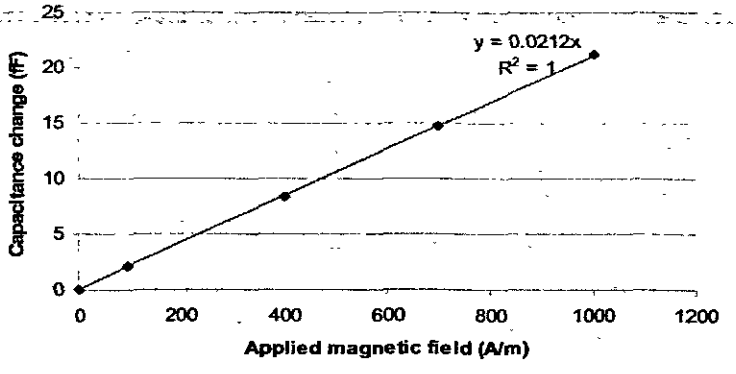

Figure 6.27: The linear relationship of the capacitance change and low applied field

The linear equation of the relationship between the capacitance changes and the applied field is extracted from the diagram in figure 6.27 with a highly good regression factor of 1.0, and can be written as

$$\Delta C = 0.0212H \tag{6.1}$$

Then the sensitivity of the capacitive sensing is given by

$$Sens = \frac{\Delta C}{H} = 0.0212 \times 10^{-15} \frac{Farad}{A/meter} \tag{6.2}$$

6.8 CIRCUIT DESIGN FOR READOUT

Capacitive Sensing Circuit is one of the most common and inexpensive measurement methods used in MEMS sensors [Kaienburg *et al*, 1998, Emmerich H & Schofthaler M, 2000, Kadar *et al*, 1994]. The design of these circuits is a highly challenging task due to the nature of MEMS sensors, which can present the analogue designer with several problems [Li X & Meijer G C M, 2002]. These include very low values of capacitors that need to be sensed and the large mismatch between them. A possible solution to these problems is by using a sensing circuit based on a fully differential cascade operational amplifier and using a correlated double sampling (CDS) analogue system as well as a very high over-sampling rate to reduce the various measurements offset and noises.

In the simulation, a bridge circuit was designed as a readout electronics system to convert the mechanical sensing system to an electrical signal voltage read out in order to measure the magnetic field using MEMS magnetic cantilever-beam [Kester W, 2007]. The circuit schematic is showed in Figure 6-28 consists of two resistors and the differential capacitors together they composed the bridge. A DC voltage source has been connected between the two mid points of the resistors and the capacitors (A, C). Point D is connected to the neutral. The voltage over the C point is depends on the values of the two capacitors, providing the resistors values are fixed. The voltage at B point is depended on the capacitance value. Therefore, any change in capacitance will led to change in voltage measured at point B. This change can be expected to be very small due to the small change in the capacitance. An amplifier has been attached to the bridge to amplifier the voltage output of the sensor.

The system has measured a very small value of DC voltage at point B when no field has applied along the vertical of the beam-length. See Figure 6.29. But, when a magnetic field has been applied along the vertical of the beam-length, an AC voltage with a double frequency of the applied field frequency has been measured at point B. This voltage is in order of nano-voltage and is proportional to the applied field, as shown in Figures 6.30, 6.31, 6.32, and 6.33.

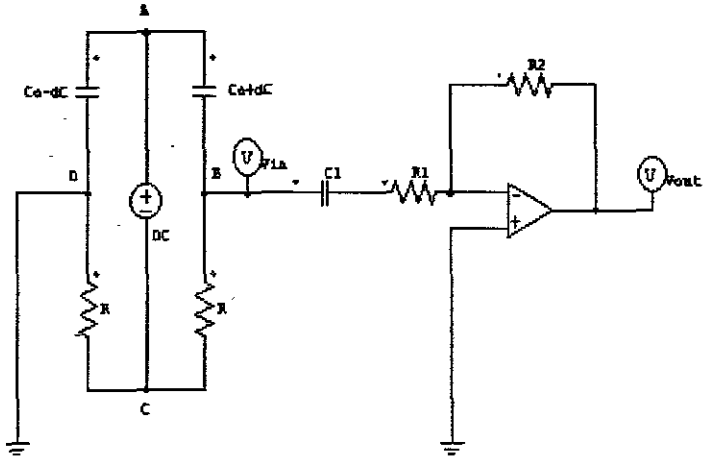

Figure 6.28: Schematic of Sensor Readout Circuit Design. Change in voltage over point B is a sign of changing in differential capacitance

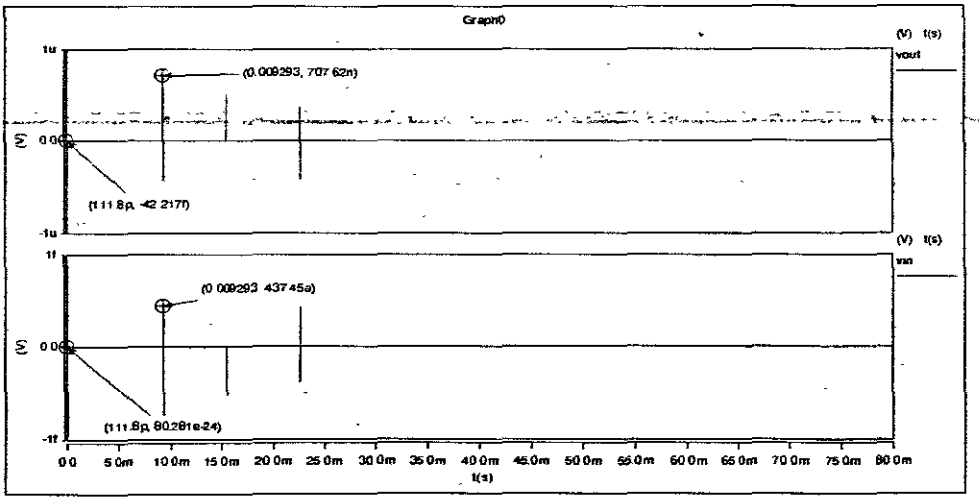

Figure 6.29: Effects of the DC voltage on the beam in other words effect of electrostatic force. A very small deflection that does not make sense in the capacitive sensing system can be occurred in a limited range of DC voltage

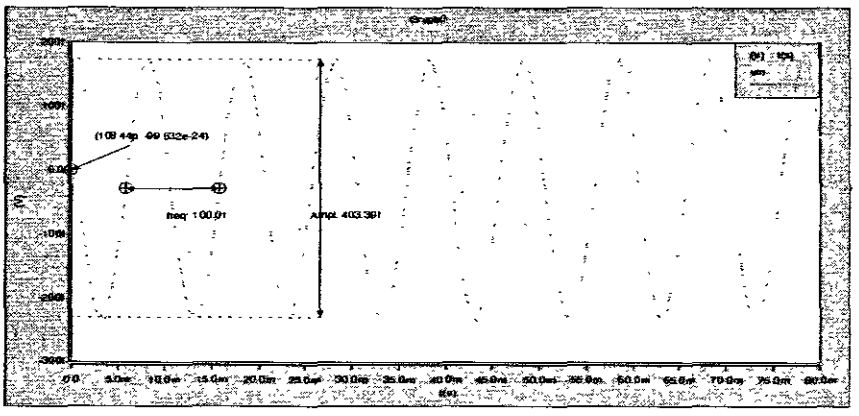

Figure 6.30: Sensor output voltages at point B of input field of 50m A/meter. The signal frequency is double of the input field signal frequency. The amplitude of the signal is proportional to the input field

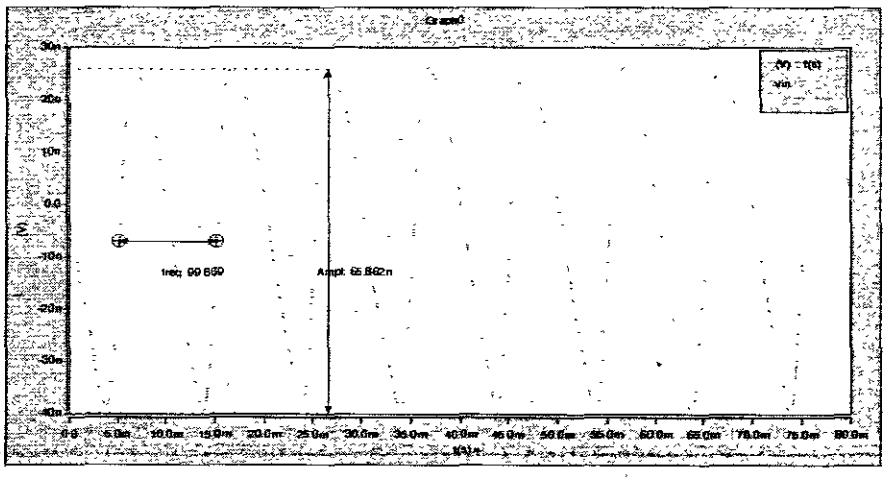

Figure 6.31: Sensor output voltages at point B of input field of 5k A/meter. The signal frequency is double of the input field signal frequency. The amplitude of the signal is proportional to the input field

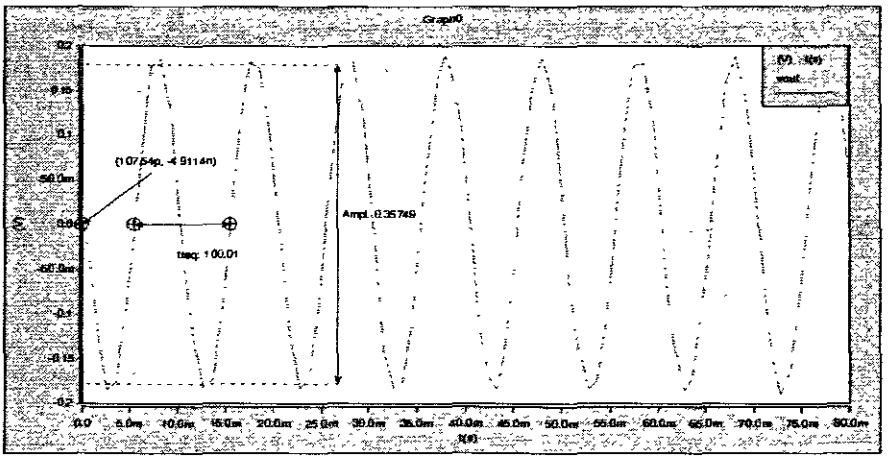

Figure 6.32: Sensor output voltage of input field of 50m A/meter. The signal frequency is double of the input field signal frequency. The amplitude of the signal is proportional to the input field

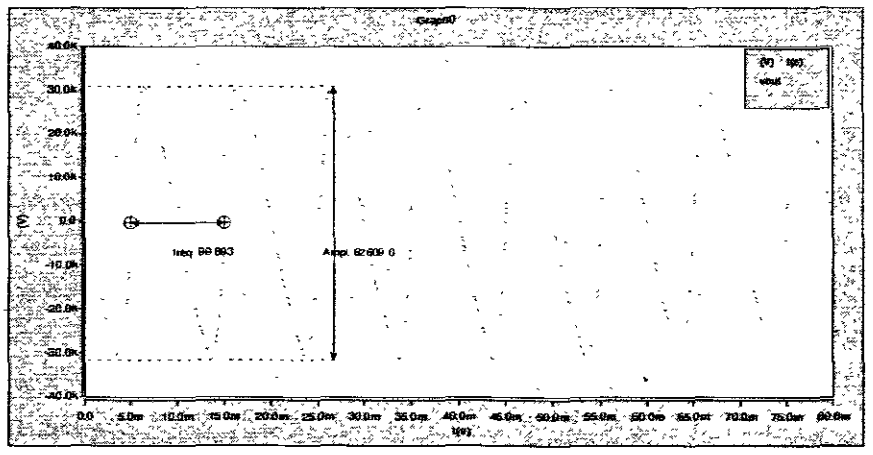

Figure 6.33: Sensor output voltage of input field of 5k A/meter. The signal frequency is double of the input field signal frequency. The amplitude of the signal is proportional to the input field

6.9 ELECTROSTATIC ANALYSIS

As the electrostatic force depends on the applied voltage, the deflection occurs from this force need to be analyzed. However, the electrostatic deflection is not the aim but it is the initial deflection that occurred before the magnetic field deflection cased. It is important, therefore, to study the effect of the electrostatic force on the capacitive sensing in order to avoid pull in voltage and other phenomena [Qiao *et al*, 2007, Lee K B, 2007]. In the simulation circuit, a DC of 0.6 V has been applied as shown in the circuit design. This value of the DC has not shown any change in the capacitance-in other words, the initial capacitance has remained as it is when no field has been applied, as outlined in the

previous sections. Optimization of the applied voltage has been studied by applying DC voltage in a range of (-1 to 1 volt), as shown in Figure 6.34.

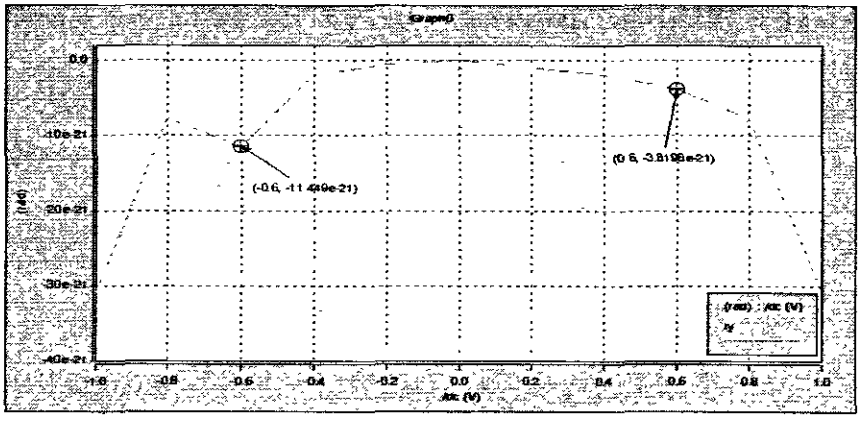

Figure 6.34: Effect of Electrostatic force when DC voltage applied and no field applied along the normal of the beam-length. Very small deflection occurred in a limited CD voltage and it does not change capacitance

As we can see, the zero deflection is at zero voltage. The deflection is increased by increasing the voltage. The deflection curve is increased very slowly in a range of (-0.8 and 0.8) and faster after reaching these two points. The deflection value caused by applying a DC of 0.6 volt is very small (-3.81E-21) compared to the deflection cased by the applied magnetic field. Therefore, any value of DC voltage in range of (-0.8 and 0.8) is preferred because it does not make sense in the capacitive system and then the initial capacitance of the capacitors are equal. The DC operating point analysis has confirmed this result, see Figure 6.35.

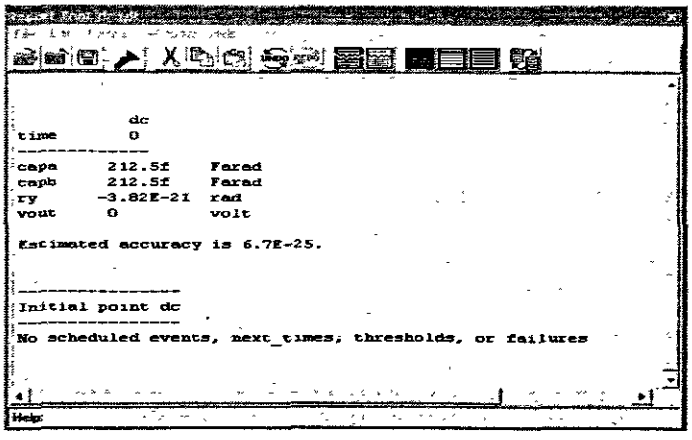

Figure 6.35: DC operating analysis point report. The analysis has been done for DC value of 0.6 volt. Very small deflection has occurred. However, the initial values of both capacitors are equal and they show zero voltage output

6.10 LINEARITY AND NON-LINEARITY OF THE SENSOR OUTPUT VOLTAGE

The measurements of the output voltage that was obtained for different values of applied magnetic field, as shown in Table 5.1 has been used to study linearity and non-linearity of the sensor output. Plotting of these measurements against the applied magnetic field and deflection has shown non-linear relation, as in Figures 6.36. The curve begins from the zero voltage and increases linearly up to some point and then change its behaviour to non-linear

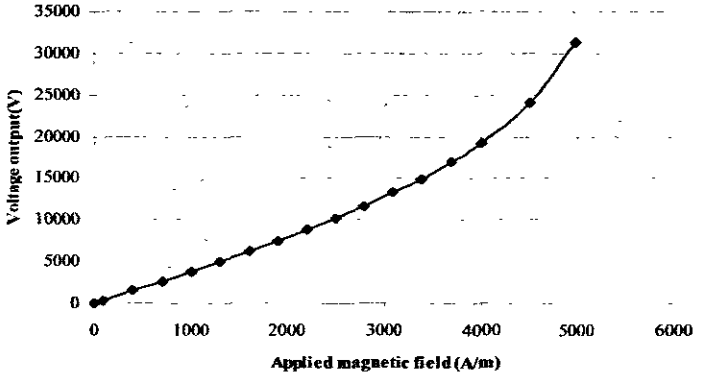

Figure 6.36: Sensor output voltage against applied magnetic field. The sensor has showed nonlinear relation when a magnetic field in range of (0 to 5k) has applied

Although, highly linear relation can be achieved if the applied field to certain range is limited, as shown in Figure 6.37. The linear equation of the sensor output of a certain range has a very good regression factor of 1.

$$V = 3.8323H \tag{6.3}$$

where V is the sensor AC voltage output and H is the applied magnetic field.

As a result of this analysis one can design a current sensor of a linear output for a certain application- in other words the range of the field produced by the current need to be specified otherwise the sensor will be influenced by a nonlinear effect for higher applied field.

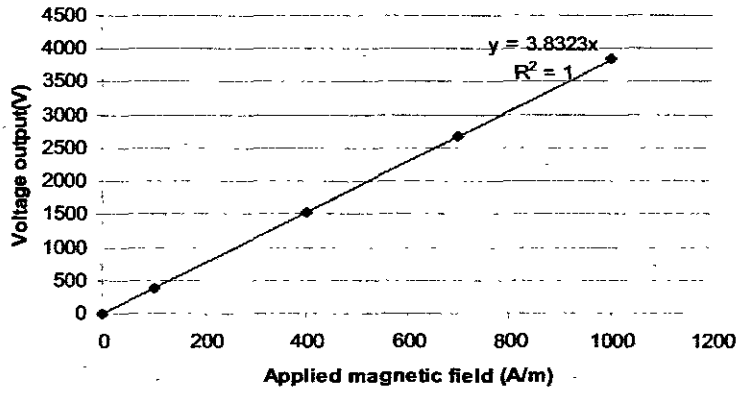

Figure 6.37: Sensor output voltage against applied magnetic field. The sensor has showed linear relation when a magnetic field in range of 0 to 2.5k has been applied

6.11 CURRENT MEASUREMENT

The externally applied current-carrying conductor is the source of the magnetic field to which the beam will respond. The magnetic force is along the vertical axis of the current- carrying conductor according to Ampere's Law [Marshall & Skitek, 1990].

6.11.1 Single wire

Figure 6-38 is showed the sensor mounted on wire carrying AC current at a certain distance (r). In this case, the sensor output voltage equation can be derived by substituting equation 4.1 into equation 6.3 as below.

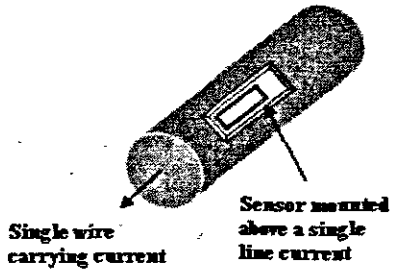

Figure 6.38: Sensor mounted above single wire

$$V = 3.8323\frac{i}{2\pi r} \tag{6.4}$$

where i is the sensor AC current input and r is the beam sensor distance from the current-carrying conductor centre. Using this equation, the Sensor response varies predictably with distance, which is shown in Figure 6.39.

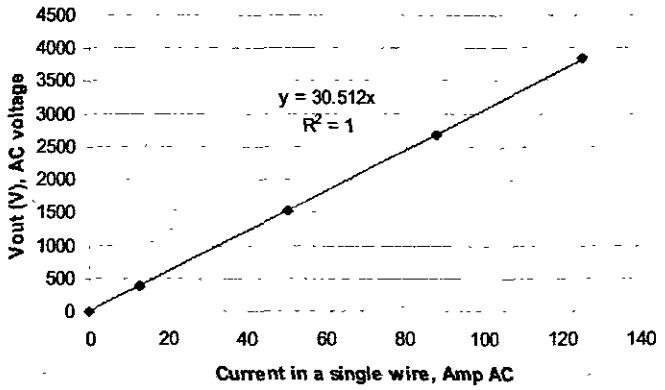

Figure 6.39: Sensor response for distance of 20mm

Figure 6-39 shows the response of the sensor when the sensor assumed to be mounted on top of the wire with a distance of 20mm above the centre of the wire. The sensor has shown linear response with a sensitivity of 30.512 V/A in current range of 6mA up to 125A at distance 20mm from the centre of the wire.

6.11.2 Double wire

Sensor mounted on top

Figure 6.40 shows one way of sensing a current flowing in a double wire. The sensor is assumed to be mounted above the wires at distance r above the centre of the wires. The distance between the two wires-centres is 2d. This way has been expressed in the schematic in Figure 6.41 in order to highlight the effective field and derivation of the total field equation.

In this case, the total field generated by the two lines current is given by equation 6.5 [Leland E S, 2007].

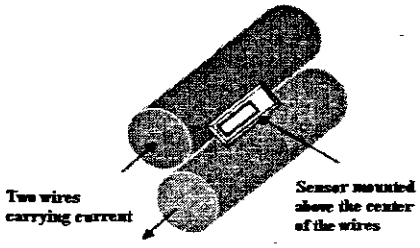

Figure 6.40: Sensor mounted above double wire

$$H_c = \frac{i}{\pi}\left(\frac{d}{r^2 + d^2}\right) \tag{6.5}$$

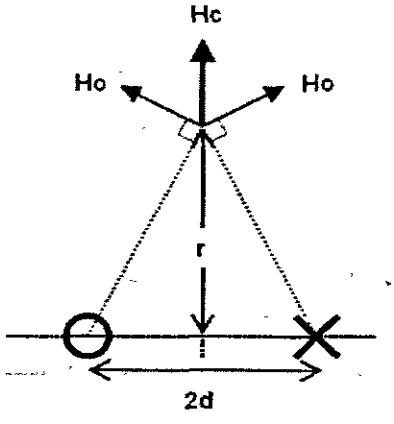

Figure 6.41: Schematic expression of the sensor above double wire

By substituting equation 6.5 into 6.4, we obtained the sensor output equation, as below.

$$V = 3.8323\frac{i}{\pi}\left(\frac{d}{r^2 + d^2}\right) \tag{6.6}$$

Sensor mounted on side

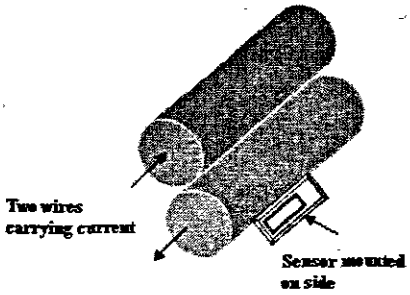

Figure 6.42: Sensor mounted on side of two wires carrying current

Figure 6.42 shows another way of sensing a current flowing in a double wire. The sensor is mounted on side of the wires at distance S from the centre of a distance 2d between the two wires-centres. This way has been expressed in the schematic shown in Figure 6.40 in order to highlight the effective field and derivation of the total field equation.

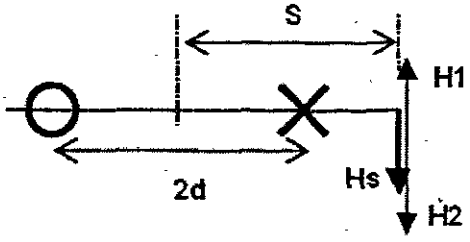

Figure 6.43: Schematic expression of the sensor above double wire

In this case, the total field generated by the two lines current is given by [Leland E S, 2007]

$$H_s = -\frac{i}{\pi}\left(\frac{d}{s^2 + d^2}\right) \tag{6.7}$$

By substituting equation 6.7 into 6.4, we obtained the sensor output equation, as below.

$$V = -3.8323\frac{i}{\pi}\left(\frac{d}{s^2 + d^2}\right) \tag{6.8}$$

6.12 SUMMARY

In conclusion, the sensor has been thoroughly simulated and the sensor equation produced which correlates closely with that of the theoretical model that was developed in the sensor design stage. The resonance frequency of the sensor structure was investigated and analyzed. The deflection of the cantilever beam due to the AC applied magnetic field has shown linear relation and the frequency of the beam motion is double of the excitation frequency signal. The effective beam dimensions, length, width, and thickness were investigated.

The behaviour of the capacitive sensing system has been analyzed in terms of linearity and nonlinearity. In a certain range of (50m A/meter to 1K A/meter), the change in the capacitance has shown a linear relationship and nonlinear beyond that. The sensitivity of the differential capacitive in the range of the linearity of the system has been calculated. The output voltage, due to the capacitance change using an integrated circuit (ICs) attached to the capacitive sensing system has been measured and analyzed in terms of linearity and nonlinearity. The electrostatic force effect due to the DC source of the ICs was investigated.

The use of the sensor in how to measure a current flowing in single or double wires was discussed in terms of the sensor position to the line current. The equation of the measurement was modelled for the linear output of the sensor in case for both single and double wires. The sensitivity of the sensor response in the linear range was calculated.

CHAPTER 7

7 CONCLUSIONS AND RECOMMENDATIONS

The objective of the research was to develop a non-contact current sensor based on MEMS technology. The primary research objective was discussed is to develop a non-contact current sensor based on MEMS technology. Secondary objectives were to investigate the design, modelling, simulation analysis of micro-structure cantilever-beam and the capacitive transducer of a current sensor.

Modelling of the equations that described the sensor dynamic has been presented. This included the modelling of the magnetic moment of a magnetic cantilever-beam placed in a field, the deflection of the beam, the natural frequency of the cantilever-beam, the maximum deflection, the change in differential capacitive sensing technique, linearity of the differential capacitive, and capacitive sensitivity. Chapter 6 also presented the circuit design that will be used for sensor readout, and the electrostatic modelling as well.

A full description of the sensor including cantilever-beam and capacitive sensing techniques, design, dimensions, materials type and their properties were presented. An introduction to the CoventorWare software and the main steps of using it to simulate a design and to analyze the sensor was presented as well.

The resonance frequency of the sensor structure was investigated and the simulation results were analyzed. The deflection of the cantilever beam due to the AC applied magnetic field has shown linear relation and the frequency of the beam motion is double of the excitation frequency signal. The effective beam dimensions, length, width, and thickness were investigated.

The behaviour of the capacitive sensing system was analyzed in terms of linearity and non-linearity. In a certain range (50m A/meter to 1K A/meter), the change in the capacitance has shown linear relationship and nonlinear beyond that. The sensitivity of the differential capacitive in the range of the linearity of the system has been calculated. The output voltage due to the capacitance change using an integrated circuit (ICs) attached to the capacitive sensing system has been measured and analyzed in terms of linearity and nonlinearity. The electrostatic force effect due to the DC source of the ICs was investigated. The use of the sensor in how to measure a current flowing in single or double wires was discussed in terms of the sensor position to the line current. The equation of the measurement was mod-

elled for the linear output of the sensor in both cases single and double wire. The sensitivity of the sensor response in the linear range was calculated.

As we understand the greatest challenges in MEMS fabrication and simulation devices are to get the simulation result in agreement with the testing results of the physical device. The difference normally happened due to the change in dimension or physical properties during the fabrication process of the sensor. As a future plan, we send the sensor design to foundry to be manufactured for experimental and further research development.

8 REFERENCES

Angelis C De, Ferrari V, Marioli D, Sardini E, Serpelloni M, & Taron A., 2007, 'Magnetically induced oscillations on a conductive cantilever for resonant microsensors', *Sensors and Actuators A, Physical*, 30 March, Vol. 135, No.1, pp. 197-202.

Bahreyni B, 2006, 'Design, Modelling, Simulation, and Testing of Resonant Micromachined Magnetic Field Sensors', PhD Thesis, University of Manitoba, Winnipeg, Canada.

Berckan E, Kapusta C J, Claydon G S, Zribi A, Meyer L J, & Tian W-C, 2006, 'MEMS-based current sensor using magnetic-to-mechanical conversion and reference components', US Patent 7,112,951 B2, 26 September.

Beroulle V, Bertrand Y, Latorre L, & Nouet P, 2001, 'Test and Testability of a Monolithic MEMS for Magnetic Field Sensing', *Journal of Electronic Testing*, October, Vol. 17, No. 5, pp. 439-450.

Bourquin F & Joly M, 2005, 'A magnet-based vibrating wire sensor: design and simulation', *Institute of physics, Smart Materials and structure*, Vol. 14, pp. 247-256.

Carvou E, Bihhan F L, Rogel R, & Bonnaud O, 2002, 'Magnetic sensors with Polysilicon TFTs', *Sensors, Proceeding of IEEE*, Vol. 2, pp. 804-809.

Cowburn R P, Moulin M, & Welland, M E, 1997, 'High sensitivity measurement of magnetic fields using microcantilevers', *Applied Physics Letters*, 13 October, Vol. 71, Issue 15, pp. 2202-2204.

DeNatale J, Borwick R, Stupar P, Anderson R, Garrett K, Morris W, & Yao J J, 2003, 'MEMS high resolution 4-20mA current sensor for industrial I/O applications', presented to *the 12th International conference on Solid State Sensors, Actuators and Microsystems*, Boston, 8-12 June, Vol. 2, pp. 1598 - 1601.

Dickinson R & Milano S, 2002, 'Isolated Loop Current Sensing Using Hall Effect Technology in an Optimized Magnetic circuit', [Online]. Available from: http://www.allegromicro.com/en/Products/Design/current_sensing/bsp_v1_52.pdf[18May 2007]

Ehrfeld W, Bley P, Gotz H P, Maner A, Mohr J, Moser H O, Munchmeyer D, Schellb W, Schmidt D, & Becker E W, 1987, 'Fabrication of Microstructures using the LIGA Process', *Proceeding of IEEE Micro Robots and Teleoperators Workshop*, Nov. 9-11, pp. 1-11.

Emmerich H & Schofthaler M, 2000, 'Magnetic field measurements with a novel surface micromachined magnetic field', *Electron Devices, IEEE Transactions*, May, Vol. 47, No. 5, pp.972-977.

Esashi M, 1993, 'Micromachining for Packaged Sensors', Paper presented to *the International conference on Solid state Sensors and Actuators, Transducers*, Yokohama, Japan, June, pp. 260-265.

Feynman R, 1992, 'There's of Room at the Bottom', *Journal of Micromechanical Systems*, March, Vol. 1, No. 1, pp. 60-66.

Fujita H, 2006, 'Characteristics of a Bulk High-Critical Temperature Superconductor Fabricated by the Shock Compaction Method: Possible Use as a Highly Sensitive Magnetic Sensor', *Journal of Physics, Conference Series*, Vol. 43, pp. 1389-1392.

Gabriel K J, 1995, 'Engineering Microscpic Machines', *Scientific American*, September, pp.150-153.

Goedeke S M, Allison S W, & Datskos P G, 2004, 'Non-contact current measurement with cobalt-coated microcantilevers', *Sensors and Actuators A*, Vol. 112, pp. 32-35.

Hardner H T, 2000, 'Characterization of Magnetic Stabiliy in Spin Valve Test Devices', *IEEE Transactions on Magnetics*, September, Vol. 36, No. 5, pp. 2584-2586.

Harmany Z., 2003, 'Effects off vacuum pressure on the resonance characteristics of MEMS cantilever structures', *NSF EE REU PENN STATE*, Annual Research Journal, Vol. 1, pp 54-57.

Howe R T & Muller R S, 1988, 'Surface micromachining for microsensors and microactuators', *Journal of Vacuum Science & Technology B: Microelectronics and Nanometer Structures*, November , Vol. 6, No. 6, pp. 1809-1813 .

Hu Y.C, Chang C M, & Huang S C, 2004, 'Some design considerations on the electrostatically actuated microstructures', *Sensors and Actuators A*, Vol. 112, pp155-161.

Ignjatovic Z & Bocko M F, 2005, 'An Interface circuit for measuring capacitance change based upon capacitance –to-duty cycle (CDC) convertor', *IEE sensors journal*, June, Vol. 5 No. 3, pp. 403-410.

Janawadkar M P, Baskaran R, Saha R, Gireesan K, Nagendran R, Vaidhyanathan L S, Jayapandian J and Radhakrishnan T S, 1999, 'SQUIDs-Highly sensitive magnetic sensor', [Online]. Available from: http://www.ias.ac.in/currsci/sep25/articles17.htm [14 June 2007].

Kadar Z, Bossche A, & Mollmger J, 1994, 'Integrated Resonant Magnetic field Sensor', *Sensors and actuators A, Physical*, 1 April, Vol. 41, Issues 1-3, pp. 66-69.

Kaienburg J, Lutz M, Maihofer B, & Schellin R. Div, 1998, 'A precise and contactless angle detection sensor using surfacemicromachining technology', *MEMS, IEEE Proceedings*, 25-29 Jan, Heidelberg, Germany, pp. 367 – 371.

Kester W, 2007, 'Bridge Circuits', [Online]. Available from: http://www.analog.com/UploadedFiles/Associated_Docs/324555617048500532024843352497435735317849058268369033Fsect2.PDF [18 May 2007].

Ko W H, Hynecek J, & Boettcher S F, 1979, 'Development of Miniature Pressure Transducer for Biomedical Applications', *Electron Devices, IEEE Transactions*, December, Vol. ED-26, No. 12, pp. 1896-1905.

Konishi S & Fujita H, 1993, 'A Conveyance System Using Air Flow Based on the Concept of Distributed Micro Motion Systems', *Proceeding of the international Conference on Solid State Sensors and Actuators, Transducers*, Yokohama, Japan, June, pp.28-31.

Koon W, 2007, 'Current sensing for Energy Metering', [Online]. Available from: http://www.analog.com/Analog_Root/static/technology/dataConverters/training/meterBackground/currentSensors/Current_sensing_for_metering.pdf [13 March 2007]

Krause H J & Kreutzbruck M.v, 2002, "Recent developments in SQUID NDE", *Physica C: Superconductivity*, March, Vol. 368, Issues 1-4, 1, pp. 70-79.

Krause H -J, Wolf W, Glaas W, Zimmermann E, Faley M, Sawade G, Mattheus R, Neudert G, Gampe U, & Krieger J, 2002, 'SQUID array for magnetic inspection of prestressed concrete bridges', *Physica C: Superconductivity*, March, Vol. 368, Issues 1-4, pp. 91-95.

Kyungwoo Lee, 2002, 'Large deflection of cantilever beam of non-linear elastic material under combined loading', *International Journal of Non-linear Mechanics*, Vol. 37, pp. 439-443.

Lee K B, 2007, 'Closed-form solutions of the parallel plate problem', *Sensors and Actuators A*, 12 Feb, Vol. 133, No. 2, pp. 518-525.

Leichle T C, von Arx M, & Allen M G, 2001, 'A Micromachined resonant magnetic field sensor', Paper presented to *the 14th IEEE International Conference, MEMS*, Interlaken, Switzerland, 21-25 Jan, pp. 274-277.

Leichle T C, Ye W, & Allen M G, 2003, 'A SUB-uW Micromachined Magnetic Compass', *proceeding of IEEE MEMS*, 19-23 Jan. pp. 514-517.

Leland E S, 2007, 'MEMS power sensors', [Online]. Available from: http://www.ucop.edu/ciee/dretd/wrkshps/documents/MEMS_Power_Sensors_02-21-2007.pdf [15 July 2007].

Lenz J E, 1990, 'A Review of Magnetic Sensors', Proceedings of IEEE 1990, June, Vol. 78, No. 6, pp. 973-989.

Li X & Meijer C M. 2002. 'An Accurate Interface for Capacitive Sensors'. *IEEE Transaction on Instrumentation and Measurement*, October, Vol. 51, No. 5. pp. 935-939.

Liu C & Yi Y W, 1999, 'Micromachined Magnetic Actuators Using Electroplated Permalloy', *IEEE Transactions on Magnetics*, May, Vol. 35, No. 3, pp.1976-1985.

Marshall S V & Skitek G G, 1990, *Electromagnetic concepts and applications*, 3rd edn, Englewood Cliffs, N.J., Prentice-Hall.

Mendels D-A, Lowe M, Cuenat A, Cain M G, Vallejo E, Ellis D, & Mendels F, 2006, 'Dynamic properties of AFM cantilevers and the calibrations of their spring constant', *IOP, Journal of Micromechanics and Microengineering*, Vol. 16, pp. 1720-1733.

Murnane S N, Barnes R N, Woodhead S R, & Amadi-Echendu J E, 1996, 'Electrostatic Modelling and Measurement of Airborne Particle Concentration', *IEEE Transaction on Instrumentation and Measurement*, April, Vol. 45, No. 2, pp. 488-492.

Nathanson H C, 1965, 'A Resonant-Gate Silicon Surface Transistor with High-Q Bandpass Properties', *Applied Physics Letter*, Vol. 7, pp. 84-86.

Nguyen Van Dau F, Schuhl A, Childress J R, & Sussiau M, 1995, 'Magnetic sensors for Nao-Tesla detection using planar Hall Effect', Paper presented to *the 8th International conference on Solid State Sensors and Actuators, and Eurosensors IX*, Stockholm, Sweden, 25-29 June, pp.241-244.

Niemainen H, , Ermolov V, Silanto S,Nybergh K, & Ryhänen T, 2004, 'Design of a Temperature-Stable RF MEM Capacitor', *Journal of Microelectromechanical system*, October, Vol. 13, No. 5, pp 705-714.

Noh H M, 2007, 'Introduction to Micro-fabrication', [Online]. Available from: http://www.mem.drexel.edu/noh/mems_course/main_files/Lecture1%20Introduction.pdf [25 July 2007].

O'Donnell T, Tipek A, Connell A, McCloskey P, & O'Mathuna S C, 2006, 'Planar fluxgate current sensor integrated in printed circuit board', *Sensors and Actuators A*, 24 May, Vol. 129, pp. 20-24.

Odawara A, Nakayama S, Ikeda M, Morooka T, Nagata A, Tsuda I, Kasai N & Chinone K, 2003, "Non-contact current measurement system using SQUID", *Physica B* 329-333, pp1517-1518.

Penna S D, 2006, 'SQUID sensor with additional compensation module for operation in an AC field', *Journal of Physics, Conference Series*, Vol. 43, pp. 1247-1249.

Petersen K E, 1982, 'Silicon as Mechanical material', *Proceeding of the IEEE*, May, Vol. 70, No. 5, pp. 420-457.

Pister K S J, 1998, 'MEMS Magnetic Sensor in Standard CMOS', [Online]. Available from: http://plasma2.ssl.berkeley.edu/ConstellationClassMissions/eyre.pdf [28 November 2006].

Qiao D-Y, Yuan W-Z, & Li X-Y, 2007, 'A two-beam method for extending the working range of electrostatic parallel-plate micro-actuators', *Journal of Electrostatics*, Vol. 65, pp. 256-262.

Ripka P, 2001, *Magnetic Sensors and Magnetometers*, Artech House, London.
Ripka P, 2004, 'Current sensors using magnetic materials', *Journal of Optoelectronics and Advanced Materials*, June, Vol. 6, No. 2, pp. 587-592.

Ripka P, Kubik J, Duffy M, Hurley W G, & O'Reilly S, 2005, 'Current Sensor in PCB Technology', *Sensors Journal, IEEE*, June, Vol. 5, No. 3, pp. 433 – 438.

Rossit C A, & Laura P A A, 2001, 'Free vibrations of a cantilever beam with a spring-mass system attached to the free end', *Ocean Engineering*, Vol. 28, pp. 933-939.

Ruan M, Shen J, & Wheeler C B, 2001; 'Latching microelectromagnetic relays', *Sensors and Actuators A*, Vol. 91, pp 346-350.

Schneider M, Castagnetti R, Allen M G, & Baltes H, 1995, 'Integrated Flux Concentrator Improves COMS Magnetotransistor', *MEMS, Proceeding IEEE*, 29 January- 2 Feb, pp. 151-156.

Salomon P R, 2007, 'Micro sensors – world wide markets and economic impact', [Online]. Available from:
http://www.enablingmnt.com/MICRO_SENSORS__WORLD_WIDE_MARKETS_AND_ECONOMIC_IMPACT_abstract_-_Eurosensors06_-Patric_Salomon.pdf [25 October 2007]

Simpson J, 2000, 'Magnetoresistive sensors based rotating probe system for detection of deep fatigue cracks under airframe fasteners', [Online]. Available from:
http://www.teccenter.org/gmr/assets/pdf/wincheski_aa00paper.pdf [06 May 2007].

Sunier R, Vancura T, Li Y, Kirstein K.-U, Baltes H, & Brand O, 2006, 'Resonant Magnetic Field Sensor with Frequency Output', *Journal of Microelectromechanical Systems IEEE*, October, Vol. 15, No. 5, pp. 1098- 1107.

Temnykh A B &. Lovelace R V E. 2001, 'Electro-mechanical resonant magnetic field sensor', Nuclear Instruments and Methods in Physics Research Section A: Accelerators, Spectrometers, Detectors and Associated Equipment, Vol. 484, Issues 1-3, 21 May 2002, pp. 95-101.

Toth F N, Bertels D, & Meijer G C M, 1996, 'A Low-Cost, Stable Reference Capacitor for Capacitive Sensor Systems', *IEEE Transaction on Instrumentation and Measurement*, April, Vol. 45, No. 2, pp.526-530.

Toth F N, Meijer G C M, & Kerkvliet M M, 1996, 'A very Accurate Measurement System for Multielectrode Capacitive Sensors', *IEEE Transaction on Instrumentation and Measurement*, April, Vol. 45, No. 2, pp. 531-535.

Van der Goes F M L & Meijer G C M, 1996, 'A Novel Low-cost Capacitive-Sensor Interface', *IEEE Transaction on Instrumentation and Measurement*, April, Vol. 45, No. 2, pp. 536-540.

Veijola T, 2001, 'Nonlinear Circuit Simulation of MEMS Components: Controlled Current Source Approach', *Proceeding of ECCTD 01*, Espoo, Finland, 28-31 Aug, Vol. 3, pp. 377-380.

Veijola T, Kuisma H, & Lahdenpera, 1998, 'Dynamic Modelling and Simulation of Microelectromechanical Devices With a Circuit Simulation Program', *Proceeding of MSM 98*, Santa Clara, 6-8 April, pp. 245-250.

White R M, 1970, 'Surface Elastic Waves', *proceeding of the IEEE*, August, Vol. 58, No. 8, pp.1238-1276.

Wise K D & Clark S K, 1978, 'Diaphragm Formation and pressure sensitivity in Batch-Fabricated Silicon Pressure Sensors', *IEDM Tech Dig*, December, pp. 96-99.

Youhe Z & Xiaojing Z, 1997, 'A variation principle on magnetoelastic interaction of Ferromagnetic thin plates', *Acta Mechanica Solida Sinca*, March, Vol. 10, No. 1, pp. 1-10.

Zheng X & Wang X, 2003, 'Large-Deflection Deformation of Ferromagnetic Plates in Magnetic Fields', *Journal of Engineering Mechanics*, February, Vol. 129, No. 2, pp. 245-248.

Zheng X J, Zhou Y H, Wang X Z, & Lee J S, 1999, 'Bending and buckling of ferroelastic plates', *Journal of Engineering Mechanics*, February, Vol. 125, No. 2, pp. 1800-185.

9 APPENDICES

9.1 APPENDIX A

Sensor Design

To create a solid model of the sensor, materials and their properties specification need to choose from the Material Properties Database (MPD) file.

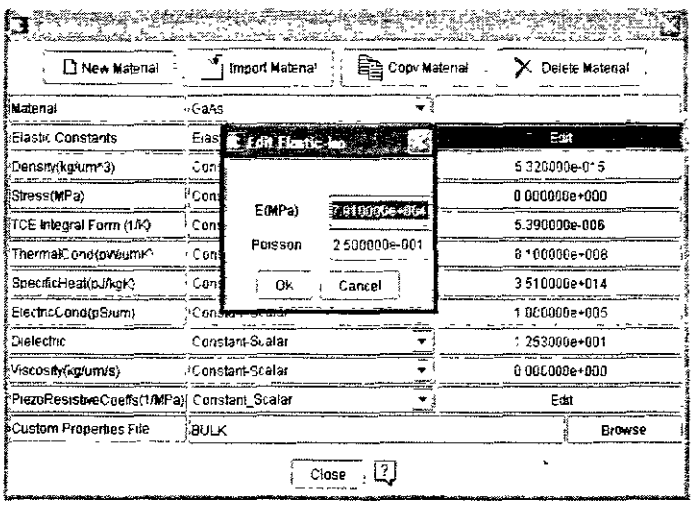

Figure 1: Materials data base settings

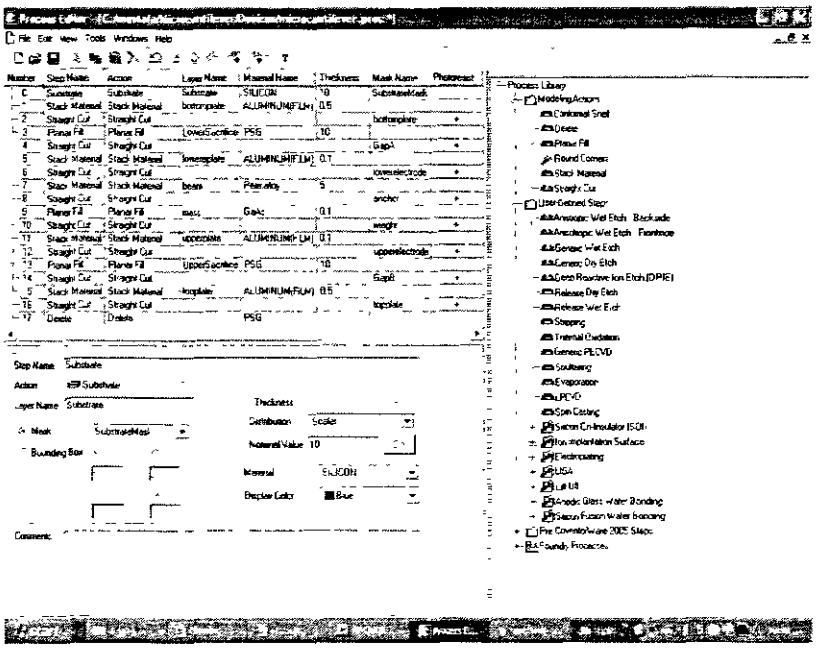

Figure 2: Deposit steps in process editor

```
LayoutEditor — Terminal
File
(c) Copyright Coventor Inc 1997-2006
LayoutEditor Build 2006 002 2236 3, Fri Mar 23 16 30 04 EDT 2007
Running Layout generator .
Netlist file C:/mustafa/Microcantilever/Schematics/microcantilever.sin
Generating for schematic component anchor anchor1
Generating for schematic component movable_magnetizable_uniformfield_magnet_bus movable_magnetizable_uniformfield_magnet_bus1
Generating for schematic component rigid_plate_contact rigid_plate_contact1
Generating for schematic component rigid_plate_contact rigid_plate_contact2
Generating for schematic component beam_1seg beam_1seg1
Generating for schematic component electrode electrode1
Creating cell microcantilever electrode electrode1
Generating for schematic component nonlinear_rigid_plate nonlinear_rigid_plate2
Creating cell microcantilever nonlinear_rigid_plate nonlinear_rigid_plate2
Generating for schematic component nonlinear_rigid_plate nonlinear_rigid_plate3
Creating cell microcantilever nonlinear_rigid_plate nonlinear_rigid_plate3
Generating for schematic component nonlinear_rigid_plate nonlinear_rigid_plate4
Creating cell microcantilever nonlinear_rigid_plate nonlinear_rigid_plate4
Generating for schematic component nonlinear_rigid_plate nonlinear_rigid_plate5
Creating cell microcantilever nonlinear_rigid_plate nonlinear_rigid_plate5
Generating for schematic component nonlinear_rigid_plate nonlinear_rigid_plate6
Creating cell microcantilever nonlinear_rigid_plate nonlinear_rigid_plate6
Generating for schematic component electrode electrode2
Creating cell microcantilever electrode electrode2
Generating for schematic component nonlinear_rigid_plate nonlinear_rigid_plate7
Creating cell microcantilever nonlinear_rigid_plate nonlinear_rigid_plate7
Generating for schematic component nonlinear_rigid_plate nonlinear_rigid_plate8
Creating cell microcantilever nonlinear_rigid_plate nonlinear_rigid_plate8
No warnings
No errors
Layout generation successful
```

Figure 3: Layout verification report

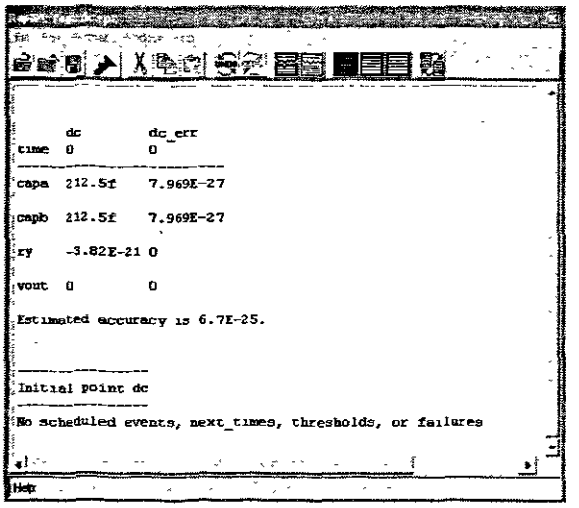

Figure 4: DC analysis report

9.2 APPENDIX B

Transient analysis of different amplitudes (50m to 5k A/m) but with a constant frequency of 50 Hz of applied magnetic field along z-axis has been simulated in order to validate and predict of the sensor behavior. Magnetization density, beam deflection, lower and upper capacitors, and voltage output has shown in figures bellow for each single simulation (2.1-2.18).

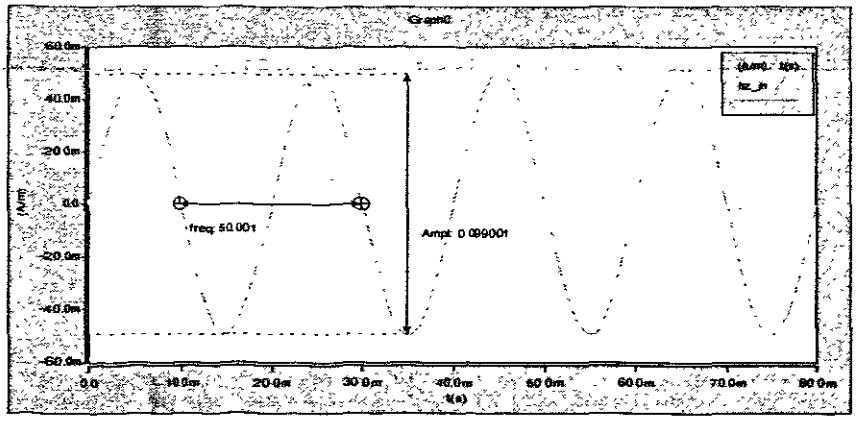

Figure1: Applied magnetic field along z-axis of 50m A/meter with 50 Hz

2.1 Results of input field Hz= 50m A/m

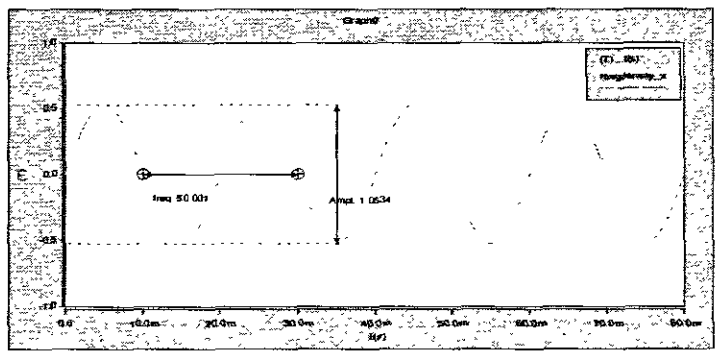

Figure 1.1: Magnetization density of the beam material of input field 50m A/meter along the beam-length (x-axis). The amplitude of the signal is increased with small value from the initial amplitude of zero input field

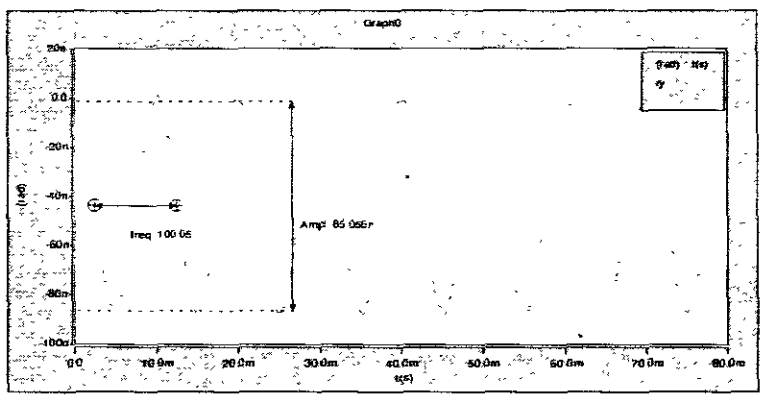

Figure 1.2: Deflection beam of input field of 50m A/meter. The signal amplitude is proportional to the input field with double frequency of the input frequency. The negative sign means the angular deflection is clockwise

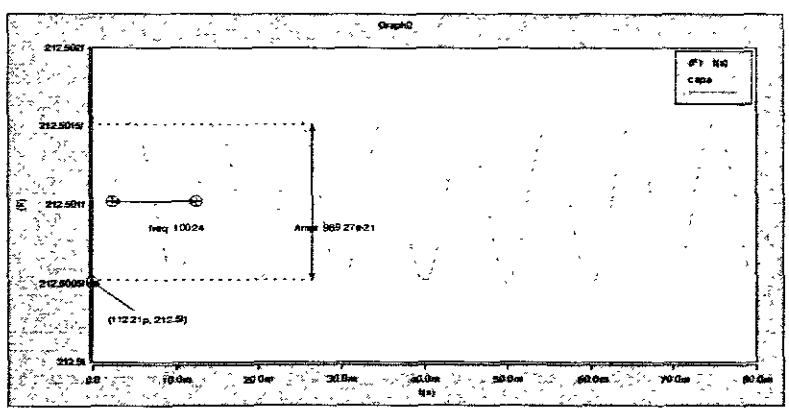

Figure 1.3: Lower capacitor signal of input field of 50m A/meter. The amplitude of the signal is increasing begins with the initial value till reach a maximum value as a function of the input field

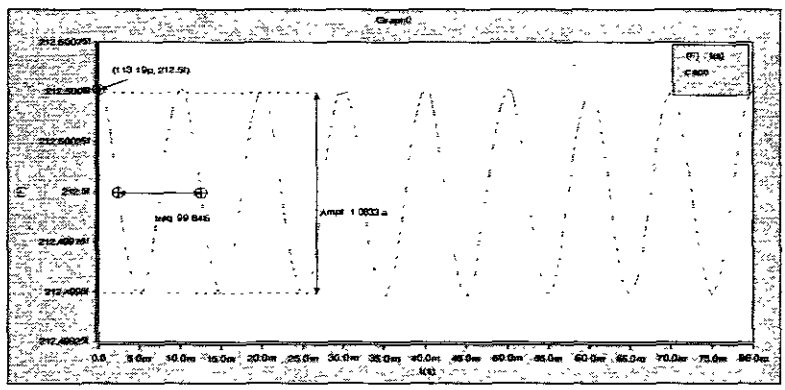

Figure 1.4: Upper capacitor signal of input field of 50m A/meter. The amplitude of the signal is decreasing begins with the initial value till reach a minimum value as a function of the input field

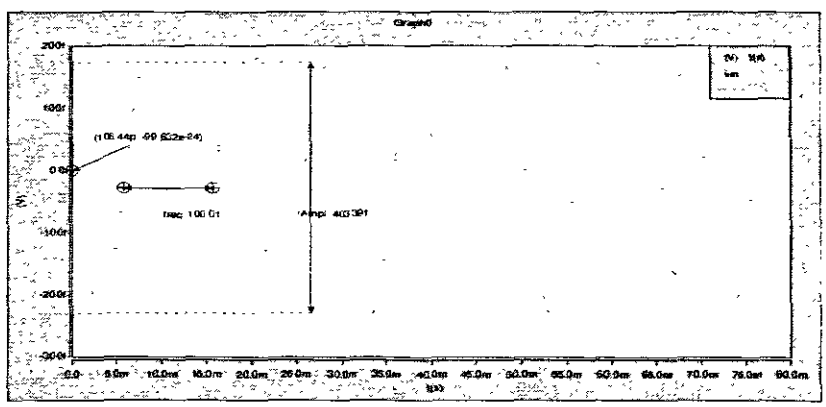

Figure 1.5: Sensor output voltage at point B of input field of 50m A/meter. The signal frequency is double of the input field signal frequency. The amplitude of the signal is proportional to the input field

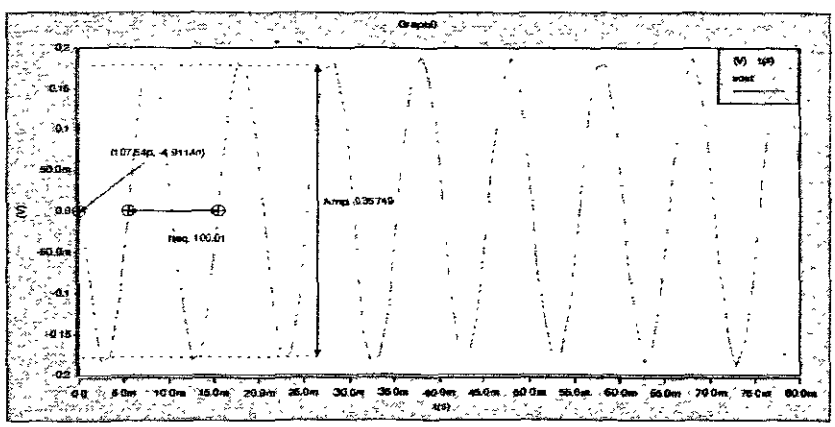

Figure 1.6: Sensor output voltage of input field of 50m A/meter. The signal frequency is double of the input field signal frequency. The amplitude of the signal is proportional to the input field

2.2 Results of input field Hz = 1 A/m

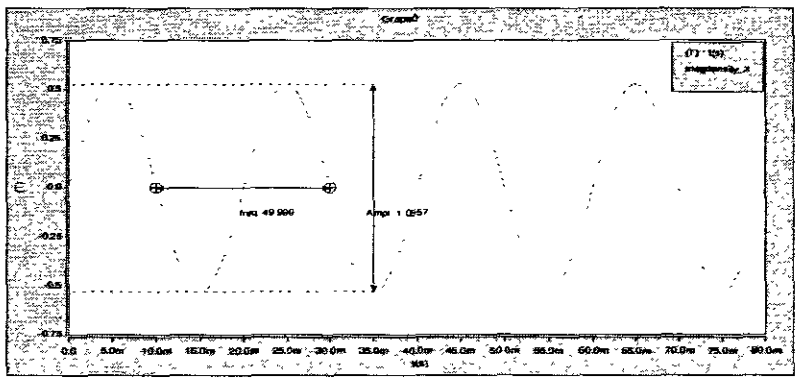

Figure 2.1: Magnetization density of the beam material of input field 1 A/meter along the beam-length (x-axis). The amplitude of the signal is increased with small value from the initial amplitude of zero input fields

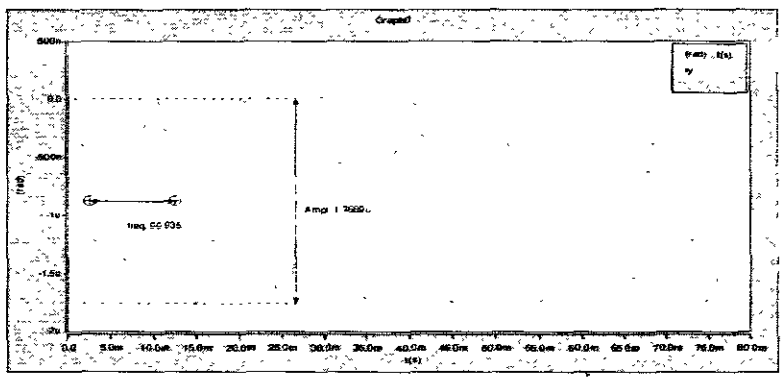

Figure 2.2: Beam deflection of input field of 1 A/meter. The signal amplitude is proportional to the input field with double frequency of the input frequency. The negative sign means the angular deflection is clockwise

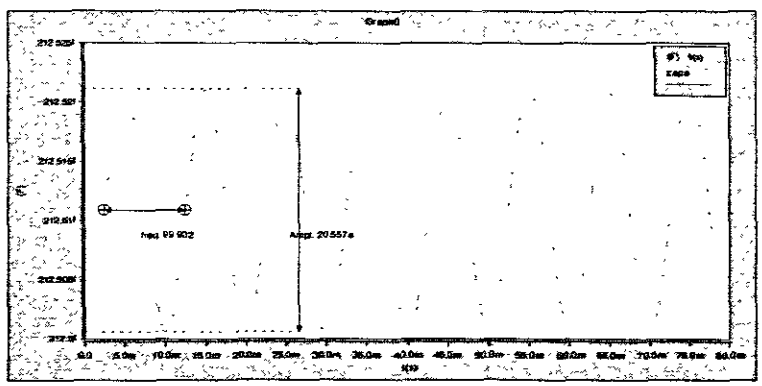

Figure 2.3: Lower capacitor signal of input field of 1 A/meter. The amplitude of the signal is increasing begins with the initial value till reach a maximum value as a function of the input field

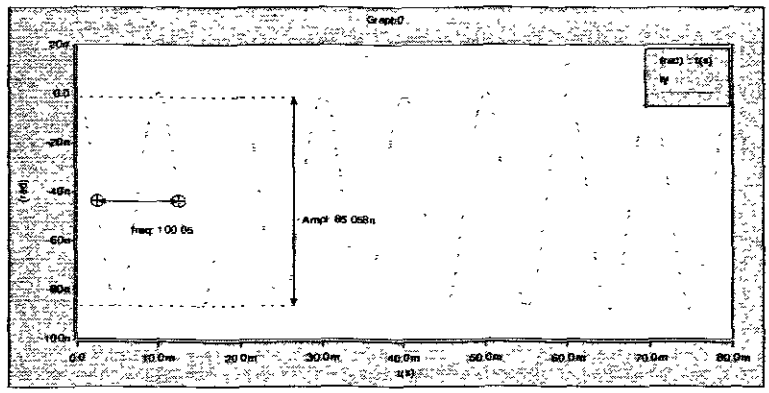

Figure 2.4: Upper capacitor signal of input field of 1 A/meter. The amplitude of the signal is decreasing begins with the initial value till reach a minimum value as a function of the input field

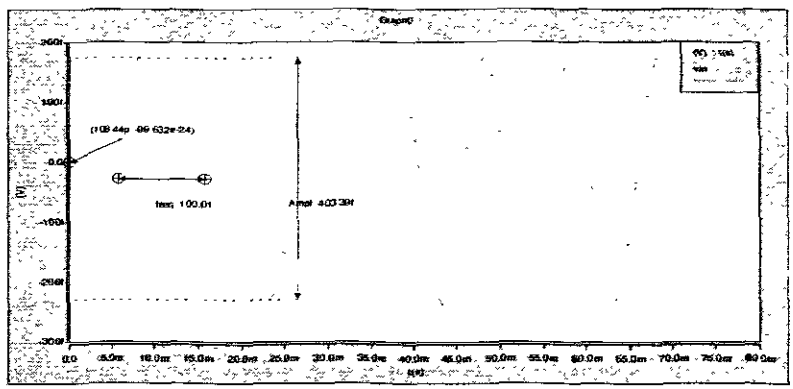

Figure 2.5: Sensor output voltage at point B of input field of 1 A/meter. The signal frequency is double of the input field signal frequency. The amplitude of the signal is proportional to the input field

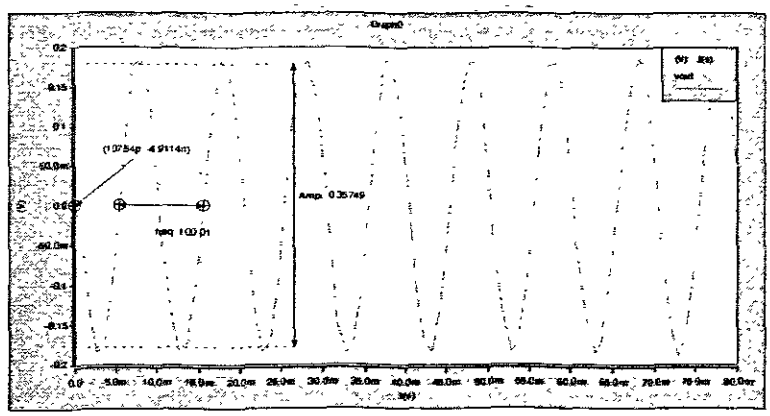

Figure 2.6: Sensor output voltage of input field of 1 A/meter. The signal frequency is double of the input field signal frequency. The amplitude of the signal is proportional to the input field

2.3 Results of input field Hz = 100 A/m

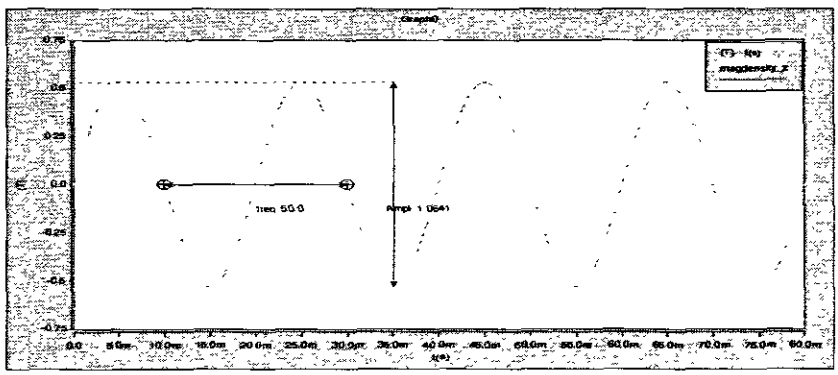

Figure 3.1: Magnetization density of the beam material of input field 100 A/meter along the beam-length (x-axis). The amplitude of the signal is increased with small value from the initial amplitude of zero input fields

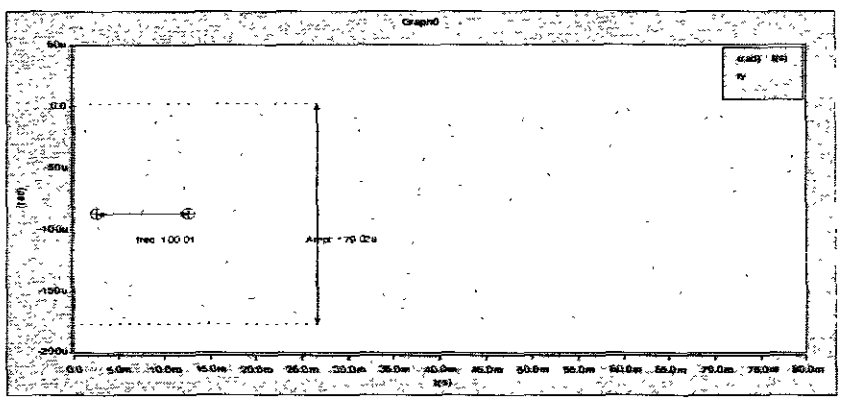

Figure 3.2: Beam deflection of input field of 100 A/meter. The signal amplitude is proportional to the input field with double frequency of the input frequency. The negative sign means the angular deflection is clockwise

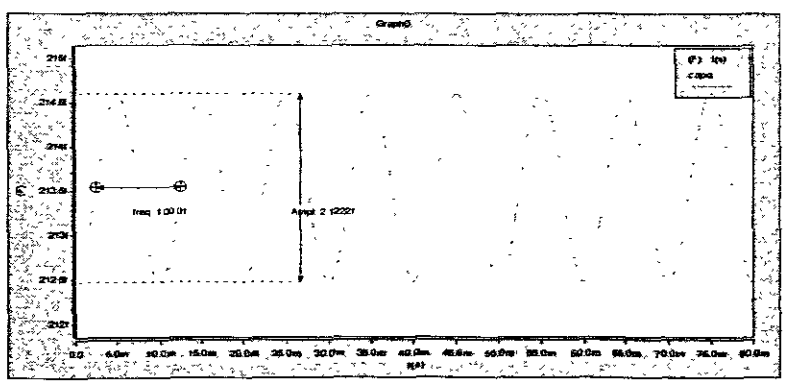

Figure 3.3: Lower capacitor signal of input field of 100 A/meter. The amplitude of the signal is increasing begins with the initial value till reach a maximum value as a function of the input field

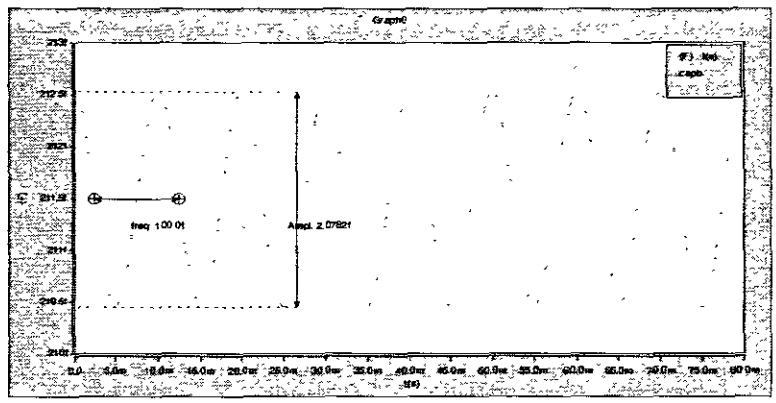

Figure 3.4: Upper capacitor signal of input field of 100 A/meter. The amplitude of the signal is decreasing begins with the initial value till reach a minimum value as a function of the input field

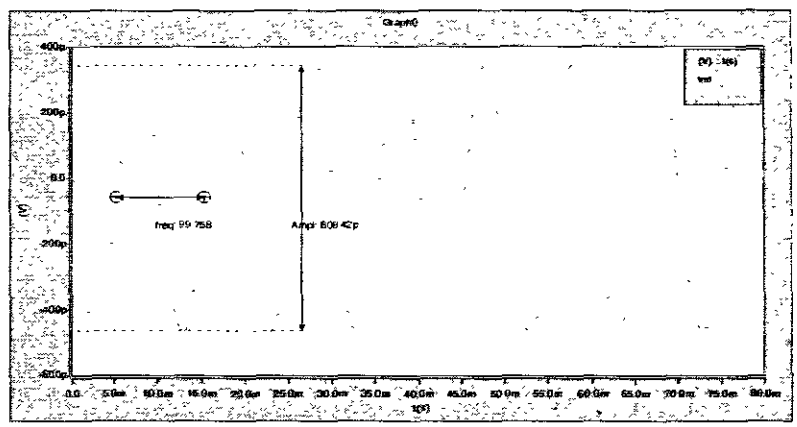

Figure 3.5: Sensor output voltage at point B of input field of 100 A/meter. The signal frequency is double of the input field signal frequency. The amplitude of the signal is proportional to the input field

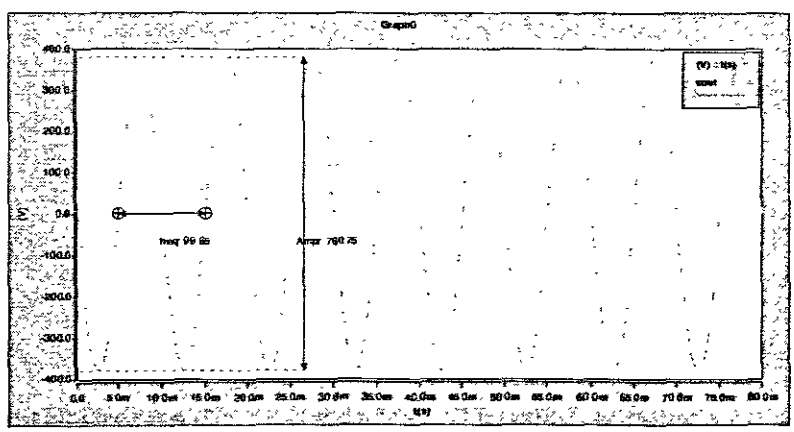

Figure 3.6: Sensor output voltage of input field of 100 A/meter. The signal frequency is double of the input field signal frequency. The amplitude of the signal is proportional to the input field

2.4 Results of input field Hz = 400 A/m

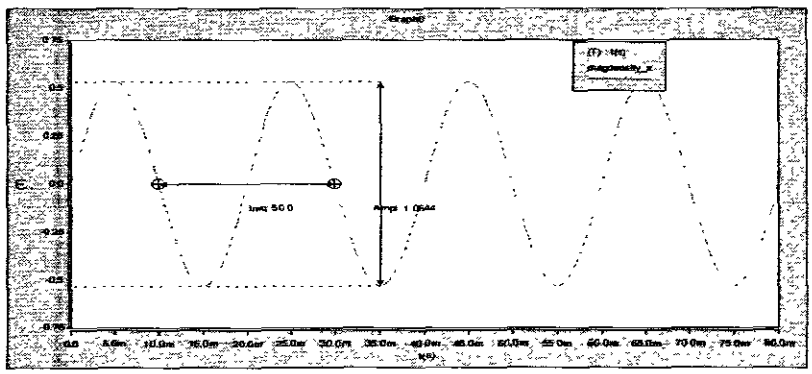

Figure 4.1: Magnetization density of the beam material of input field 400 A/meter along the beam-length (x-axis). The amplitude of the signal is increased with small value from the initial amplitude of zero input fields

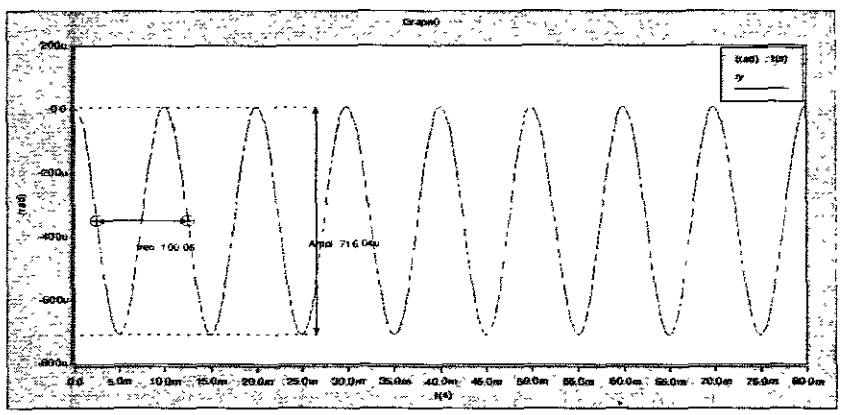

Figure 4.2: Beam deflection of input field of 400 A/meter. The signal amplitude is proportional to the input field with double frequency of the input frequency. The negative sign means the angular deflection is clockwise

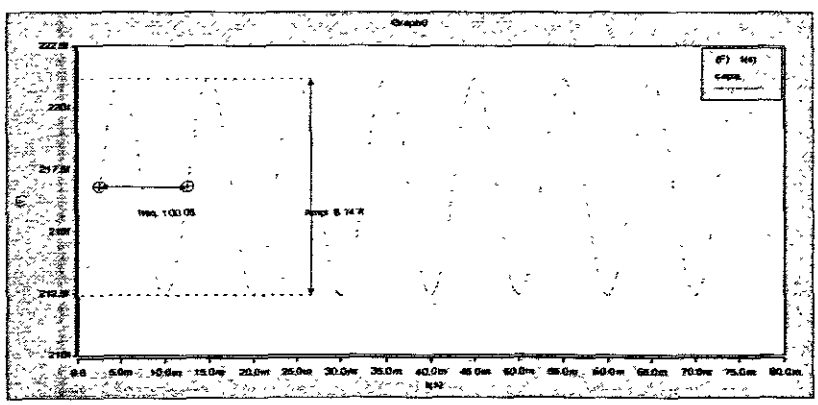

Figure 4.3: Lower capacitor signal of input field of 400 A/meter. The amplitude of the signal is increasing begins with the initial value till reach a maximum value as a function of the input field

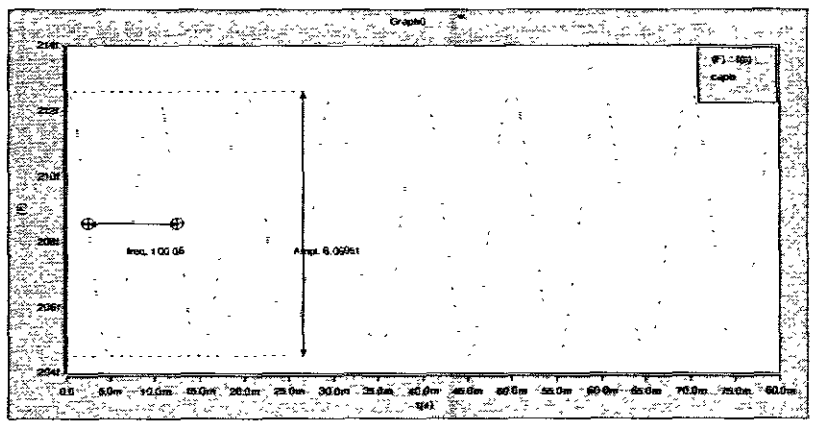

Figure 4.4: Upper capacitor signal of input field of 400 A/meter. The amplitude of the signal is decreasing begins with the initial value till reach a minimum value as a function of the input field

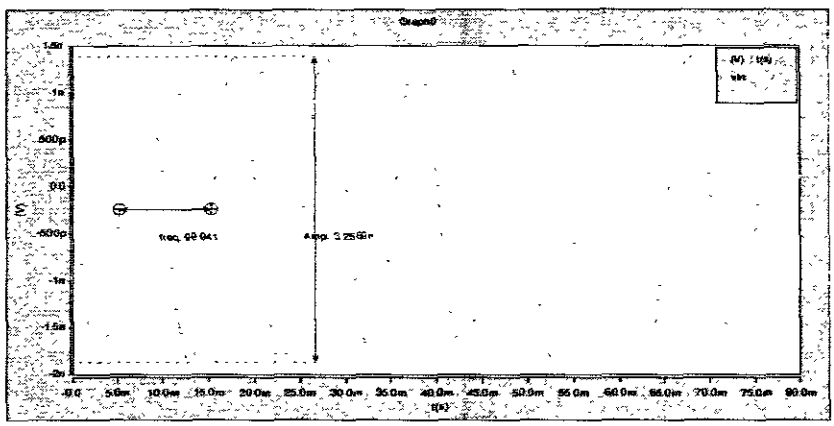

Figure 4.5: Sensor output voltage at point B of input field of 400 A/meter. The signal frequency is double of the input field signal frequency. The amplitude of the signal is proportional to the input field

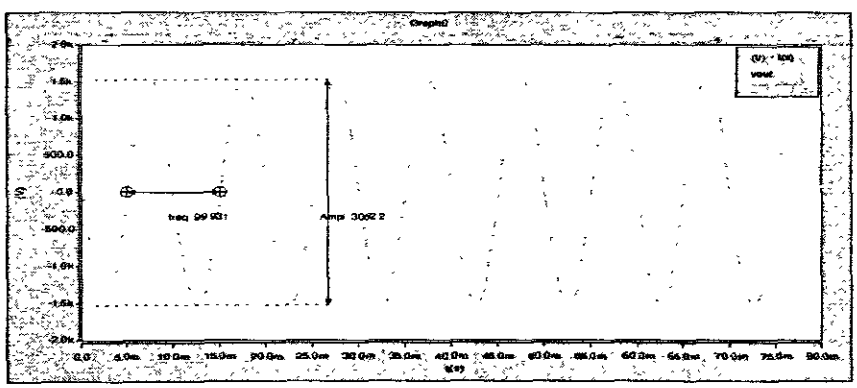

Figure 4.6: Sensor output voltage of input field of 400 A/meter. The signal frequency is double of the input field signal frequency. The amplitude of the signal is proportional to the input field

2.5 Results of input field of 700 A/m

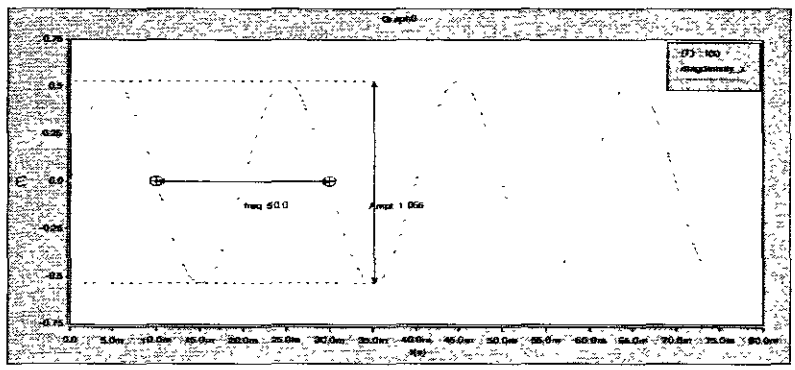

Figure 5.1: Magnetization density of the beam material of input field 700 A/meter along the beam-length (x-axis). The amplitude of the signal is increased with small value from the initial amplitude of zero input fields

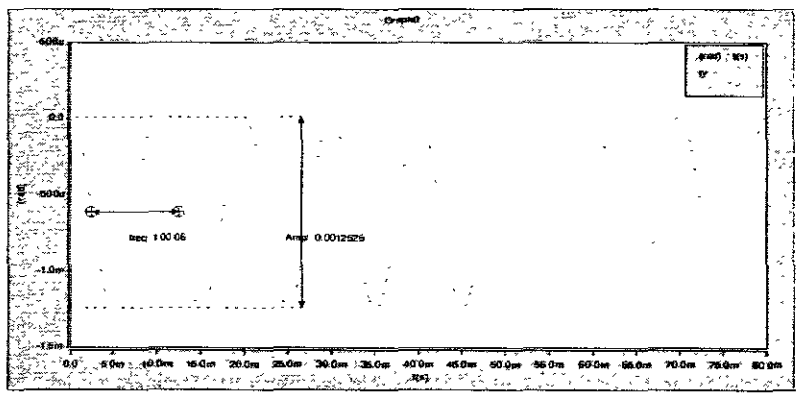

Figure 5.2: Beam deflection of input field of 700 A/meter. The signal amplitude is proportional to the input field with double frequency of the input frequency. The negative sign means the angular deflection is clockwise

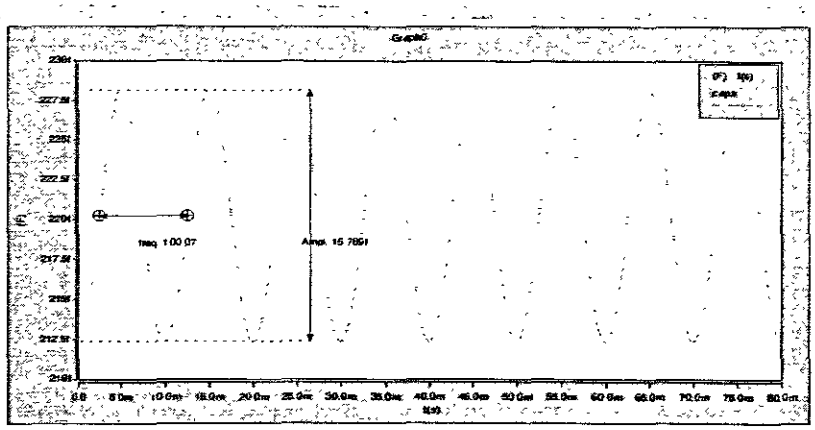

Figure 5.3: Lower capacitor signal of input field of 700 A/meter. The amplitude of the signal is increasing begins with the initial value till reach a maximum value as a function of the input field

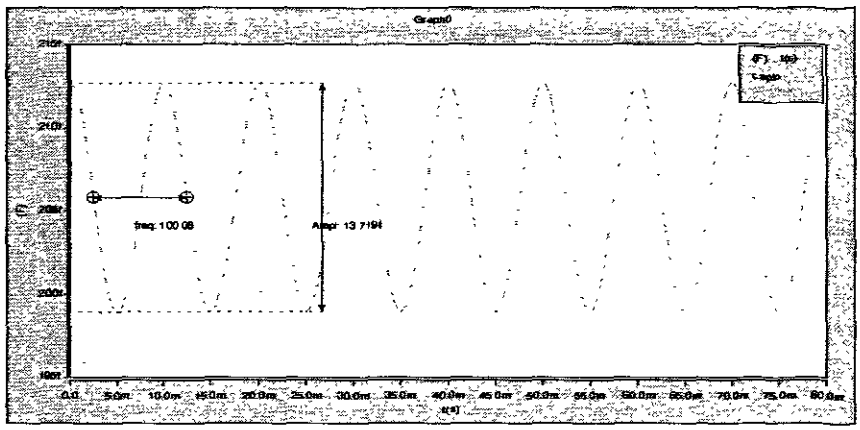

Figure 5.4: Upper capacitor signal of input field of 700 A/meter. The amplitude of the signal is decreasing begins with the initial value till reach a minimum value as a function of the input field

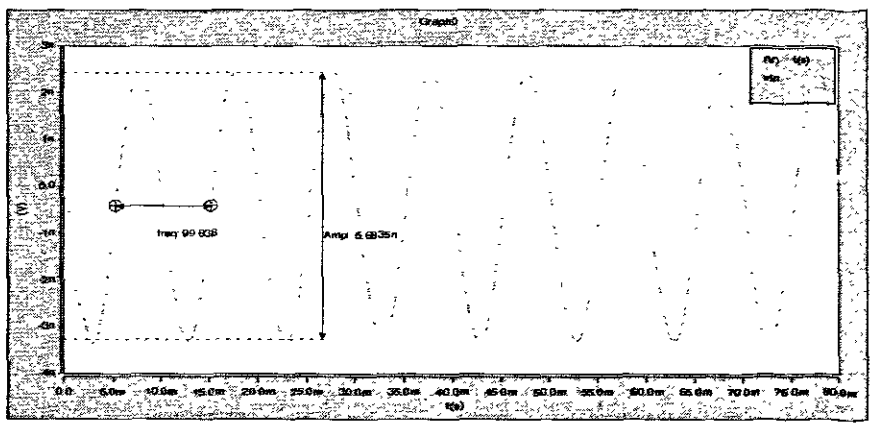

Figure 5.5: Sensor output voltage at point B of input field of 700 A/meter. The signal frequency is double of the input field signal frequency. The amplitude of the signal is proportional to the input field

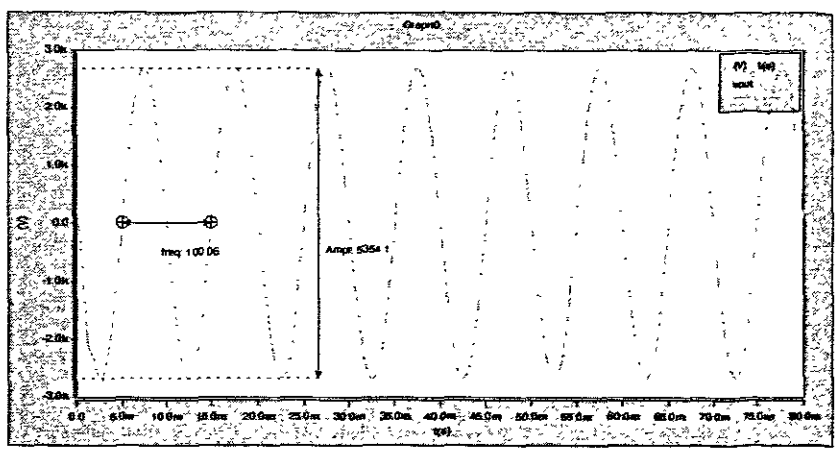

Figure 5.6: Sensor output voltage of input field of 700 A/meter. The signal frequency is double of the input field signal frequency. The amplitude of the signal is proportional to the input field

2.6 Results of input field of 1 k A/m

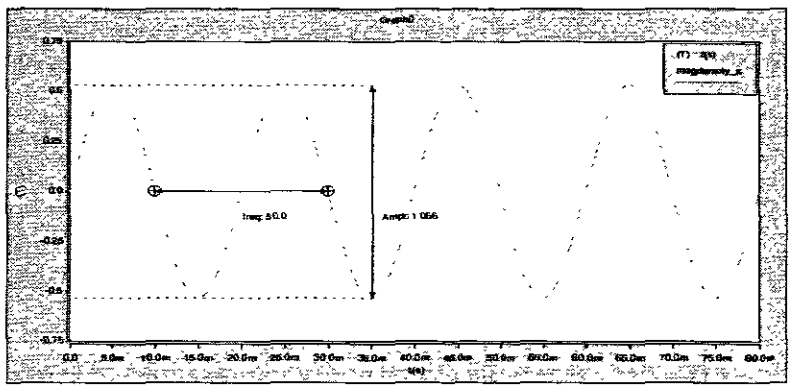

Figure 6.1: Magnetization density of the beam material of input field 1k A/meter along the beam-length (x-axis). The amplitude of the signal is increased with small value from the initial amplitude of zero input fields

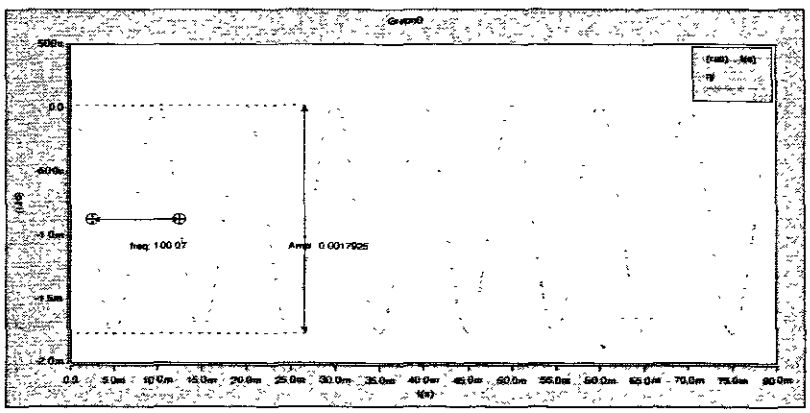

Figure 6.2: Beam deflection of input field of 1k A/meter. The signal amplitude is proportional to the input field with double frequency of the input frequency. The negative sign means the angular deflection is clockwise

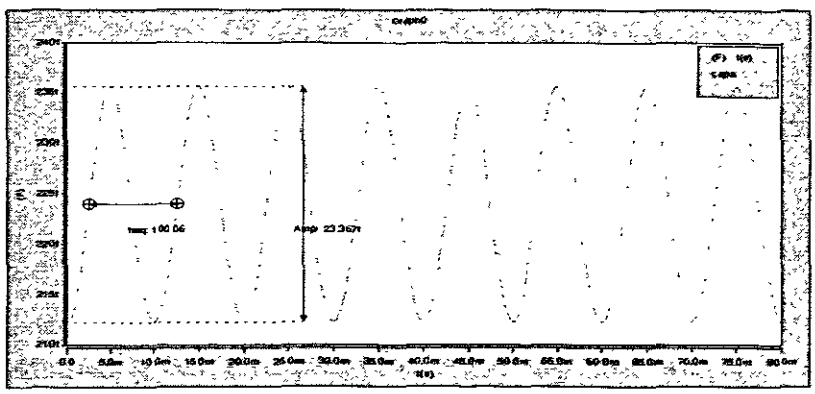

Figure 6.3: Lower capacitor signal of input field of 1k A/meter. The amplitude of the signal is increasing begins with the initial value till reach a maximum value as a function of the input field

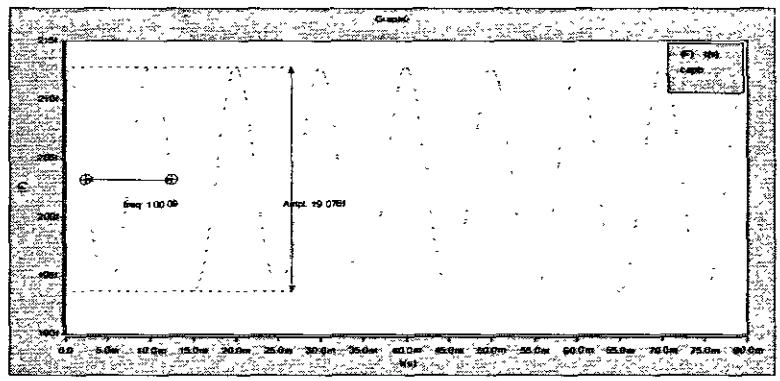

Figure 6.4: Upper capacitor signal of input field of 1k A/meter. The amplitude of the signal is decreasing begins with the initial value till reach a minimum value as a function of the input field

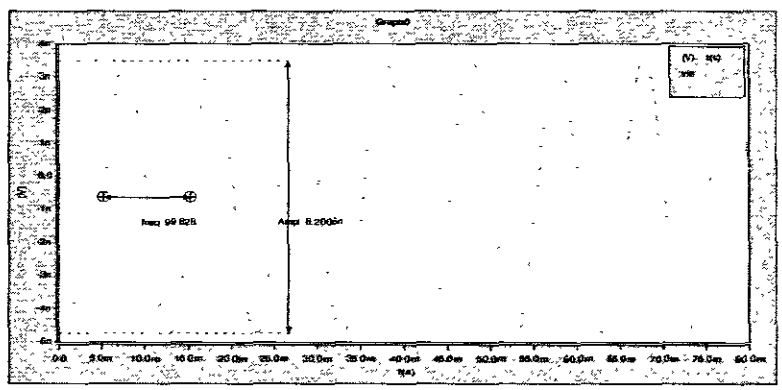

Figure 6.5: Sensor output voltage at point B of input field of 1k A/meter. The signal frequency is double of the input field signal frequency. The amplitude of the signal is proportional to the input field

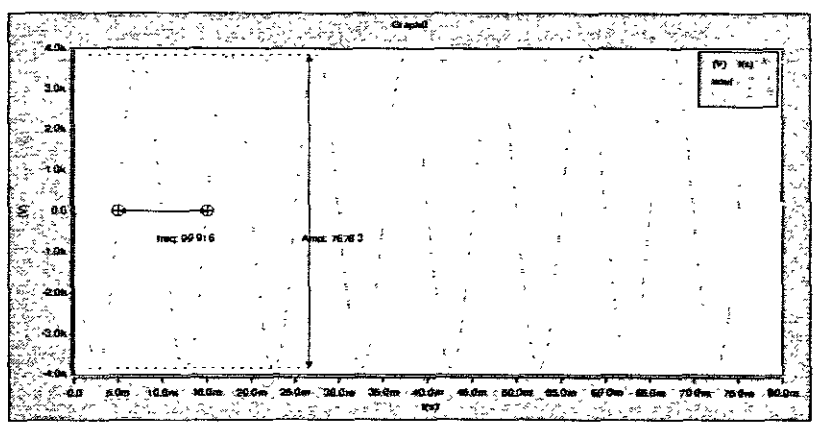

Figure 6.6: Sensor output voltage of input field of 1k A/meter. The signal frequency is double of the input field signal frequency. The amplitude of the signal is proportional to the input field

2.7 Results of input field of 1.3 k A/m

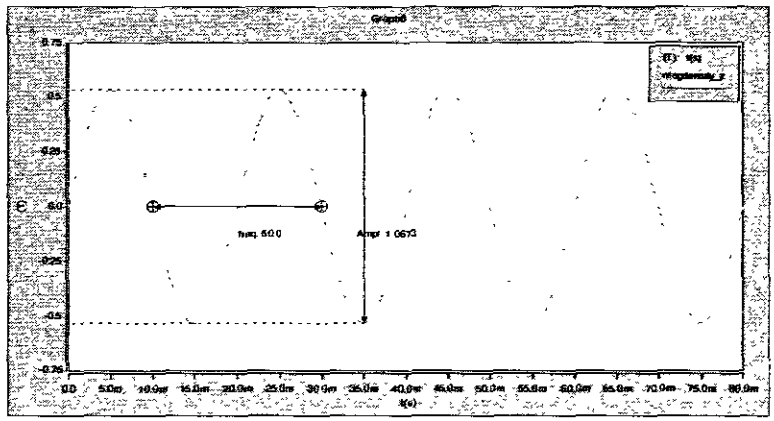

Figure 7.1: Magnetization density of the beam material of input field 1.3k A/meter along the beam-length (x-axis). The amplitude of the signal is increased with small value from the initial amplitude of zero input fields

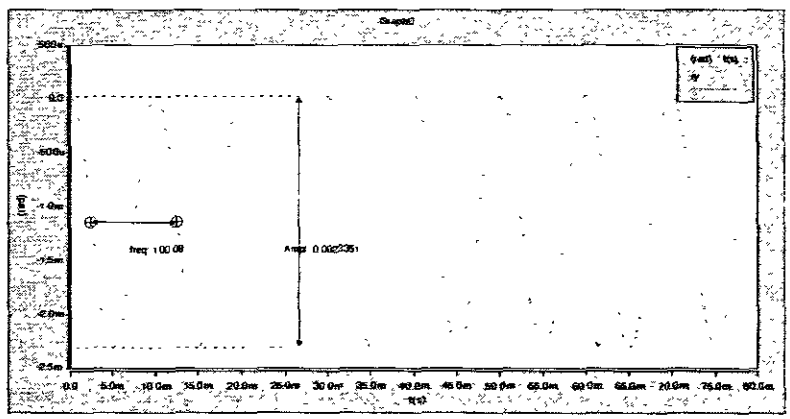

Figure 7.2: Beam deflection of input field of 1.3k A/meter. The signal amplitude is proportional to the input field with double frequency of the input frequency. The negative sign means the angular deflection is clockwise

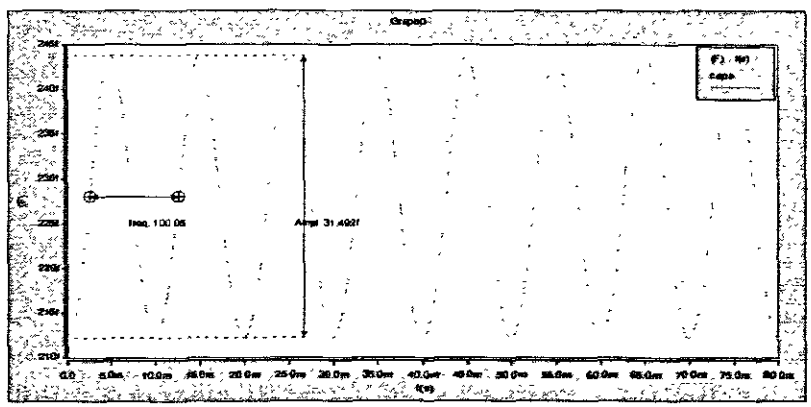

Figure 7.3: Lower capacitor signal of input field of 1.3k A/meter. The amplitude of the signal is increasing begins with the initial value till reach a maximum value as a function of the input field

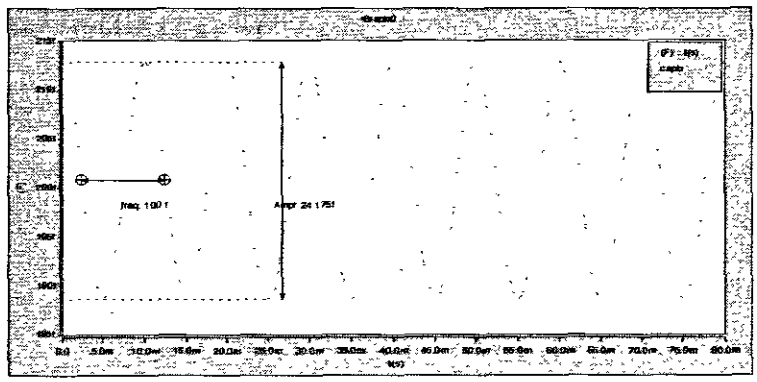

Figure 7.4: Upper capacitor signal of input field of 1.3k A/meter. The amplitude of the signal is decreasing begins with the initial value till reach a minimum value as a function of the input field

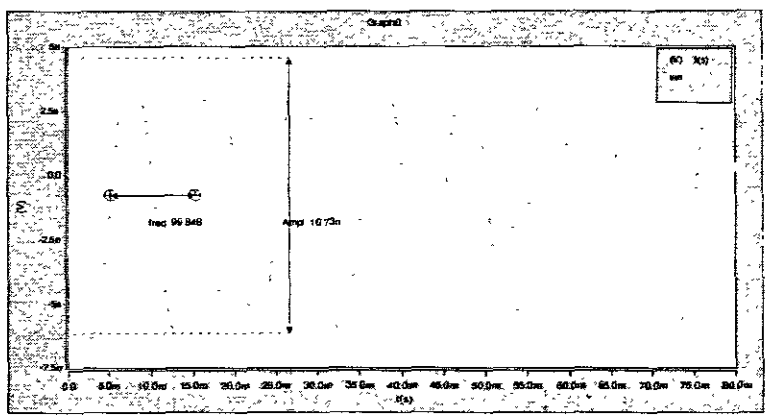

Figure 7.5: Sensor output voltage at point B of input field of 1.3k A/meter. The signal frequency is double of the input field signal frequency. The amplitude of the signal is proportional to the input field

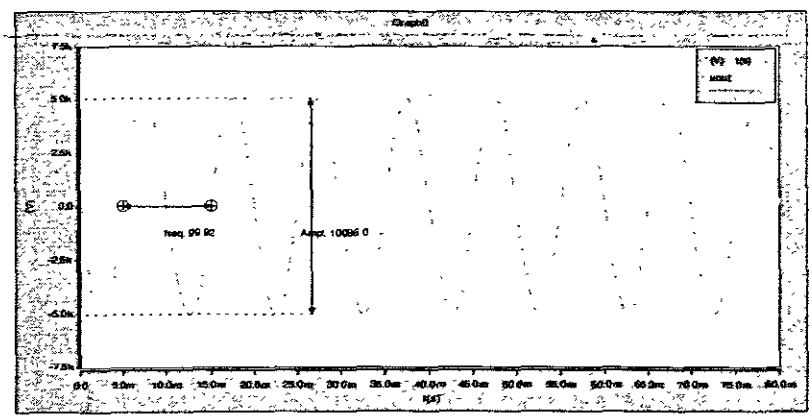

Figure 7.6: Sensor output voltage of input field of 1.3k A/meter. The signal frequency is double of the input field signal frequency. The amplitude of the signal is proportional to the input field

2.8 Results of input field of 1.6 k A/m

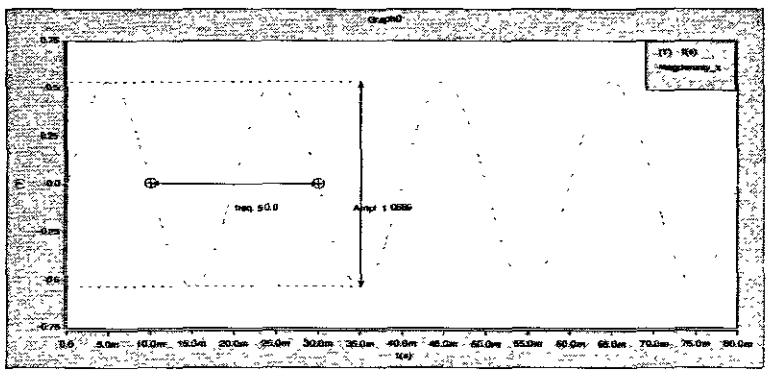

Figure 8.1: Magnetization density of the beam material of input field 1.6k A/meter along the beam-length (x-axis). The amplitude of the signal is increased with small value from the initial amplitude of zero input fields

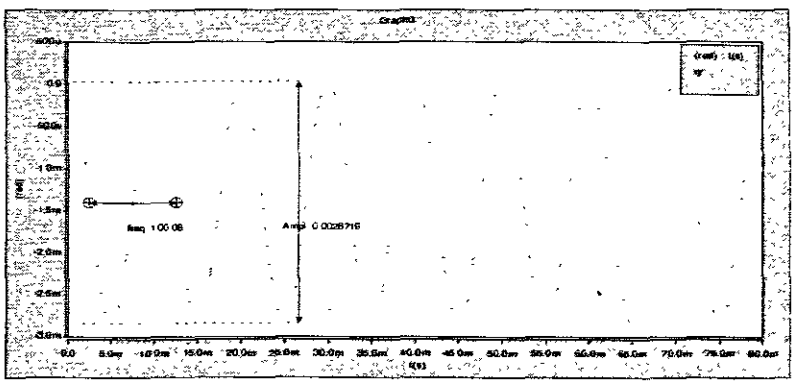

Figure 8.2: Beam deflection of input field of 1.6k A/meter. The signal amplitude is proportional to the input field with double frequency of the input frequency. The negative sign means the angular deflection is clockwise

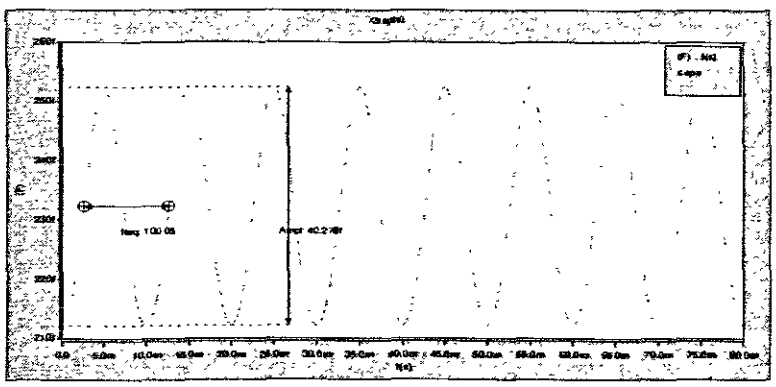

Figure 8.3: Lower capacitor signal of input field of 1.6k A/meter. The amplitude of the signal is increasing begins with the initial value till reach a maximum value as a function of the input field

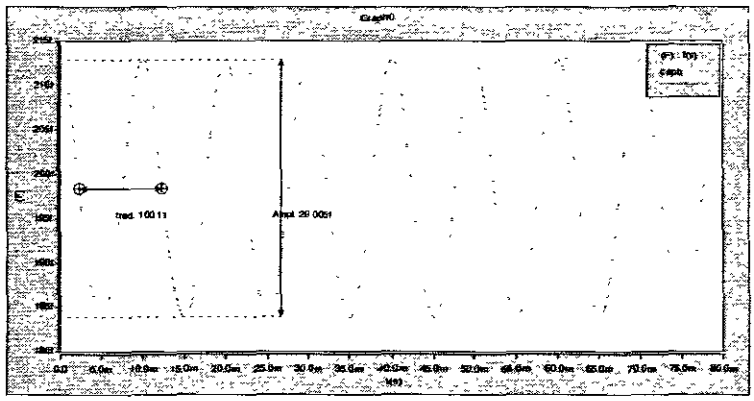

Figure 8.4: Upper capacitor signal of input field of 1.6k A/meter. The amplitude of the signal is decreasing begins with the initial value till reach a minimum value as a function of the input field

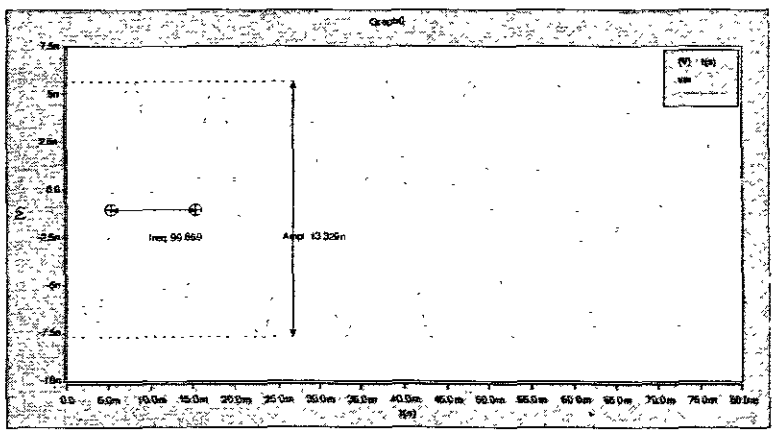

Figure 8.5: Sensor output voltage at point B of input field of 1.6k A/meter. The signal frequency is double of the input field signal frequency. The amplitude of the signal is proportional to the input field

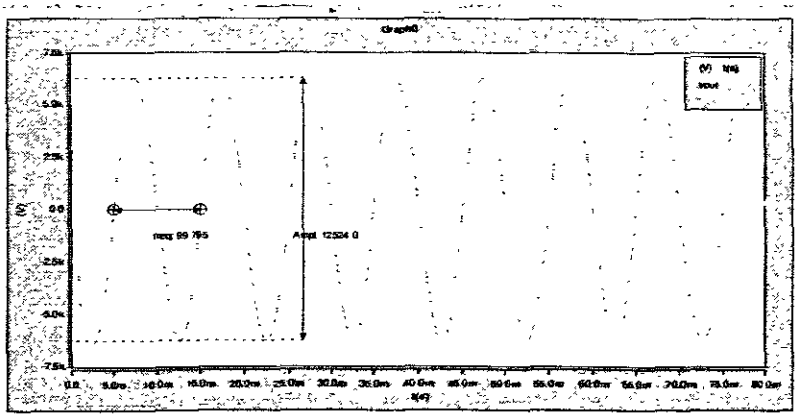

Figure 8.6: Sensor output voltage of input field of 1.6k A/meter. The signal frequency is double of the input field signal frequency. The amplitude of the signal is proportional to the input field

2.9 Results of input field of 1.9 k A/m

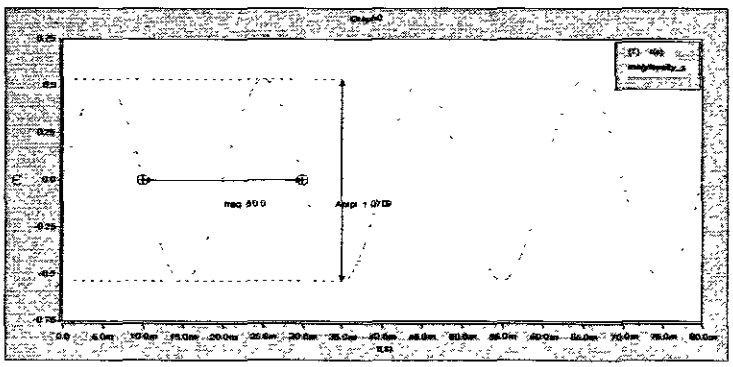

Figure 9.1: Magnetization density of the beam material of input field 1.9k A/meter along the beam-length (x-axis). The amplitude of the signal is increased with small value from the initial amplitude of zero input fields

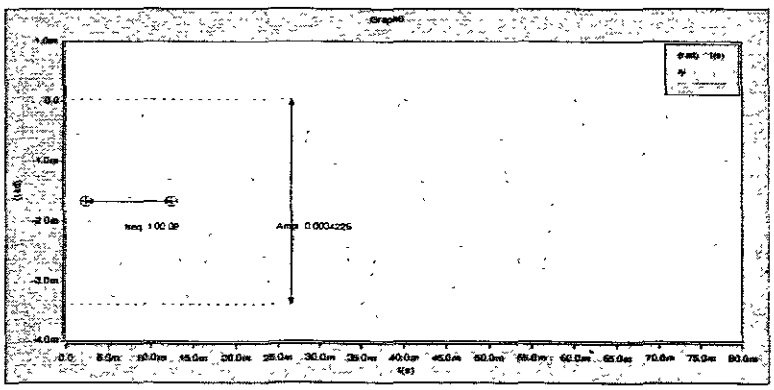

Figure 9.2: Beam deflection of input field of 1.9k A/meter. The signal amplitude is proportional to the input field with double frequency of the input frequency. The negative sign means the angular deflection is clockwise

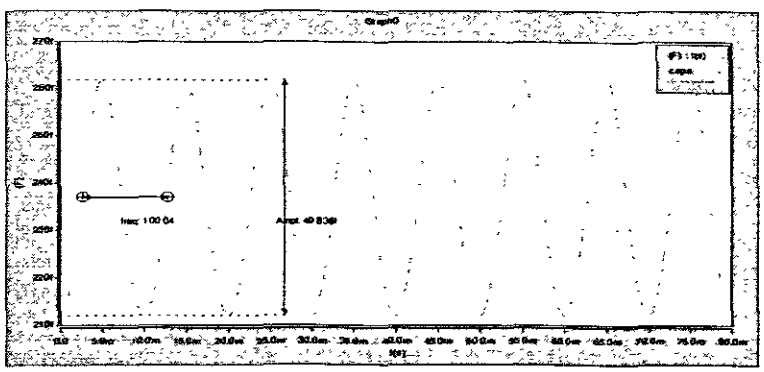

Figure 9.3: Lower Capacitor signal of input field of 1.9k A/meter. The amplitude of the signal is increasing begins with the initial value till reach a maximum value as a function of the input field

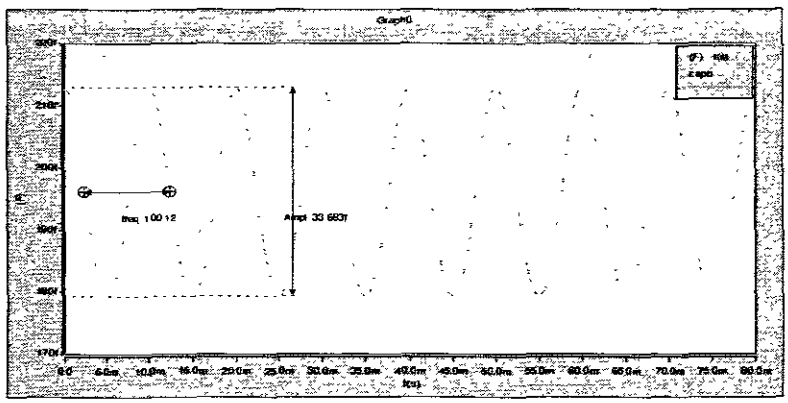

Figure 9.4: Upper capacitor signal of input field of 1.9k A/meter. The amplitude of the signal is decreasing begins with the initial value till reach a minimum value as a function of the input field

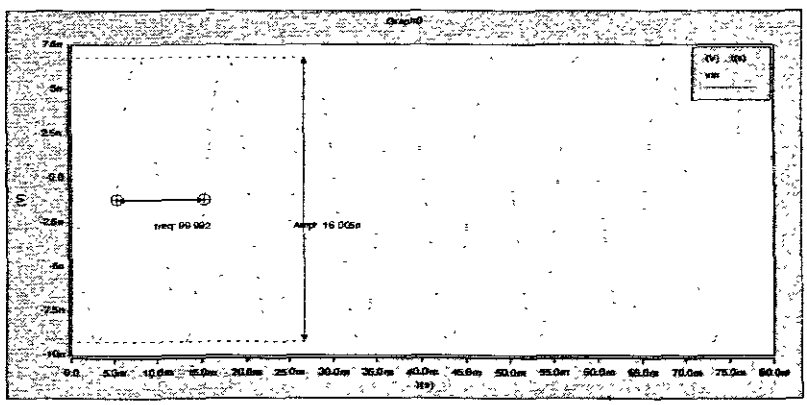

Figure 9.5: Sensor output voltage at point B of input field of 1.9k A/meter. The signal frequency is double of the input field signal frequency. The amplitude of the signal is proportional to the input field

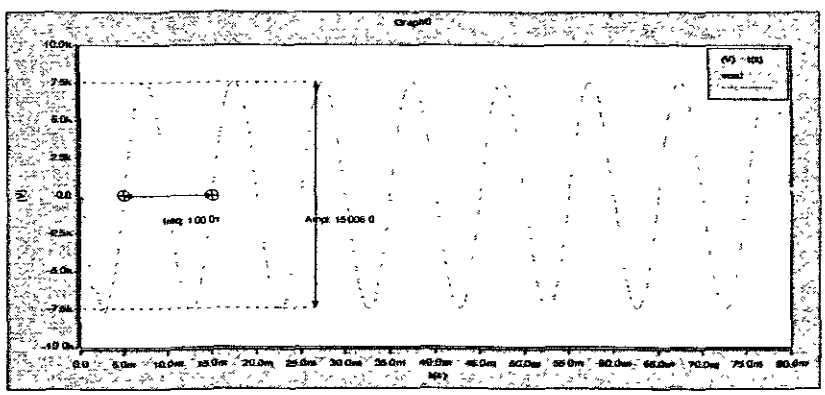

Figure 9.6: Sensor output voltage of input field of 1.9k A/meter. The signal frequency is double of the input field signal frequency. The amplitude of the signal is proportional to the input field

2.10 Results of input field of 2.2 k A/m

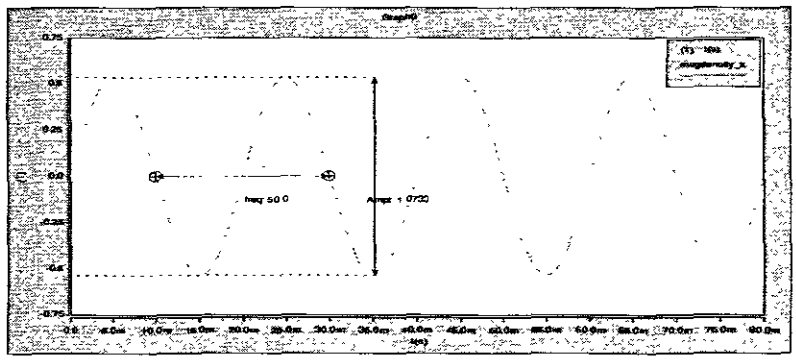

Figure 10.1: Magnetization density of the beam material of input field 2.2k A/meter along the beam-length (x-axis). The amplitude of the signal is increased with small value from the initial amplitude of zero input fields

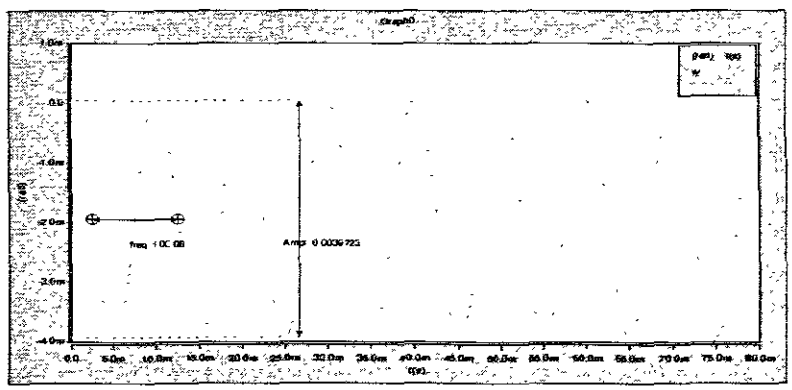

Figure 10.2: Beam deflection of input field of 2.2k A/meter. The signal amplitude is proportional to the input field with double frequency of the input frequency. The negative sign means the angular deflection is clockwise

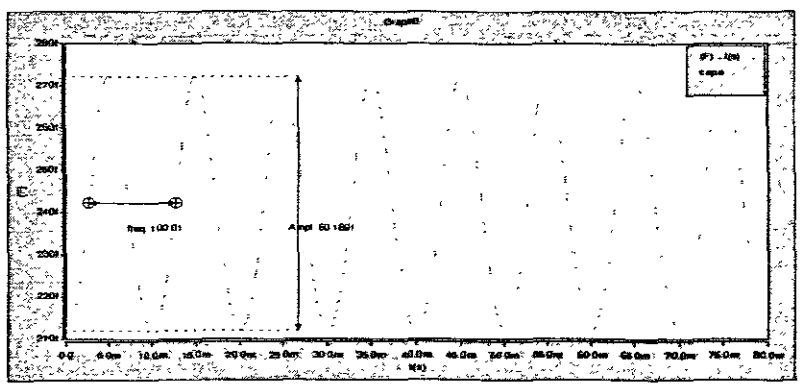

Figure 10.3: Lower capacitor signal of input field of 2.2k A/meter. The amplitude of the signal is increasing begins with the initial value till reach a maximum value as a function of the input field

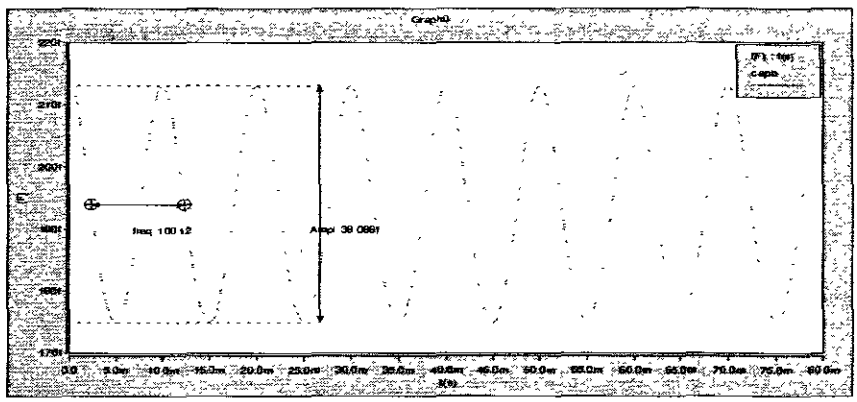

Figure 10.4: Upper capacitor signal of input field of 2.2k A/meter. The amplitude of the signal is decreasing begins with the initial value till reach a minimum value as a function of the input field

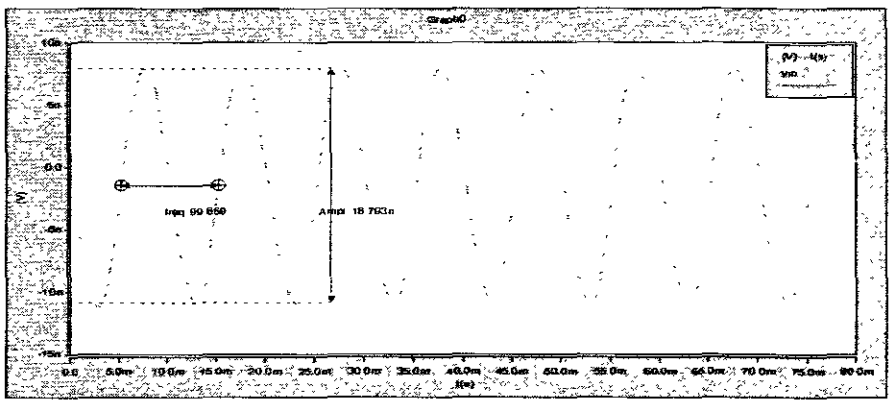

Figure 10.5: Sensor output voltage at point B of input field of 2.2k A/meter. The signal frequency is double of the input field signal frequency. The amplitude of the signal is proportional to the input field

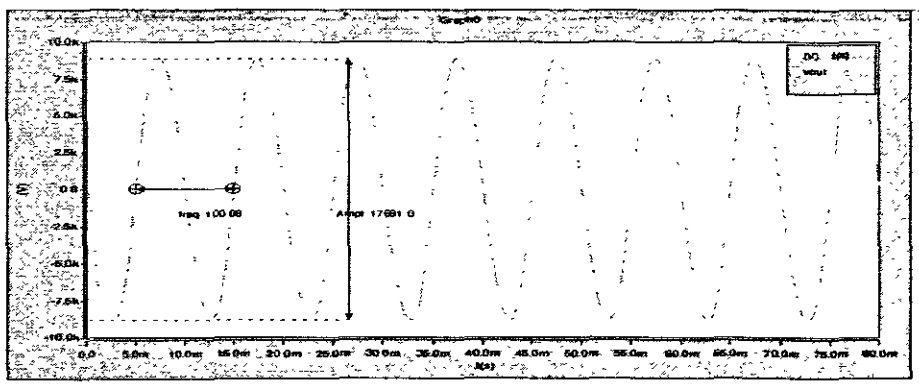

Figure10.6: Sensor output voltage of input field of 2.2k A/meter. The signal frequency is double of the input field signal frequency. The amplitude of the signal is proportional to the input field

2.11 Results of input field of 2.5 k A/m

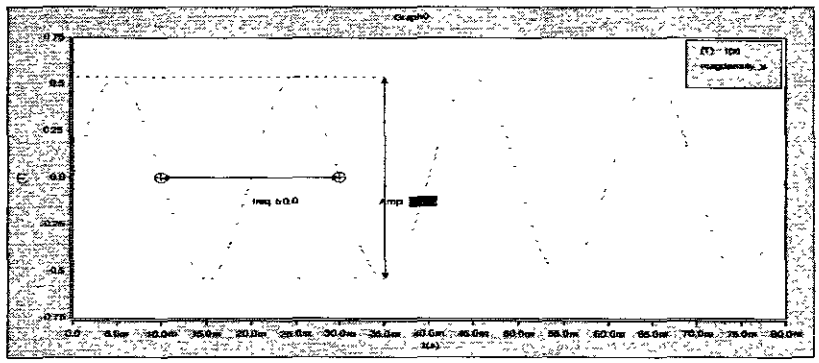

Figure 11.1: Magnetization density of the beam material of input field 2.5k A/meter along the beam-length (x-axis). The amplitude of the signal is increased with small value from the initial amplitude of zero input fields

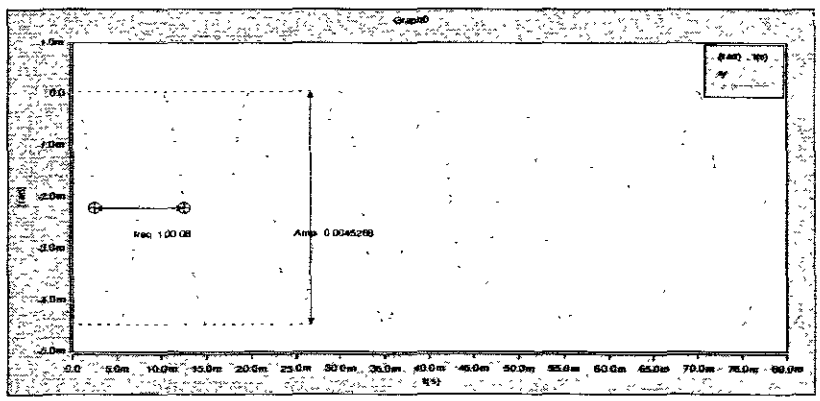

Figure 11.2: Beam deflection of input field of 2.5k A/meter. The signal amplitude is proportional to the input field with double frequency of the input frequency. The negative sign means the angular deflection is clockwise

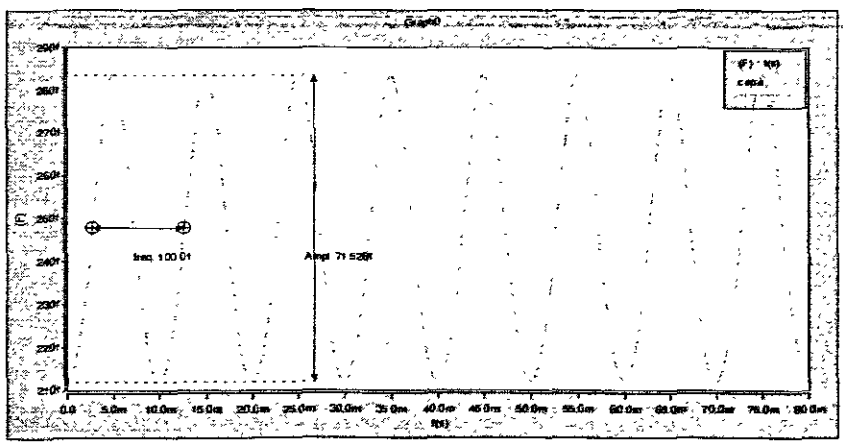

Figure 11.3: Lower capacitor signal of input field of 2.5k A/meter. The amplitude of the signal is increasing begins with the initial value till reach a maximum value as a function of the input field

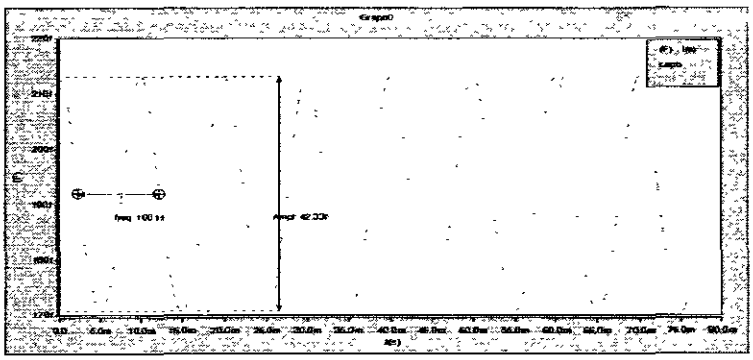

Figure 11.4: Upper capacitor signal of input field of 2.5k A/meter. The amplitude of the signal is decreasing begins with the initial value till reach a minimum value as a function of the input field

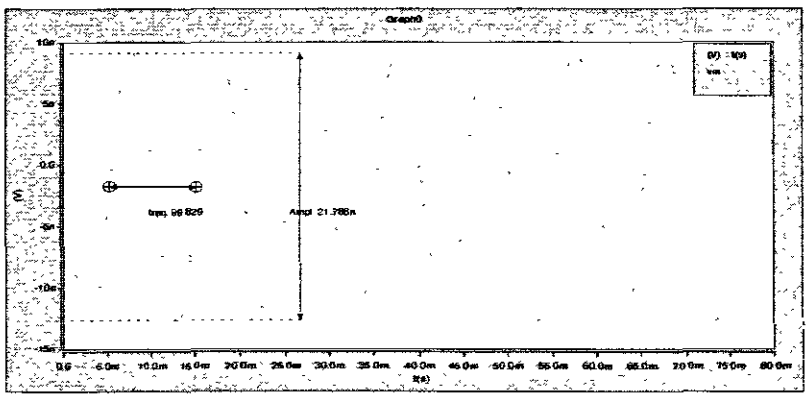

Figure 11.5: Sensor output voltage at point B of input field of 2.5k A/meter. The signal frequency is double of the input field signal frequency. The amplitude of the signal is proportional to the input field

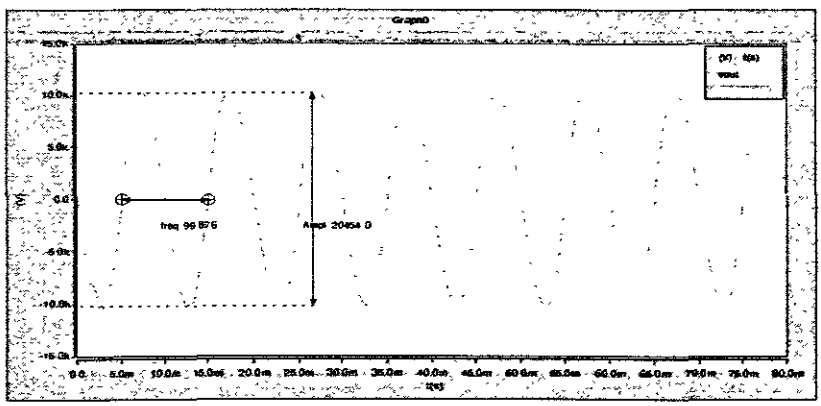

Figure 11.6: Sensor output voltage of input field of 2.5k A/meter. The signal frequency is double of the input field signal frequency. The amplitude of the signal is proportional to the input field

2.12 Results of input field of 2.8 k A/m

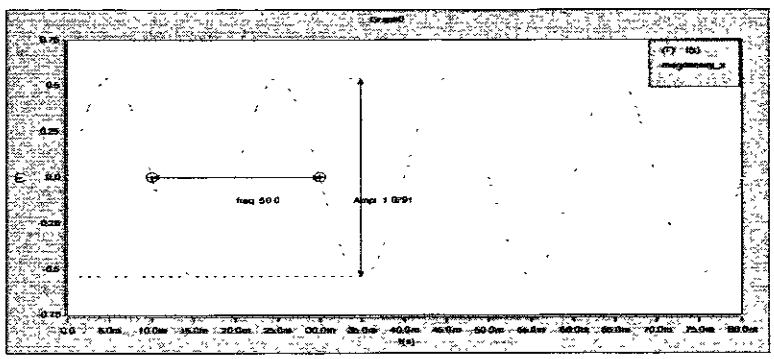

Figure 12.1: Magnetization density of the beam material of input field 2.8k A/meter along the beam-length (x-axis). The amplitude of the signal is increased with small value from the initial amplitude of zero input fields

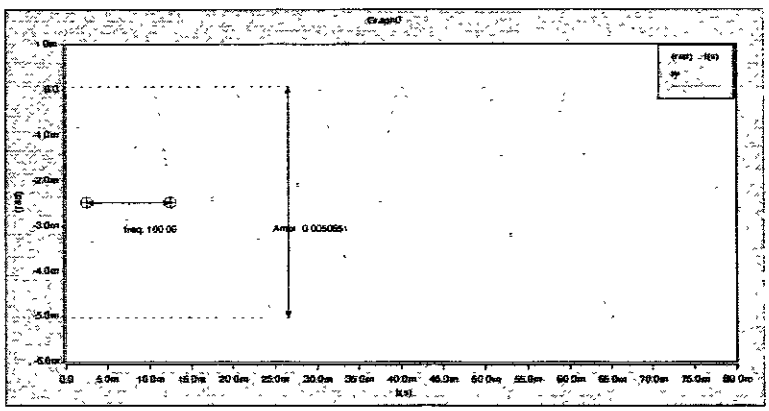

Figure 12.2: Beam deflection of input field of 2.8k A/meter. The signal amplitude is proportional to the input field with double frequency of the input frequency. The negative sign means the angular deflection is clockwise

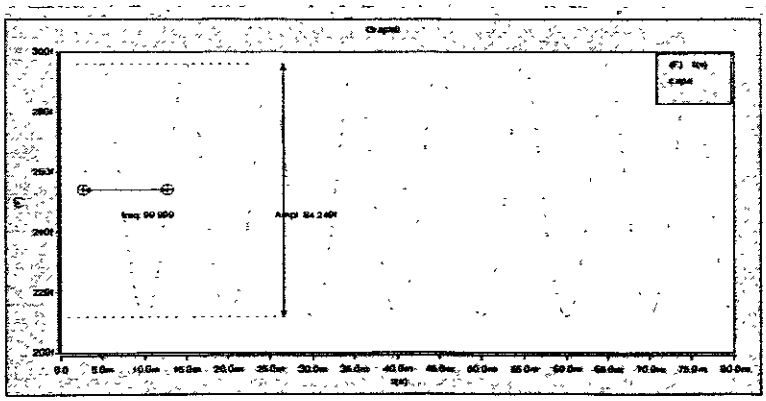

Figure 12.3: Lower capacitor signal of input field of 2.8k A/meter. The amplitude of the signal is increasing begins with the initial value till reach a maximum value as a function of the input field

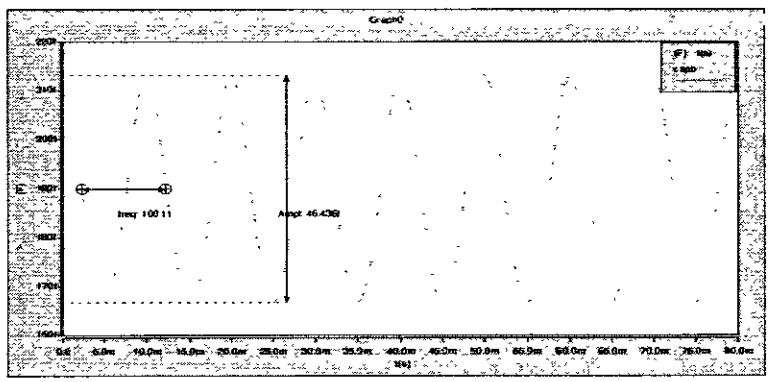

Figure 12.4: Upper capacitor signal of input field of 2.8k A/meter. The amplitude of the signal is decreasing begins with the initial value till reach a minimum value as a function of the input field

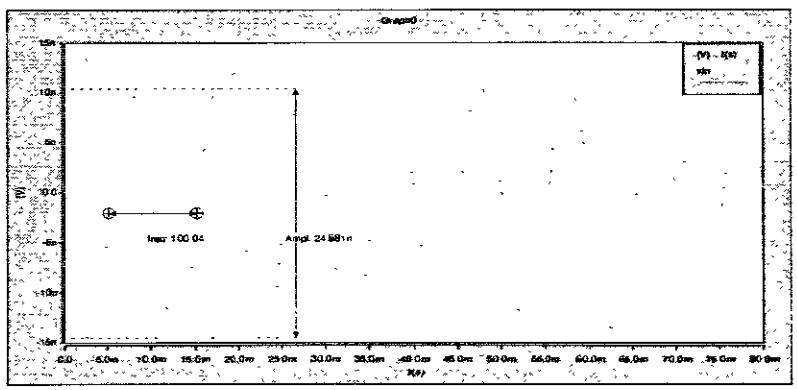

Figure 12.5: Sensor output voltage at point B of input field of 2.8k A/meter. The signal frequency is double of the input field signal frequency. The amplitude of the signal is proportional to the input field

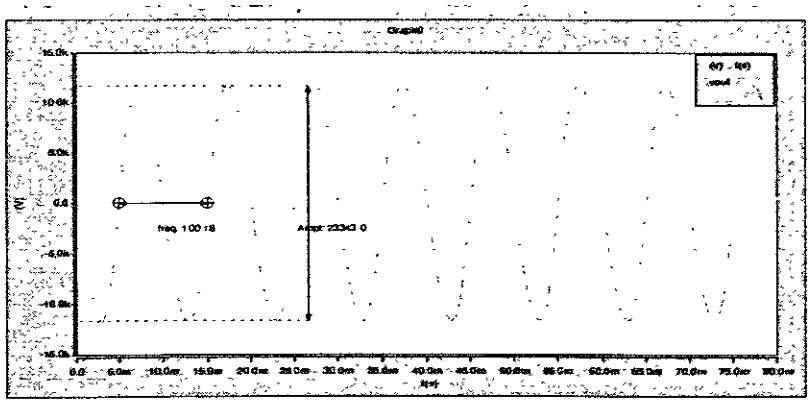

Figure 12.6: Sensor output voltage of input field of 2.8k A/meter. The signal frequency is double of the input field signal frequency. The amplitude of the signal is proportional to the input field

2.13 Results of input field of 3.1 k A/m

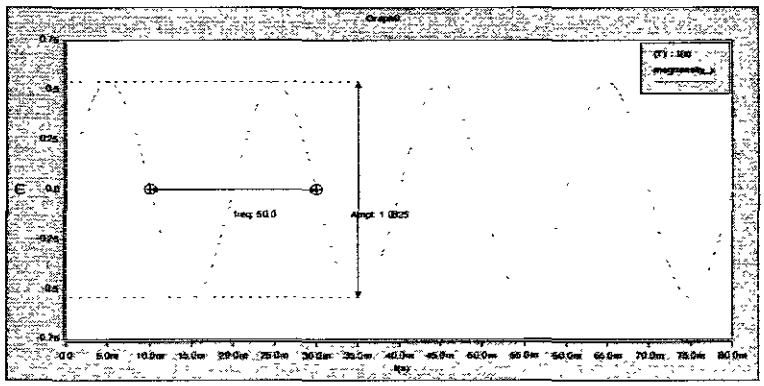

Figure 13.1: Magnetization density of the beam material of input field 3.1k A/meter along the beam-length (x-axis). The amplitude of the signal is increased with small value from the initial amplitude of zero input fields

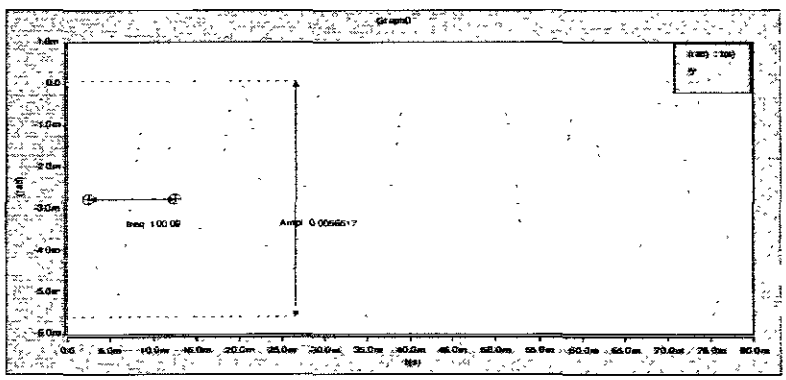

Figure 13.2: Beam deflection of input field of 3.1k A/meter. The signal amplitude is proportional to the input field with double frequency of the input frequency. The negative sign means the angular deflection is clockwise

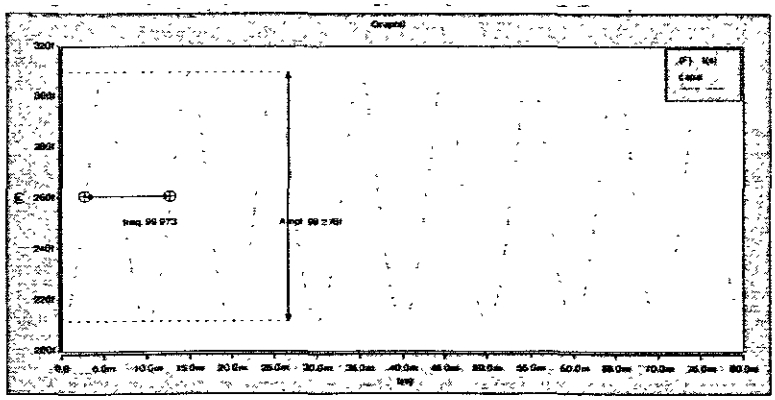

Figure 13.3 Lower capacitor signal of input field of 3.1k A/meter. The amplitude of the signal is increasing begins with the initial value till reach a maximum value as a function of the input field

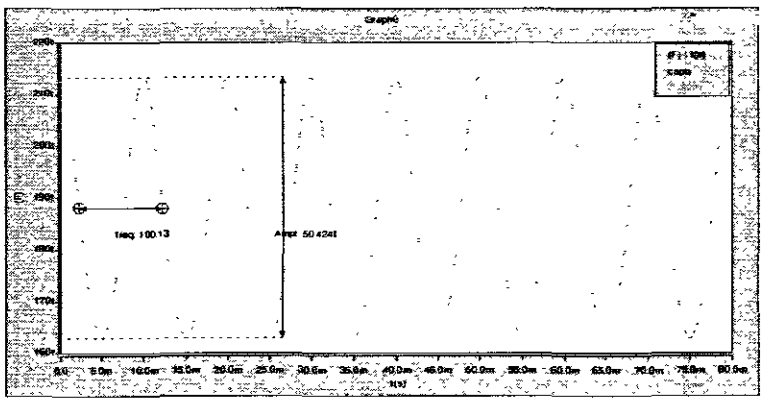

Figure 13.4: Upper capacitor signal of input field of 3.1k A/meter. The amplitude of the signal is decreasing begins with the initial value till reach a minimum value as a function of the input field

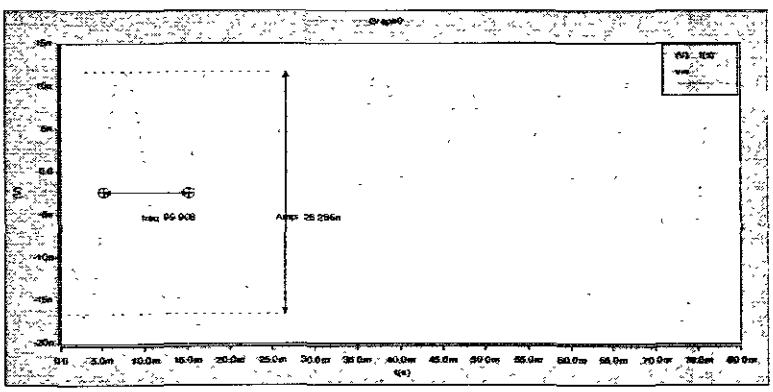

Figure 13.5: Sensor output voltage at point B of input field of 3.1k A/meter. The signal frequency is double of the input field signal frequency. The amplitude of the signal is proportional to the input field

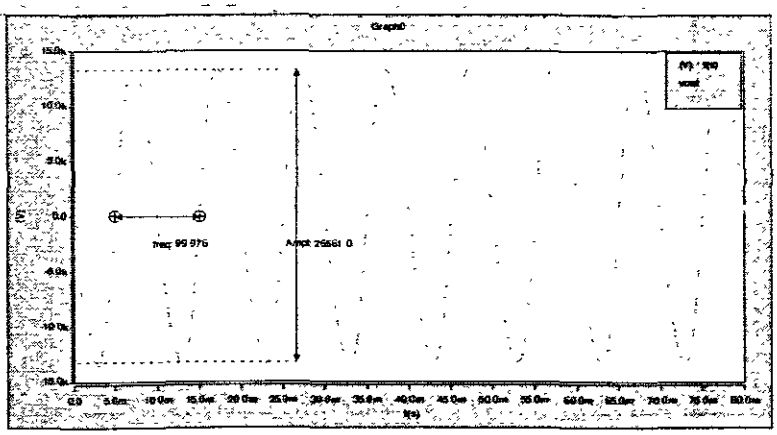

Figure 13.6: Sensor output voltage of input field of 3.1k A/meter. The signal frequency is double of the input field signal frequency. The amplitude of the signal is proportional to the input field

2.14 Results of input field of 3.4 k A/m

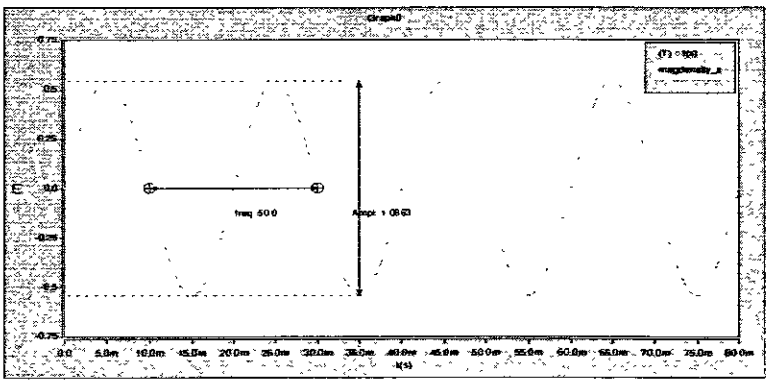

Figure 14.1: Magnetization density of the beam material of input field 3.4k A/meter along the beam-length (x-axis). The amplitude of the signal is increased with small value from the initial amplitude of zero input fields

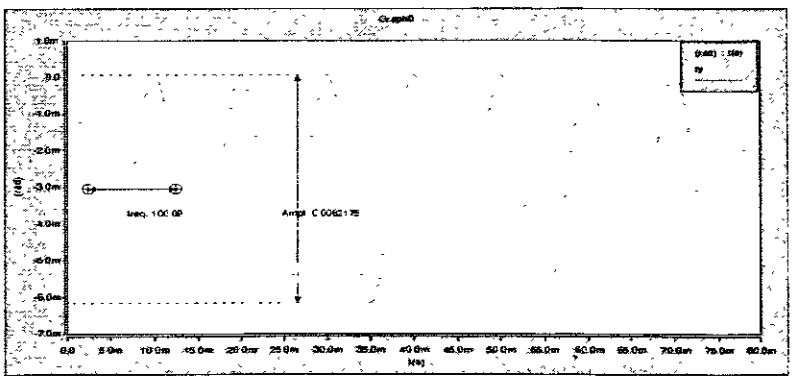

Figure 14.2: Beam deflection of input field of 3.4k A/meter. The signal amplitude is proportional to the input field with double frequency of the input frequency. The negative sign means the angular deflection is clockwise

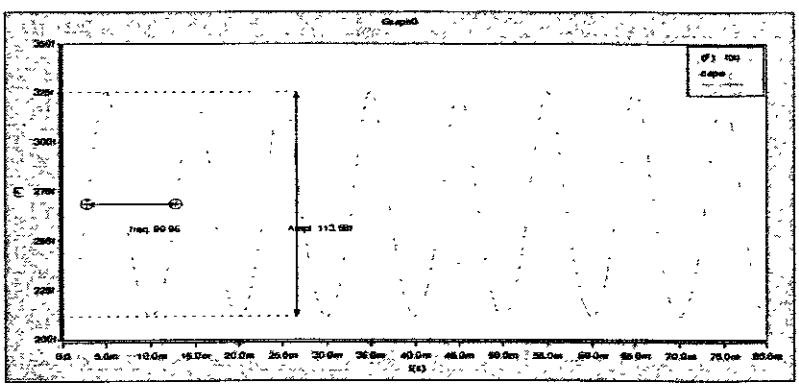

Figure 14.3: Lower capacitor signal of input field of 3.4k A/meter. The amplitude of the signal is increasing begins with the initial value till reach a maximum value as a function of the input field

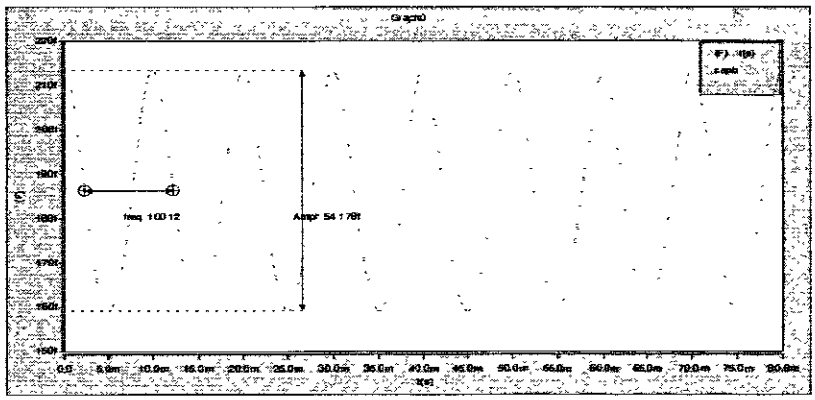

Figure 14.4: Upper capacitor signal of input field of 3.4k A/meter. The amplitude of the signal is decreasing begins with the initial value till reach a minimum value as a function of the input field

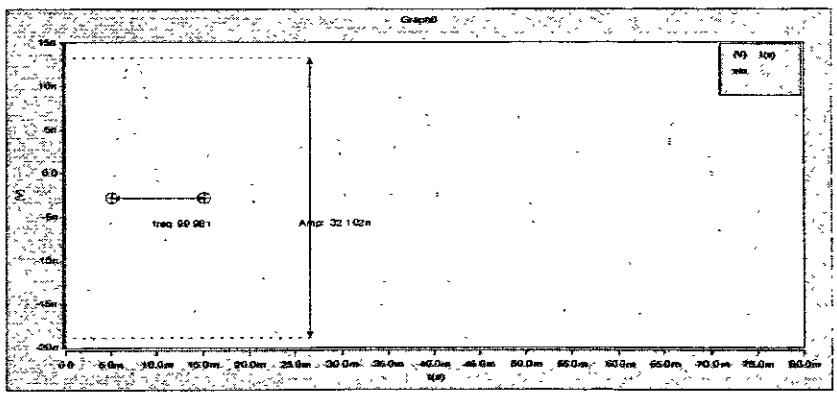

Figure 14.5: Sensor output voltage at point B of input field of 3.4k A/meter. The signal frequency is double of the input field signal frequency. The amplitude of the signal is proportional to the input field

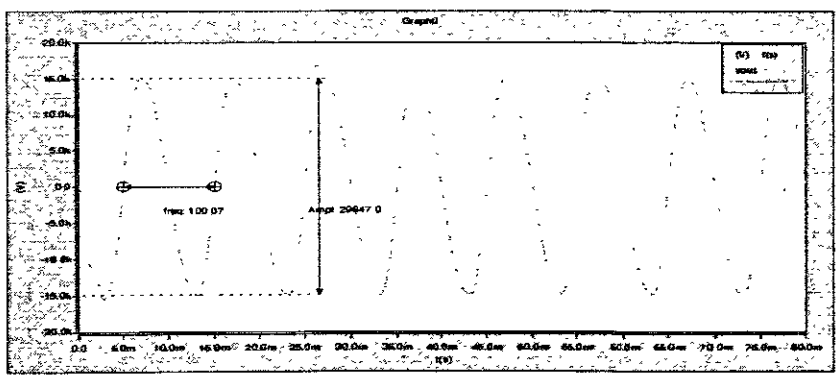

Figure 14.6: Sensor output voltage of input field of 3.4k A/meter. The signal frequency is double of the input field signal frequency. The amplitude of the signal is proportional to the input field

2.15 Results of input field of 3.7 k A/m

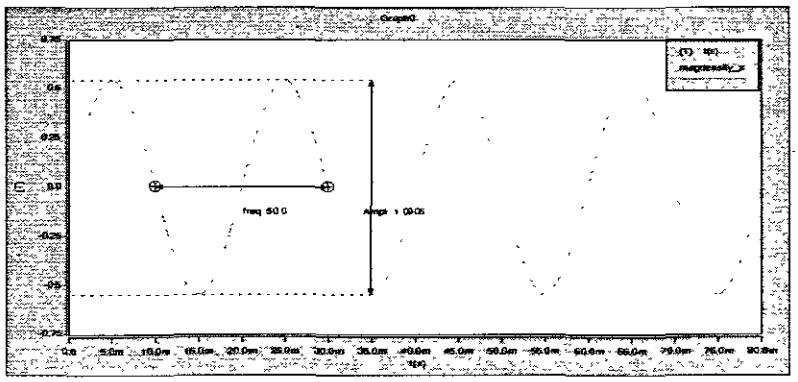

Figure 15.1: Magnetization density of the beam material of input field 3.7k A/meter along the beam-length (x-axis). The amplitude of the signal is increased with small value from the initial amplitude of zero input fields

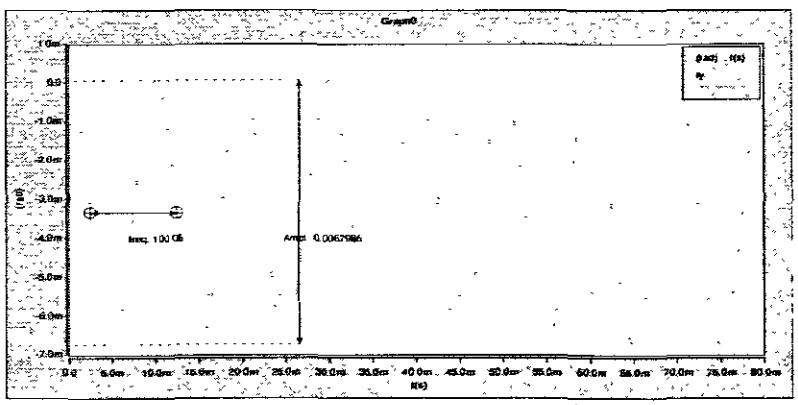

Figure 15.2: Beam deflection of input field of 3.7k A/meter. The signal amplitude is proportional to the input field with double frequency of the input frequency. The negative sign means the angular deflection is clockwise

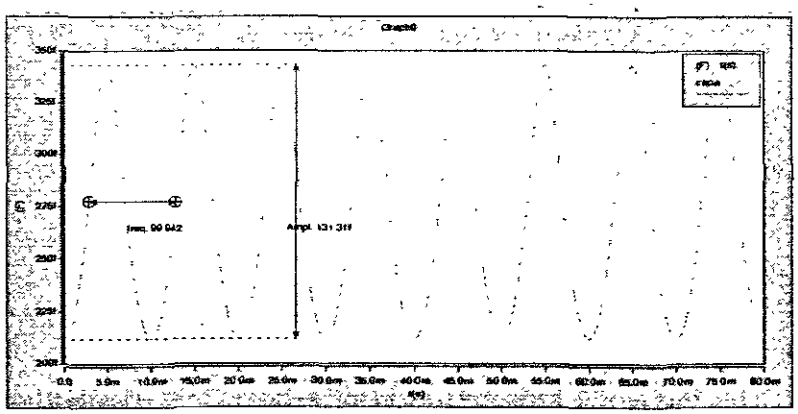

Figure 15.3: Lower capacitor signal of input field of 3.7k A/meter. The amplitude of the signal is increasing begins with the initial value till reach a maximum value as a function of the input field

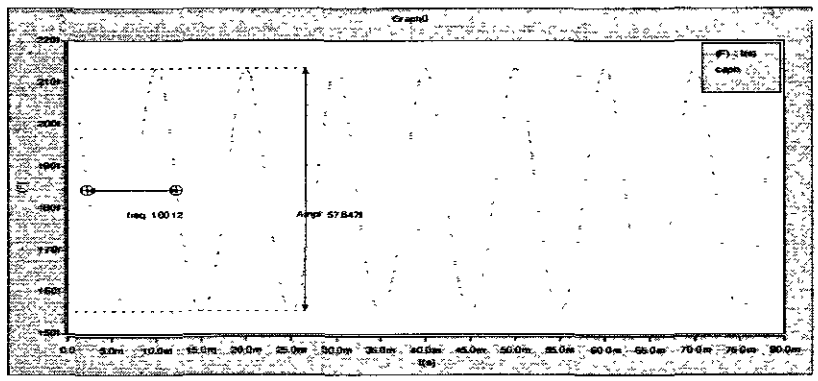

Figure 15.4: Upper capacitor signal of input field of 3.7k A/meter. The amplitude of the signal is decreasing begins with the initial value till reach a minimum value as a function of the input field

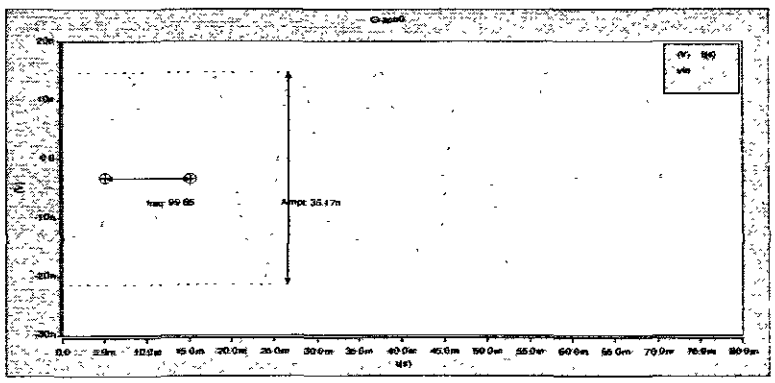

Figure 15.5: Sensor output voltage at point B of input field of 3.7k A/meter. The signal frequency is double of the input field signal frequency. The amplitude of the signal is proportional to the input field

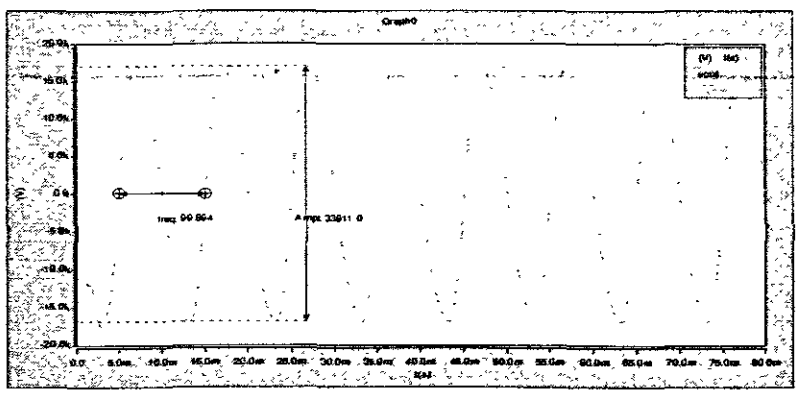

Figure 15.6: Sensor output voltage of input field of 3.7k A/meter. The signal frequency is double of the input field signal frequency. The amplitude of the signal is proportional to the input field

2.16 Results of input field of 4 k A/m

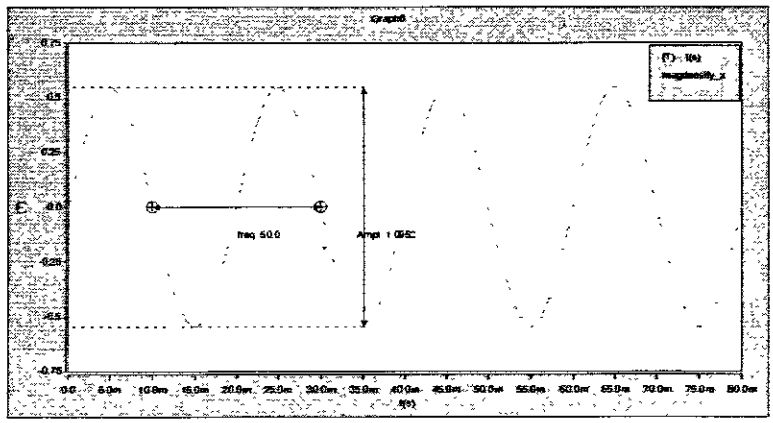

Figure 16.1: Magnetization density of the beam material of input field 4k A/meter along the beam-length (x-axis). The amplitude of the signal is increased with small value from the initial amplitude of zero input fields

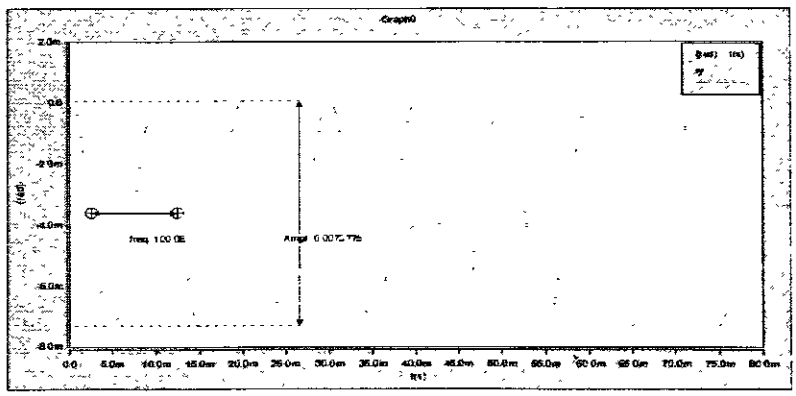

Figure 16.2: Beam deflection of input field of 4k A/meter. The signal amplitude is proportional to the input field with double frequency of the input frequency. The negative sign means the angular deflection is clockwise

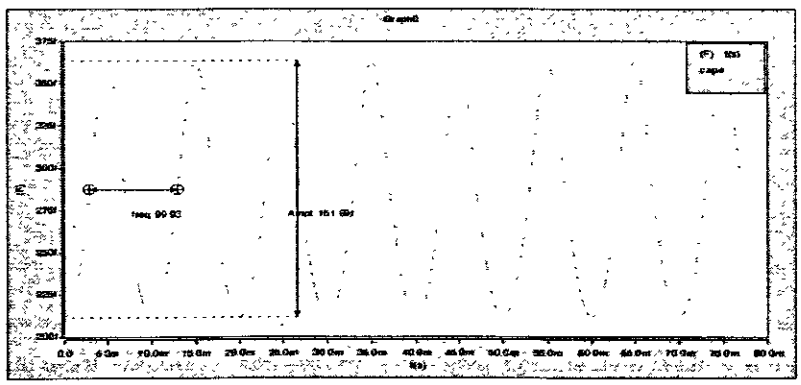

Figure 16.3: Lower capacitor signal of input field of 4k A/meter. The amplitude of the signal is increasing begins with the initial value till reach a maximum value as a function of the input field

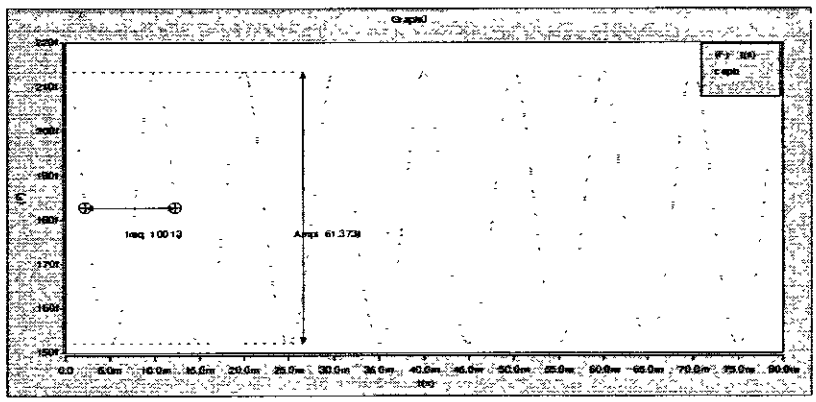

Figure 16.4: Upper capacitor signal of input field of 4k A/meter. The amplitude of the signal is decreasing begins with the initial value till reach a minimum value as a function of the input field

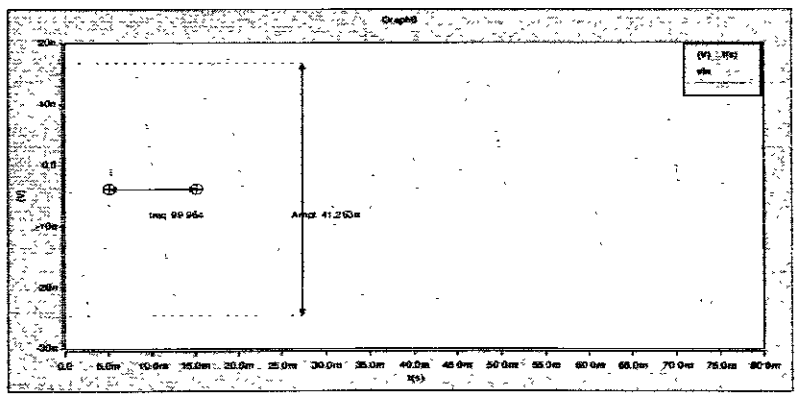

Figure 16.5: Sensor output voltage at point B of input field of 4k A/meter. The signal frequency is double of the input field signal frequency. The amplitude of the signal is proportional to the input field

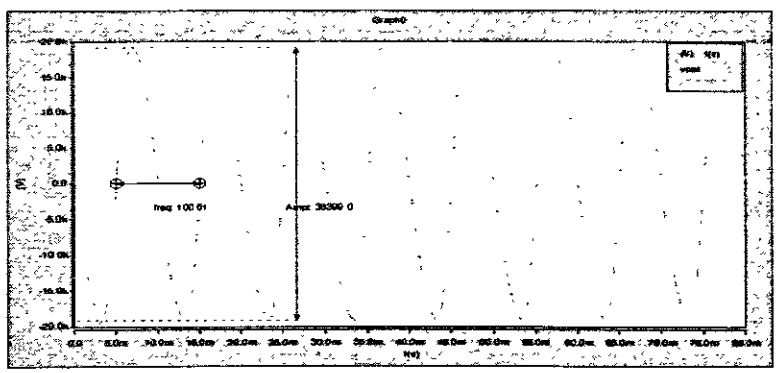

Figure 16.6: Sensor output voltage of input field of 4k A/meter. The signal frequency is double of the input field signal frequency. The amplitude of the signal is proportional to the input field

2.17 Results of input field of 4.5 k A/m

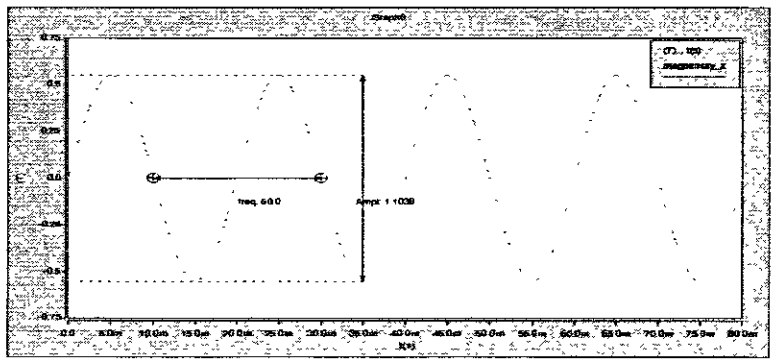

Figure 17.1: Magnetization density of the beam material of input field 4.5k A/meter along the beam-length (x-axis). The amplitude of the signal is increased with small value from the initial amplitude of zero input fields

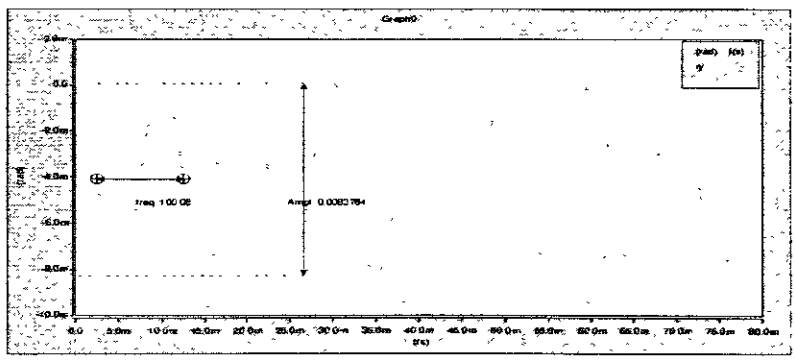

Figure 17.2: Beam deflection of input field of 4.5k A/meter. The signal amplitude is proportional to the input field with double frequency of the input frequency. The negative sign means the angular deflection is clockwise

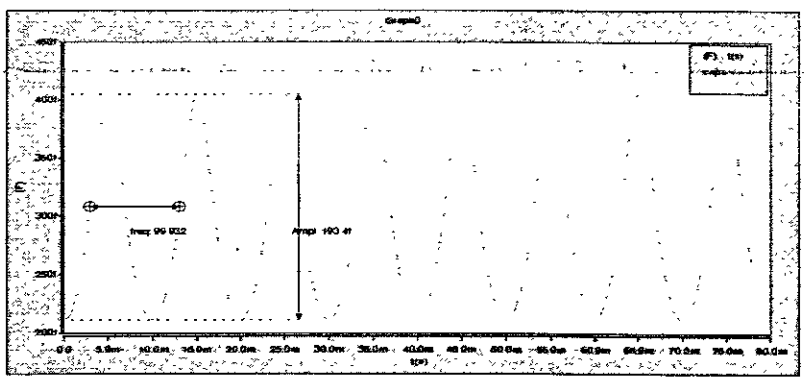

Figure 17.3: Lower capacitor signal of input field of 4.5k A/meter. The amplitude of the signal is increasing begins with the initial value till reach a maximum value as a function of the input field

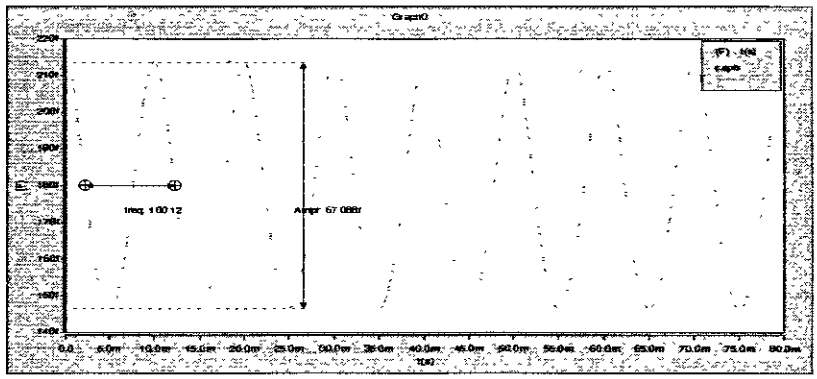

Figure 17.4: Upper capacitor signal of input field of 4.5k A/meter. The amplitude of the signal is decreasing begins with the initial value till reach a minimum value as a function of the input field

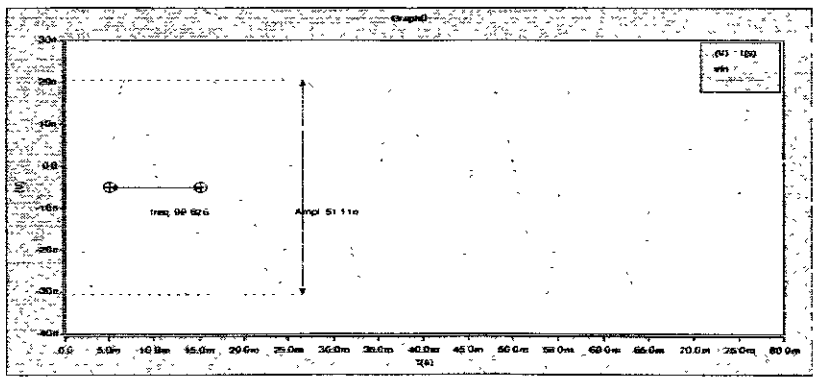

Figure 17.5: Sensor output voltage at point B of input field of 4.5k A/meter. The signal frequency is double of the input field signal frequency. The amplitude of the signal is proportional to the input field

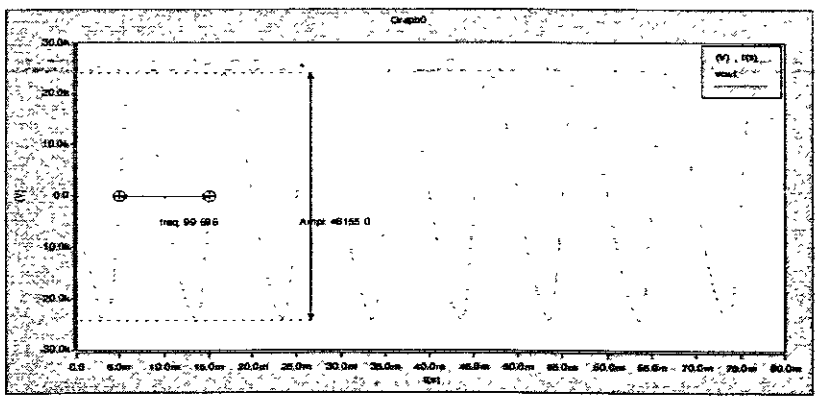

Figure 17.6: Sensor output voltage of input field of 4.5k A/meter. The signal frequency is double of the input field signal frequency. The amplitude of the signal is proportional to the input field

2.18 Results of input field of 5 k A/m

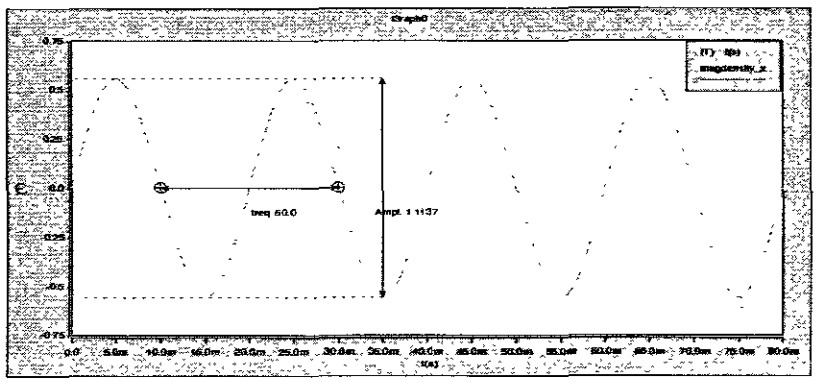

Figure 18.1: Magnetization density of the beam material of input field 5k A/meter along the beam-length (x-axis). The amplitude of the signal is increased with small value from the initial amplitude of zero input fields

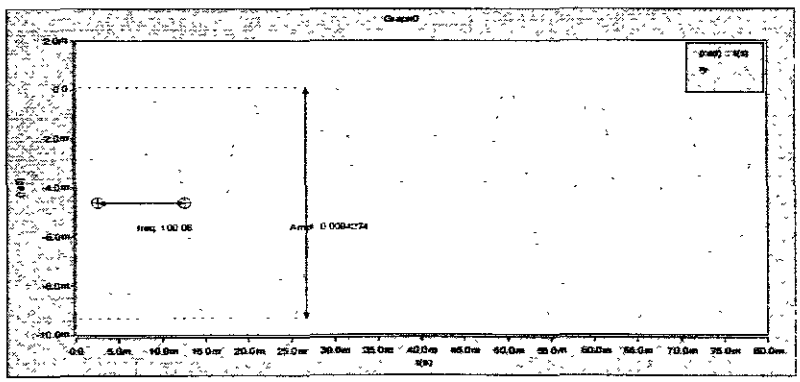

Figure 18.2: Beam deflection of input field of 5k A/meter. The signal amplitude is proportional to the input field with double frequency of the input frequency. The negative sign means the angular deflection is clockwise

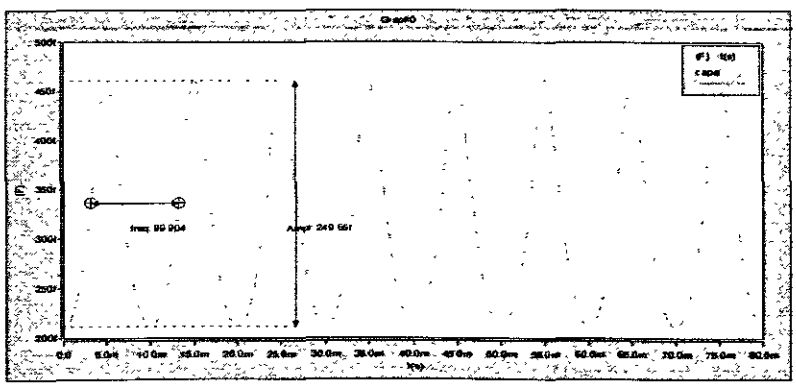

Figure 18.3: Lower capacitor signal of input field of 5k A/meter. The amplitude of the signal is increasing begins with the initial value till reach a maximum value as a function of the input field

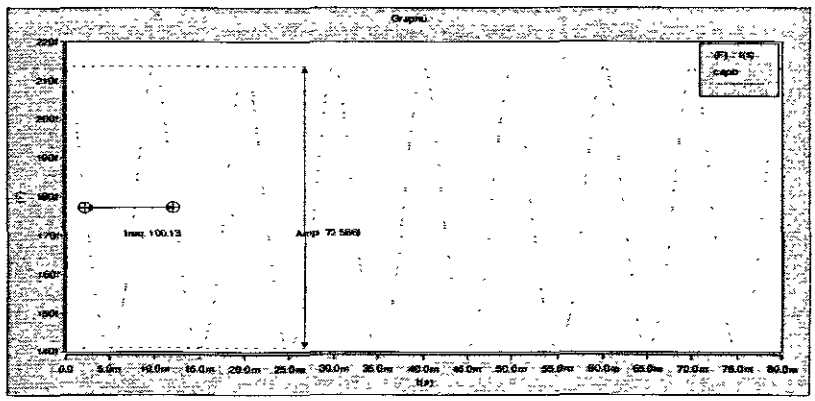

Figure 18.4: Upper capacitor signal of input field of 5k A/meter. The amplitude of the signal is decreasing begins with the initial value till reach a minimum value as a function of the input field

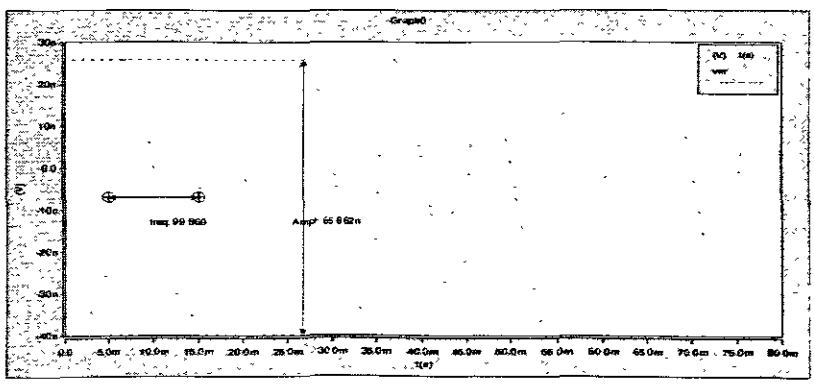

Figure 18.5: Sensor output voltage at point B of input field of 5k A/meter. The signal frequency is double of the input field signal frequency. The amplitude of the signal is proportional to the input field

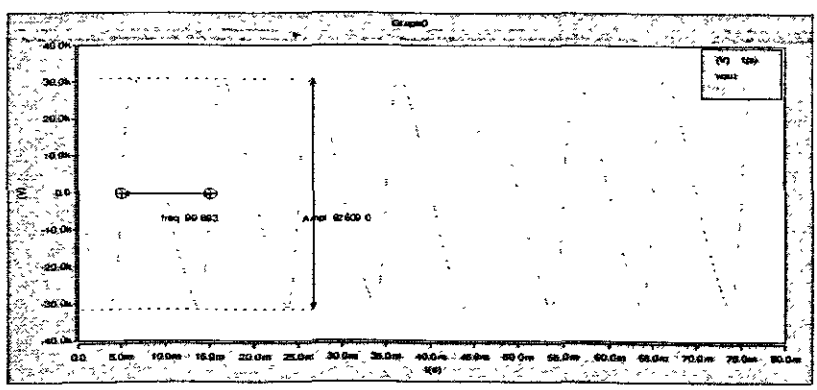

Figure 18.6 Sensor output voltage of input field of 5k A/meter. The signal frequency is double of the input field signal frequency. The amplitude of the signal is proportional to the input field